

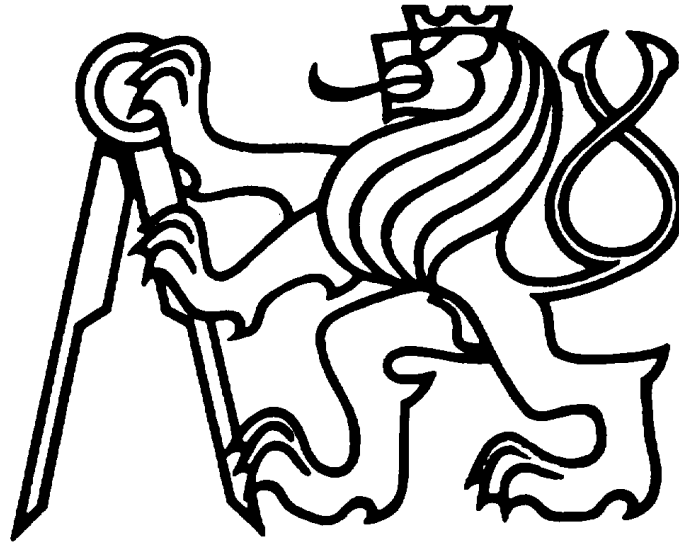
Czech Technical University in Prague
Faculty of Nuclear Sciences and Physical Engineering

DOCTORAL THESIS

Prague, April 2011

Ing. Radek Hofman

Czech Technical University in Prague
Faculty of Nuclear Sciences and Physical Engineering
Department of Mathematics



**APPLICATION OF ADVANCED DATA
ASSIMILATION METHODS IN OFF-SITE
CONSEQUENCE ASSESSMENT**

Radek Hofman

A thesis submitted in fulfillment of the requirements for the degree of
“Doctor of Philosophy” abbreviated to “Ph.D.”

Prague, April 2011

Acknowledgment

First of all, I would like to thank my advisor Dr. Petr Pecha for his patient guidance, support and inspiration.

I would also like to express my deepest gratitude to Dr. Václav Šmídl for his helpful suggestions and consultations. My special thanks go to Dr. Kamil Dedecius for being my colleague and a friend.

Last, but not least, I am very grateful to Andrea and my family for their love. It would have been impossible for me to go this far without their unconditional support and help.

Prague, April 2011

Radek Hofman

Financial support has been provided from the grants GAČR 02/07/1596, MŠMT 1M0572, and MVČR VG20102013018.

Abstract

The task of the decision support in the case of a radiation accident is to provide up-to-date information on the radiation situation, prognosis of its future evolution and possible consequences. The reliability of predictions can be significantly improved using data assimilation, which refers to a group of mathematical methods allowing an efficient combination of observed data with a numerical model. The dissertation concerns application of the advanced data assimilation methods in the field of radiation protection. We focus on assessment of off-site consequences in the case of a radiation accident when radionuclides are released into the environment.

The main contribution of this thesis is the development of sequential data assimilation methods for the early and the late phase of a radiation accident. Data assimilation is understood here as a particular case of recursive Bayesian estimation. Instead of using traditional estimation methods for state-space models based on Kalman filtering, we focused on sequential Monte Carlo methods, specifically particle filtering and marginalized particle filtering.

Firstly, data assimilation methodology for the early phase of an accident was developed. It employs particle filtering with adaptive selection of proposal density for estimation of the most important variables describing the aerial propagation of radionuclides. The general methodology is applicable to all parametrized atmospheric dispersion models. It is demonstrated on a simulated release, where a bias of the basic meteorological inputs and the source term is corrected using inference of gamma dose measurements.

Secondly, for the purpose of data assimilation in the late phase, we extended the idea of marginalized particle filtering to analytically intractable approximate filters, e.g. ensemble filters. The result is a hybrid data assimilation methodology, where multiple ensemble filters are run in parallel. The methodology was applied for joint estimation of the spatial distribution of deposition on terrain and estimation of the speed of radionuclides removal due to environmental processes in a simulated release scenario.

The proposed methodologies are implemented in an assimilation subsystem, which is a part of the decision support system HARP (HAzardous Radioactivity Propagation).

Contents

List of Figures	ix
List of Tables	xiii
Notational Conventions	xv
List of Acronyms	xix
1 Introduction	1
1.1 Motivation	1
1.2 Data Assimilation in Radiation Protection	2
1.3 State of the Art	3
1.3.1 Data Assimilation in the Early Phase	3
1.3.2 Data Assimilation in the Late Phase	5
1.3.3 Evaluation of Performance	6
1.4 Specific Goals of the Dissertation	6
1.5 Outline of the Dissertation	7
2 Physical Background	9
2.1 Atmospheric Dispersion Modeling	9
2.1.1 From Advection to Diffusion	9
2.1.2 Classifications of Air Pollution Models	11
2.1.3 Gaussian Models	14
2.2 Radiological Quantities	19
2.2.1 Radioactive Decay and Radioactivity	19
2.2.2 Calculation of Absorbed Doses	20
2.3 Developed Atmospheric Dispersion Model	23
2.3.1 Model Inputs and Outputs	23
2.3.2 Numerical Evaluation of Gaussian Puff Model under Variable Meteorological Conditions	24
2.3.3 Numerical Evaluation of Cloudshine Dose Rate	26

3	Data Assimilation	29
3.1	Introduction and Terminology	29
3.1.1	Data Assimilation Cycle	29
3.1.2	Identification of Data Assimilation with Bayesian Estimation	30
3.2	Recursive Bayesian Filtering	31
3.3	Kalman Filter	32
3.3.1	Suboptimal Solution for Nonlinear Model	34
3.4	Ensemble Filters	34
3.4.1	Ensemble Kalman Filter	34
3.4.2	Ensemble Square Root Filter	38
3.4.3	Sampling Error Issues in Ensemble Filtering	40
3.5	Particle Filter	42
3.5.1	Degeneracy Problem and Re-sampling	45
3.5.2	Choice of Proposal Density	47
3.5.3	Practical Evaluation of Weights	49
3.6	Marginalized Particle Filter	50
4	MPF Framework for Tuning of Ensemble Filters	53
4.1	Modification of MPF Algorithm for Suboptimal Conditional Filters	53
4.2	Estimation of Inflation Factor, Observation Error Variance, and Length-scale Parameter	54
4.3	Simulation Studies	56
4.3.1	Lorenz-96 Model	56
4.3.2	Stationary Parameters	56
4.3.3	Adaptive Estimation in Perfect Model Scenario	58
4.3.4	Model with Random Perturbations	60
4.4	Summary	61
5	Data Assimilation in the Early Phase	65
5.1	Problem Statement	65
5.2	Proposed Data Assimilation Methodology	66
5.2.1	State Evolution Model	66
5.2.2	Observation Operator	67
5.2.3	Data Assimilation Algorithm	67
5.2.4	Evaluation of Radiological Quantities of Interest	68
5.3	Application to Gaussian Puff Model	69
5.3.1	Parametrization of Gaussian Puff Model	69
5.3.2	Observation Operator	70
5.3.3	Evaluation of Weights	70
5.3.4	Adaptive Selection of Proposal Density	71
5.4	Numerical Experiment	71
5.4.1	Computational and Observational Grids	72
5.4.2	Simulation of Observations	73

5.4.3	Results	75
5.5	Summary	79
6	Data Assimilation in the Late Phase	81
6.1	Problem Statement	81
6.2	Data Assimilation Scenario	81
6.3	Proposed Data Assimilation Methodology	83
6.3.1	State Evolution Model	83
6.3.2	Observation Operator	84
6.3.3	Evaluation of Weights	85
6.4	Numerical Experiment	85
6.4.1	Computational and Observational Grids	86
6.4.2	Estimation of Prior Distribution of Deposition	86
6.4.3	Simulation of Observations	87
6.4.4	Selection of Prior Ensemble	89
6.4.5	Results	89
6.5	Summary	92
7	Developed Software	93
7.1	Visualization System	93
7.2	Preprocessor of Meteorological Data	93
7.3	Framework for Monte Carlo Sampling	95
8	Conclusion	97
8.1	Summary of Contributions	97
8.2	Future Research Directions	99
	Appendix A	101
	Appendix B	103
	Bibliography	105
	Index	113

List of Figures

2.1.1	Illustration of the Gaussian plume model.	14
2.1.2	Illustration of the principle used for modeling of the reflections as a superposition of multiple plumes released from virtual sources below the ground and above the top of mixing layer	18
2.2.1	Illustration of the relative decrease of groundshine dose from deposition of ^{134}Cs in time due to the radioactive decay and the environmental removal.	23
2.3.1	Illustration of numerical integration scheme of the Gaussian puff propagation. Between time steps t and $t + 1$, the puff is integrated forward in using elemental shifts k	25
3.1.1	Illustration of basic principle of sequential data assimilation.	30
3.4.1	Correlation function given by (3.4.21) with different values of the length-scale parameter l	42
3.4.2	Illustration of the effect of covariance localization; (a) contour plot of spatial covariance (without localization) of a point denoted with the red circle with the rest of the polar computational grid; (b)–(d) resulting covariance after application of the localization using localization matrices given by (3.4.21) with increasing value of the length-scale parameter l	43
3.5.1	Illustration of basic principle of re-sampling in PF. The piecewise-constant blue line denotes the cumulative weight $\sum_i w^{(i)}$ of $N = 10$ particles. The higher the weight $w^{(i)}$, the longer the interval I (3.5.17) and the higher the probability that random samples $u_i \sim \mathcal{U}[0, 1)$, denoted with dashed lines, are from I . Particle 1 was copied twice, particle 2 once, particle 5 for three times, particle 6 once, particle 8 twice and particle 10 once.	46
3.6.1	Illustration of a 2-dimensional state $\mathbf{x} = [x_1, x_2]^T$ estimated using MPF. Resulting joint estimate of the posterior pdf is in the linear-Gaussian part of the state, x_1 , estimated using the optimal Kalman filter and approximated using a particle filter in the non-linear and/or non-Gaussian part of the full state vector, x_2	52

4.3.1	Estimation of stationary parameters on rectangular grid. Top: marginal log-likelihood (4.3.2) of the tuned parameters Δ, l . Labels of the contour lines denote difference from the maximum which is marked by a circle. Bottom: Time average of RMSE (4.3.3).	58
4.3.2	Position of the particles $\Delta_t^{(i)}, l_t^{(i)}$ denoted by '+' on the background of stationary contours of marginal log-likelihood.	59
4.3.3	Estimation of system (4.3.5) with time-varying α_t of triangular profile displayed at the bottom. Posterior densities of the parameters are displayed via their mean value (blue line) and region between minimum and maximum value of the particles (gray area).	62
5.4.1	Illustration of computational grid and monitoring network.	72
5.4.2	Time integrated gamma dose evaluated for the first three hours of the release with the nominal model (left) and the twin model (right). . . .	75
5.4.3	Comparison of the nominal model, the twin model and the assimilated model in time steps $t = 6, 12, 18$. The misfit of the wind direction in the last hour is due to the lack of measurements in the area.	76
5.4.4	Estimated values of magnitude of release, wind speed and wind direction. Green lines: values used for simulation of measurements; red lines: estimated values of physical quantities; blue dots: values of particles with nonzero weights.	77
5.4.5	Estimated values of magnitude of release, wind speed and wind direction. Green lines: values used for simulation of measurements; red lines: estimated values; gray areas: regions between minimum and maximum values of the particles.	77
5.4.6	Time evolution of time integrated doses \mathcal{D}^c given by the twin model (blue solid lines), the nominal model (green solid lines), and the assimilated model (red dashed lines) at receptor locations 14, 15, 16, 27, 28, 29, 40 and 41 (see Table 5.1).	78
6.4.1	Illustration of computational and observational grids. We focus on the eastern half of the zone of emergency planning.	87
6.4.2	Left column: Visualization of initial deposition of the twin model $\mathbf{d}_0^{\text{twin}}$ (top) and of the initial ensemble mean (bottom). Right column: Interpolation of $\mathbf{d}_0^{\text{twin}}$ projected into the space of observations using (6.4.4) (top) and interpolation of the initial ensemble mean projected into the space of observations using (6.4.4) (bottom).	88
6.4.3	Weights of candidates $\mathbf{d}_0^{(i)}$ on members of initial ensemble.	89
6.4.4	Results for a selected observation location. Blue line: true deposition (twin model); green dots: measurements and their standard deviations; cyan dots: prior estimates (forecasts); gray area: standard deviation of the forecast error; red dots: posterior estimates.	90

6.4.5 Visualization of assimilation results in time steps 0, 8, 16, and 24. Nominal model (prior mean), twin model (measurements) and assimilated model (posterior mean) are in first, second and third column, respectively. Color scale is the same as in Figure 6.4.2.	91
7.2.1 Spatial data visualization system. Visualization of a simulated release from the Czech NPP Temelin.	94
7.2.2 Meteorological data preprocessor. Visualization of a sample wind field describing the flow in vicinity of the Czech NPP Dukovany. HIRMAL data on the red rectangular grid is interpolated into the points of the green polar grid used by the HARP system.	94
7.2.3 A diagram of the Monte Carlo framework for repetitive evaluation of dispersion models.	95
7.3.1 Example of a graphical output from the system. Background: visualization of expected spatial distribution of total committed dose for adults based on a sample two-year meteorological sequence (17520 hourly releases). Foreground: histogram representing distribution of committed doses in the highlighted point close to the source.	96

List of Tables

1.1	Summary of the key properties of the early and the late phase of radiation accident.	4
2.1	Discretization of parameters for evaluation of pre-calculated values of gamma dose rate from a radionuclide ^{41}Ar dispersed in air.	26
4.1	Best stationary choices of nuisance parameters for EnSRF according to two criteria.	57
4.2	Adaptive tuning of $\mathbf{x}_t^p = [\Delta_t, l_t]^T$ and the resulting analysis RMSE error, averaged over assimilation steps between $t = 1000$ and $t = 100000$, std denotes standard deviation of the estimates from the mean over time.	60
4.3	Adaptive tuning of $\mathbf{x}_t^p = [\Delta_t, r_t, l_t]^T$ and the resulting analysis RMSE error, averaged over assimilation steps between $t = 1000$ and $t = 100000$, std denotes standard deviation of the estimates from the mean over time.	60
4.4	Adaptive tuning of $\mathbf{x}_t^p = [\Delta_t, l_t, r_t]^T$ for system with random model errors (4.3.5) with variance $\alpha = 4$. The resulting analysis RMSE error is averaged over assimilation steps between $t = 1000$ and $t = 100000$, time averages of parameter estimates are displayed in tandem with standard deviation of the estimates from the mean over time. Both algorithms were run with $N = 10$ and $\overline{N_{\text{eff}}} = 0.8N$	61
5.1	Coordinates of the receptors comprising radiation monitoring network in the numerical example.	73
5.2	Parameters of nominal and twin model. Nominal values $Q^{i,*}, u_t^*, \phi_t^*$ of physical quantities treated as uncertain. “Real” values $Q^{i,r}, u_t^r, \phi_t^r$ of the quantities used for simulation of measurements. Sought values of variables $\boldsymbol{\theta}_t^r = (\omega_1^r, \xi_t^r, \psi_t^r)$ transforming the nominal values into the real values using parameterizations (5.3.1)–(5.3.3).	74
6.1	Parameters treated as uncertain during Monte Carlo sampling of candidates on ensemble members.	87
6.2	Comparison of “true” parameters used for simulation of measurements with those estimated using the data assimilation procedure.	92

Notational Conventions

Operators, intervals	
\equiv	equivalence by definition
\propto	proportionality, equivalence up to a constant factor
\int_{Ω}	integration over set Ω
$\sum_{i=a}^b$	summation over indices $i = a, \dots, b$
\circ	Schur (element-wise) matrix product
$\langle a, b \rangle$	closed interval from a to b
(a, b)	open interval from a to b
$(a, b), \langle a, b \rangle$	left-open and right-open intervals from a to b , respectively
Algebraic notation	
\mathbb{R}	set of real numbers
\mathbb{R}^+	set of positive real numbers
\mathbb{N}	set of natural numbers
$a \in \mathbb{R}$	scalar value
$\mathbf{A} \in \mathbb{R}^{m \times n}$	matrix of dimension $m \times n$
$\mathbf{a} \in \mathbb{R}^n$	column vector of length n
$\mathbf{I} \in \mathbb{R}^{n \times n}$	identity matrix of dimension $n \times n$
$\mathbf{A}[i, j]$	element of matrix \mathbf{A} in i th row and j th column
$\mathbf{a}[i]$	i th element of column vector \mathbf{a}
\mathbf{A}^T	transpose of matrix \mathbf{A}
$\det \mathbf{A}$	determinant of matrix \mathbf{A}
$\ \cdot\ $	Euclidean norm
Probability and statistical modeling	
$\mathbb{E}[\cdot]$	expected value of argument \cdot
$p(\mathbf{a} \mathbf{b})$	probability density function determined by its argument \mathbf{a} conditioned on \mathbf{b}
$\Pr(\cdot)$	probability of argument \cdot
$\mathcal{N}(\mu, \sigma^2)$	Gaussian (normal) distribution with mean value μ and variance σ^2
$\mathcal{N}(\boldsymbol{\mu}, \boldsymbol{\Sigma})$	multidimensional Gaussian (normal) distribution with mean value $\boldsymbol{\mu}$ and covariance matrix $\boldsymbol{\Sigma}$

Probability and statistical modeling - continued	
$t\mathcal{N}(\mu, \sigma^2, (a, b))$	Gaussian distribution with mean value μ and variance σ^2 truncated on interval (a, b)
$\log\mathcal{N}(\mu, \sigma^2)$	log-normal distribution with mean value μ and variance σ^2
$\mathcal{U}(a, b)$	uniform distribution on interval $\langle a, b \rangle$
$\delta(x)$	Dirac δ -distribution
$\mathbf{x}_{i:j} = [x_i, \dots, x_j]$	ordered set of variables $x_k, k = i, \dots, j$
Atmospheric dispersion modeling	
C	(activity) concentration in air
\bar{C}	mean value of concentration over time
C'	stochastic fluctuation of concentration
$\mathbf{u} = (u_1, u_2, u_3)$	wind vector with components u_1, u_2, u_3
$\bar{\mathbf{u}}$	mean value of wind speed components over time
\mathbf{u}'	stochastic fluctuation of wind speed components
$\mathbf{s} = (s_1, s_2, s_3)$	spatial location in 3-dimensional space with coordinated s_1, s_2, s_3
$\mathbf{s}^R = (s_1^R, s_2^R, s_3^R)$	coordinates of receptor R
$\mathbf{s}^P = (s_1^P, s_2^P, s_3^P)$	coordinates of center of Gaussian puff P
K_1, K_2, K_3	eddy diffusivity coefficients in directions s_1, s_2, s_3
$\sigma_1, \sigma_2, \sigma_3$	dispersion coefficients of Gaussian puff in directions s_1, s_2, s_3
Q^i	magnitude of release from instantaneous source of pollution
H	height of release
H_{ef}	effective height of release
H_{mix}	height of mixing layer
Radiological quantities and modeling	
A	activity of a radionuclide
λ	radionuclide-dependent radioactive decay constant
$T_{1/2}$	radionuclide-dependent physical half-life
E	energy of gamma decay of a radionuclide
Φ	effective flux of gamma rays
B	build-up factor
μ_a	absorption coefficient
μ	linear attenuation coefficient
ρ	density of air
K	dose conversion coefficient
$D_c(\mathbf{s}^R)$	gamma dose rate from cloudshine at receptor R
$\mathcal{D}_c(\mathbf{s}^R, \tau_1, \tau_2)$	gamma dose rate from cloudshine at receptor R integrated over time interval (τ_1, τ_2)
$D_g(\mathbf{s}^R)$	gamma dose rate from groundshine at receptor R

Radiological quantities and modeling - continued

DF_g	radionuclide-dependent integrated dose rate conversion factor for groundshine
SF	shielding factor
SD	spatial deposition
f_R	factor of radioactive decay
f_E	factor of environmental removal
d^f	fraction of fast component of environmental removal
T^f	half-life of fast component of environmental removal
d^s	fraction of slow component of environmental removal
T^s	half-life of slow component of environmental removal

Bayesian filtering

\mathcal{M}_t	nonlinear state evolution operator
\mathcal{H}_t	nonlinear observation operator
\mathbf{M}_t	matrix of linear state evolution operator
\mathbf{H}_t	matrix of linear observation operator
$\bar{\mathbf{x}}_{t t-1}$	prior state estimate (prior ensemble sample mean)
$\bar{\mathbf{x}}_{t t}$	posterior state estimate (posterior ensemble sample mean)
$\mathbf{P}_{t t-1} = \mathbf{S}_{t t-1} \mathbf{S}_{t t-1}^T$	prior forecast error covariance matrix (prior ensemble sample covariance)
$\mathbf{P}_{t t} = \mathbf{S}_{t t} \mathbf{S}_{t t}^T$	posterior forecast error covariance matrix (posterior ensemble sample covariance)
\mathbf{R}_t	observation error covariance matrix
\mathbf{Q}_t	state evolution model error
\mathbf{K}_t	Kalman gain
$\mathbf{X}_{t t-1} = [\mathbf{x}_{t t-1}^1, \dots, \mathbf{x}_{t t-1}^M]$	prior ensemble
$\mathbf{X}_{t t} = [\mathbf{x}_{t t}^1, \dots, \mathbf{x}_{t t}^M]$	posterior ensemble
$\tilde{\mathbf{X}}_t = [\tilde{\mathbf{x}}_t^1, \dots, \tilde{\mathbf{x}}_t^M]$	deviations of ensemble members from ensemble mean
$\tilde{\mathbf{K}}_t$	Kalman gain for update of deviations from ensemble mean
$\mathbf{D}_t = [\mathbf{y}_t^1, \dots, \mathbf{y}_t^M]$	ensemble of perturbed observation vectors
$\mathbf{x}^{(i)}$	i th particle
$w^{(i)}$	normalized weight of i th particle
$\tilde{w}^{(i)}$	weight of i th particle before normalization
$\ln \tilde{w}^{(i)}$	weight of i th particle before normalization in logarithmic scale
M	ensemble size
N	number of particles
$\Psi_{a \times b}$	matrix of all ones of dimension $a \times b$
Δ	multiplicative inflation factor
ρ	covariance localization matrix
l	length-scale of localization function
$\overline{N_{\text{eff}}}$	estimate of effective number of particles

Data assimilation in the early phase and the late phase

θ_t	vector of parameters (control variables)
η_t	immutable control variables
ν_t	mutable control variables
\mathcal{S}_t^R	set of receptor locations
\mathcal{S}_t	set of computational grid-points
τ	continuous time
Δ_τ	length of time step
ω_1	control variable parameterizing magnitude of release
ξ_t	control variable parameterizing wind speed
ψ_t	control variable parameterizing wind direction
Q^i	magnitude of release
u_t	wind speed
ϕ_t	wind direction
$Q^{i,*}, u_t^*, \phi_t^*$	nominal values of control variables (location parameters)
$Q^{i,r}, u_t^r, \phi_t^r$	“true” values of control variables used for evaluation of twin model

List of Acronyms

ADM	Atmospheric Dispersion Model
EKF	Extended Kalman Filter
EnKF	Ensemble Kalma Filter
HARP	HAzardous Radioactivity Propagation
HIRLAM	HIgh Resolution Limited Area Model
IAEA	International Atomic Energy Agency
KF	Kalman Filter
MPF	Marginalized Particle Filter
NPP	Nuclear Power Plant
OSCAAR	Off-Site Consequence Analysis code for Atmospheric Releases in reactor accidents
PF	Particle Filter
RIMPUFF	RIIsø Mesoscale PUFF model
RODOS	Real-time Online DecisiOn Support system for nuclear emergency management
RMSE	Root Mean Square Error
SIR	Sampling Importance Re-sampling
SIS	Sampling Importance Sampling
TDS	Tele-Dosimetric System
UKF	Unscented Kalman Filter
UTM	Universal Transverse Mercator
i.i.d.	independent, identically distributed (random variable)
pdf	probability density function

Chapter 1

Introduction

1.1 Motivation

On June 27, 1954, the USSR's Obninsk Nuclear Power Plant (NPP) became the world's first nuclear power plant to generate electricity for a power grid, and produced around 5 megawatts of electric power. Nowadays, there are more than 400 nuclear power reactors in operation worldwide with the total share of 15% of produced electricity (Lillington, 2004). Although the old-fashioned reactors are replaced by the modern ones satisfying strict safety criteria, there is still a potential for failures due to malfunctions, natural disasters or man-made errors. This can result in a release of radioactive substances into the environment (Saji, 2003).

In the case of a radiation accident, the risk evaluation and the decision-making process focused on protecting the public have the highest priority. The task of the decision support is to provide reliable and up-to-date information on the radiation situation, prognosis of its future evolution and possible consequences. Knowledge of spatial distribution of radionuclides and prediction of the future evolution are essential for planning of effective countermeasures. Historically, accidents in nuclear facilities have revealed unsatisfactory level of preparedness and lack of adequate modeling tools. Great attention has been paid to this topic since the Chernobyl disaster (Onishi et al., 2007). Nowadays, decision makers dispose of complex computer systems intended to provide assistance to them throughout various phases of the accident, e.g., (Päsler-Sauer, 2000; Pecha et al., 2007; Thykier-Nielsen et al., 1999).

During the last decades, a great progress has been made in our understanding the atmospheric dispersion and related natural phenomena. Despite all the effort, the stochastic nature of involved physical processes, the deficiencies in their mathematical conceptualization and particularly ignorance of the initial conditions prevent obtaining of accurate results. The only way how to attain satisfactory accuracy of the model forecasts is exploitation of observational data, which represent the only connection with the physical reality. Observations are often sparse in both time and space and it is not possible to get a complete picture of radiological situation based on monitoring data alone, especially during the first hours after the accident.

Data assimilation provides a framework for optimal combination of numerical model predictions and the available observational data (Kalnay, 2003). It makes possible to consistently account for uncertainties in the model, its inputs and observations, and produces probabilistic answers which are more informative than those deterministic. Data assimilation is a compromise between the pure modeling approach on one hand and the data mining approach on the other hand. Nowadays, data assimilation arise in many scientific areas. The main fields of its application are meteorology, oceanography and hydrology (Park and Xu, 2009; Wang et al., 2000). This work addresses the problem of exploitation of advanced data assimilation methods in the field of radiation protection.

1.2 Data Assimilation in Radiation Protection

We are concerned with application of data assimilation in the case of a severe radiation accident, when an accidental release of radionuclides into the environment occurred and it is likely to require at least partial implementation of countermeasures. The main objective of data assimilation is to estimate the true scale of the accident and predict its consequences in order to improve reliability of the decision support through different phases of the accident.

The time tract of an accidental release of radionuclides can be formally split into two consecutive phases:

Early phase begins when the radionuclides are released into the environment. We focus on atmospheric releases, when the effluent forms a radioactive plume advected by the wind field and dispersed by turbulent processes. The plume causes external irradiation from *cloudshine* and internal irradiation due to inhalation. Duration of this phase is from a few hours up to several days and let it formally ends when the plume leaves the area of interest. The main objectives of data assimilation in the early phase are (i) on-line estimation of radiation situation and its evolution and (ii) estimation of committed population doses.

Late phase covers latter stages of the accident and immediately follows after the early phase. After the plume passage, there is no more irradiation due to cloudshine, however, on the ground remains deposited radioactive material. It causes external irradiation from *groundshine* and internal irradiation from inhalation due to resuspension and ingestion. This phase ends when radiation levels resume to background values. The main objectives of data assimilation in the late phase are (i) identification of contaminated areas and (ii) estimation of radiation levels and the speed of the radionuclides removal for purposes of long-term forecasting. The estimates enter subsequent models of radionuclides propagation through the different compartments of the environment.

Data assimilation is potentially applicable in both phases, however, different physical processes, time scales etc., determine specific requirements on assimilation inputs and

target fields of predictions. The key properties of the early and the late phase are summarized in Table 1.1.

1.3 State of the Art

1.3.1 Data Assimilation in the Early Phase

Particular data assimilation algorithm for the early phase must be constructed for a given class of atmospheric dispersion models.

Assimilation of Lagrangian Particle Models

Lagrangian particle model is a Monte Carlo dispersion model, where the spreading of pollutants is simulated using a large number of particles released from the source, each of them carrying some elemental activity. Trajectories of particles are given by a meteorological forecast entering the model. Random perturbations are added to the wind speed of the particles in order to simulate stochastic turbulent processes in the atmosphere. In this model, the three-dimensional space is divided into partial volumes. At each time step, movement of all the particles is traced and the activity concentration in each partial volume is obtained by summing up the activity assigned to particles within the volume. When a new set of observations is available, the assimilation procedure is performed as a modification of the number of particles in the partial volumes, e.g. (Zheng et al., 2007). Between consecutive measurement updates, the redistributed particles are propagated forward in time by the meteorological forcing.

The advantage of Lagrangian models is their capability to account for many physical processes in a natural way. Their application in data assimilation allows for local assimilation of the activity concentrations and thus the results better consider local variations in terrain, meteorology etc. The disadvantage is the fact, that a large number of particle trajectories must be computed to simulate a release using this type of model. Such an assimilation algorithm based on this approach model must be run on a supercomputer in order to meet the strict time constraints in the early phase.

Assimilation of Parameterized Models

A substantial reduction of the computational complexity can be reached by the use of a deterministic model parametrized by a set of control variables. The term *control variables* refers to a selected subset of inputs to the model and parameters influencing its result. The set is selected using the uncertainty and sensitivity studies performed with dispersion models, (Eleveld et al., 2007; Rao, 2005; Twenhöfel et al., 2007). Given some particular values of control variables, concentration in air is calculated simply by evaluation of the model as a deterministic function of the variables. Contrary to Lagrangian particle models, direct assimilation of concentration values in the grid points is not possible with these models. Modification of the analytical shape of the plume

PHASES OF REACTOR ACCIDENT		
Property	Early phase	Late phase
Duration	This phase starts when the radionuclides are released into the environment and lasts from few hours to days until the plume leaves the area of interest	The phase begins immediately after the early phase and lasts until the radiation levels resume to background values (years)
Pathways of irradiation	(i) External irradiation from the cloud and the deposition (ii) Internal irradiation from inhalation	(i) External irradiation from deposition (ii) Internal irradiation from ingestion and inhalation of resuspended material
Typical countermeasures	Iodine prophylaxis, sheltering, evacuation	Food bans, relocation, amelioration (liming, fertilization) and decontamination of selected areas (ploughing, soil removal)
Possible sources of observations	(i) Radiation monitoring network (ii) Airborne and ground-based mobile groups	(i) Thermoluminescent dosimetry network (ii) Airborne and ground-based mobile groups (iii) Laboratory analysis, monitoring
Main objectives of data assimilation in this phase	(i) On-line (step-wise) estimation of the affected area and committed doses. (ii) Determination of source term, correction of meteorological and other inputs	(i) Identification of contaminated area and radiation levels (ii) Estimation of the speed of the radionuclides removal for purposes of long-term forecasting

Table 1.1: Summary of the key properties of the early and the late phase of radiation accident.

would forbid its propagation in the next time step. Data assimilation is then formulated as an optimization of the control variables in order to reach the best correspondence of model forecast with available observations. These estimates may in turn re-enter atmospheric dispersion models, resulting in a greatly improved dose rate assessment. Parameters not included in the set of control variables are not treated as uncertain but they are initialized with a fixed value.

The most simple methods for optimization of the control variables are not probabilistic and minimize just a loss function measuring point-wise distance between model and observations. Eleveld et al. (2007) presented a simple assimilation scheme for tuning of the effective release height and the wind direction of the Gaussian plume model. This idea is more developed in (Pecha and Hofman, 2008), where a segmented version of the Gaussian plume model (Hofman et al., 2008) is used and the set of optimized control variables is extended to address their time variability. The advantage of this method is its simplicity and a potential for extension of the set of optimized control variables. The disadvantage is the fact that the method does not consider error statistics of the model and observations, contrary to variational methods, where the difference between the model forecast and the observations is weighted with appropriate error statistics. Assimilation schemes based on variational approach are described in (Jeong et al., 2005; Kovalets et al., 2009; Quelo et al., 2005). Here, all the optimized control variables are treated as time invariant.

More advanced methods are based on sequential data assimilation. Drews et al. (2005) described extended Kalman filtering of the Gaussian plume. Here, the set of optimized control variables is restricted to the ratio of the release rate and the wind speed, the wind direction and the plume height. Similar assimilation scheme is proposed in (Astrup et al., 2004) describing assimilation of the RIMPUFF model (Thykier-Nielsen et al., 1999). A continuous release is with the RIMPUFF (RIsø Mesoscale PUFF) model approximated by a sequence of overlapping puffs. This allows inclusion of complex meteorological and other local characteristics. Control variables are radioactive inventories of partial puffs and the wind direction affecting spatial positions of the puffs within the computation domain. The number of control variables changes dynamically as new puffs are released and other puffs leave the domain. This assimilation methodology for the early phase is implemented in the RODOS (Real-time Online Decision Support System for nuclear emergency management), (Palma et al., 2003).

1.3.2 Data Assimilation in the Late Phase

The basic aspects of modeling and assimilation in the late phase are formulated in (Gering et al., 2004). Modeling in the late phase covers a broad range of disciplines focusing on different problems, e.g., contamination of arable soil and urban areas, contamination of water resources, propagation of radionuclides in the food chain, etc. In (Yuschenko et al., 2005), the method *iterations to optimal solution* is applied for assimilation of an aquatic model with observations of the Black Sea contamination after the Chernobyl accident. The details regarding this simple empirical interpolation method can be found

in (Daley, 1993).

In (Palma, 2005), the ensemble Kalman filtering (EnKF) based data assimilation system for assimilation of the groundshine measurements with a radio-ecological model is described. The system is a part of the RODOS. EnKF introduced by Evensen (1994) is proposed here as the most promising approach for data assimilation in the late phase.

1.3.3 Evaluation of Performance

The performance assessment of data assimilation methods is in the field of radiation protection problematic. The dispersion modeling of radioactive pollutants has its specific properties and the existing data sets from experiments with non-radioactive pollutants are not suitable. Since there is a lack of observational data sets from the real reactor accidents, the measurements used for validation of data assimilation methods are simulated using the *twin experiments* (Eleveld et al., 2007). It means, that the measurements are generated using a model of the system under investigation, initialized by some reference values. Observations are sampled from the model output fields in locations of the receptor points. From the theoretic point of view, the twin experiments are useful, because they make possible to evaluate assimilation performance against a known “background truth” and the convergence can be easily assessed. The method also provides a transparent tool for controlling of measurement error type and magnitude.

1.4 Specific Goals of the Dissertation

The contributions of this dissertation are presented in three separate parts. The first part concerns development of the marginalized particle framework for analytically intractable filters. The second and the third parts are devoted to the application of particle filtering and marginalized particle filtering in the early and the late phase, respectively. Specific goals of respective parts are discussed below.

The main contributions of the first part presented in Chapter 4 are as follows:

- The extension of marginalized particle filtering on analytically intractable approximative filters and formulation of a framework for on-line tuning of ensemble filters resulting in a hybrid data assimilation method.
- The comparison of the new adaptive method with the “best tuned” ensemble filters on data assimilation scenarios with 40-variable Lorenz-96 model.

The main contributions of the second part presented in Chapter 5 are as follows:

- The formulation of a new data assimilation methodology for estimation of selected control variables of a parametrized atmospheric dispersion model in the Bayesian framework using particle filtering.

- The implementation of the Gaussian puff model and the nonlinear observation operator transforming the activity concentration in air into the time integrated gamma dose rate.
- The demonstration of the assimilation algorithm resulting from the new methodology on a simulated release scenario. The source term, the wind speed, and the wind direction of the Gaussian puff model are estimated using the time integrated gamma dose rate measurements.

The main contributions of the third part presented in Chapter 6 are as follows:

- The formulation of a new data assimilation methodology for the late phase in the Bayesian framework and exploiting the extension of marginalized particle filtering presented in Chapter 4.
- The implementation of the groundshine dose evolution model and the observation operator for spatial interpolation of the deposition fields.
- The demonstration of the developed assimilation algorithm resulting from the new methodology on a simulated release scenario. Spatial distribution of the deposition on terrain is estimated together with the speed of radionuclides removal.

1.5 Outline of the Dissertation

The work is organized as follows: Chapter 2.1 gives a brief review of atmospheric dispersion modeling and relations between the basic radiological quantities. The atmospheric dispersion model developed in this work is presented here. Chapter 3 describes the theory of sequential data assimilation and puts it into context of Bayesian filtering. A new method for tuning of ensemble filters is described in Chapter 4. Chapters 5 and 6 concern the proposed assimilation methodology for the early and the late phase, respectively. A brief review of developed software is given in Chapter 7. Conclusion and future research direction are given in Chapter 8.

Chapter 2

Physical Background

2.1 Atmospheric Dispersion Modeling

Atmospheric dispersion modeling is the mathematical simulation of how air pollutants disperse in the ambient atmosphere. Dispersion models are computer codes solving equations describing the propagation of pollutants given the initial conditions, i.e., the meteorological conditions (wind speed and direction, precipitation) and the process conditions (heat capacity of the plume, terrain roughness, etc.) prevailing in the atmospheric boundary layer. Output from such a dispersion model is a 3-dimensional field of pollutant concentration in air. In the case of radioactive pollutants, the output is given in terms of activity concentration in air [$Bq\ m^{-3}$].

Atmospheric dispersion models are basic tools for decision makers when assessing the atmospheric radionuclide releases. The models predict concentration of pollutants in the downwind directions from the source. Combined with the information on demography, the models can estimate expected exposure of population to ionizing radiation, and consequently, the health effects in terms of total committed doses. Nowadays, there exist various approaches to atmospheric dispersion modeling.

2.1.1 From Advection to Diffusion

In the following text in this chapter, the subscript i iterates over the set $\{1, 2, 3\}$ denoting the three spatial coordinates.

Following Barratt (2001), let us assume a release of a material into the atmosphere. If no chemical reactions and molecular diffusion are assumed, the concentration of material, C , resulting from the release is given by the advection equation

$$\frac{\partial C}{\partial \tau} + \frac{\partial}{\partial s_i} (u_i C) = 0, \quad (2.1.1)$$

where $\mathbf{u} = (u_1, u_2, u_3)$ are the wind speed components in directions $\mathbf{s} = (s_1, s_2, s_3)$ and $C = C(\mathbf{s}, \tau)$ is a function describing concentration of the pollutant in space and time. As the actual wind speed is not known and it can not be incorporated into the

equation, we assume that the wind speed at a certain time can be described according to the scheme

$$u_i = \bar{u}_i + u'_i, \quad (2.1.2)$$

where \bar{u} is the mean wind speed during a time period and the second term u' stands for a stochastic component, fluctuation of the wind due to the momentary turbulence. This scheme implies also fluctuation of the concentration

$$C = \bar{C} + C', \quad (2.1.3)$$

where \bar{C} is the concentration taken over a time period and C' is a stochastic fluctuation. The stochastic fluctuation terms are assumed to have zero mean values

$$\bar{C}' = 0, \quad \bar{u}'_i = 0. \quad (2.1.4)$$

Substituting (2.1.2, 2.1.3) into (2.1.1) yields

$$\frac{\partial C}{\partial \tau} + \frac{\partial}{\partial s_i} [(\bar{u}_i + u'_i)(\bar{C} + C')] = 0. \quad (2.1.5)$$

Exploiting linearity of the differentiation operator $\partial/\partial s_i$ and averaging over time yields

$$\frac{\partial \bar{C}}{\partial \tau} + \frac{\partial}{\partial s_i} (\bar{u}_i \bar{C}) + \frac{\partial}{\partial s_i} (\overline{u'_i C'}) = 0, \quad (2.1.6)$$

where the terms $\overline{u'_i C'}$ and $\bar{C}' u'_i$ are zero due to (2.1.4).

To describe the mean stochastic turbulent flux term $\overline{u'_i C'}$, we introduce the eddy diffusivity coefficients K_i . Turbulent *diffusion* is a diffusion process by which substances are mixed in the atmosphere or in any fluid system due to eddy motion. As the turbulent fluxes $\overline{u'_i C'}$ can be measured only with fast-response instruments and it is difficult to treat them theoretically by analogy with the molecular case, the turbulent flux is commonly assumed to be directly proportional to the mean gradient

$$\overline{u'_i C'} = -K_i \frac{\partial \bar{C}}{\partial s_i}, \quad (2.1.7)$$

where K_i are *diffusivity coefficients* in units $m^2 s^{-1}$. The negative sign is included so that the flux is down the gradient, i.e., from the high values of C to the low values. The mean wind components and the mean concentration represent average values over the time scale T_a and the corresponding spatial scale s_a . Typical values of T_a are a few minutes in magnitude. Fluctuation in smaller scales is assumed to be turbulent and is included in K_i . Substituting (2.1.7) into (2.1.6) gives

$$\frac{\partial \bar{C}}{\partial \tau} + \frac{\partial}{\partial s_i} (\bar{u}_i \bar{C}) = \frac{\partial}{\partial s_i} \left(K_i \frac{\partial \bar{C}}{\partial s_i} \right). \quad (2.1.8)$$

Expanding the second term on the left side of (2.1.8) and assuming that the atmosphere is incompressible,

$$\frac{\partial u_1}{\partial s_1} + \frac{\partial u_2}{\partial s_2} + \frac{\partial u_3}{\partial s_3} = 0,$$

the second term on the left side of (2.1.8) vanishes and we obtain the *advection-diffusion equation*

$$\frac{\partial \bar{C}}{\partial \tau} + \bar{u}_i \frac{\partial \bar{C}}{\partial s_i} = \frac{\partial}{\partial s_i} \left(K_i \frac{\partial \bar{C}}{\partial s_i} \right). \quad (2.1.9)$$

It describes the relationship between the spatial and the temporal behavior of concentration. When combined with appropriate initial conditions and boundary conditions, this equation forms the basis for the dispersion modeling and may be solved for various scenarios. In this equation, both the pollution transport by the advection and the diffusion due to the atmospheric turbulence are represented. However, (2.1.9) is not possible to solve analytically for completely general functional forms for the diffusivity coefficients K_i and the wind speed components u_i .

2.1.2 Classifications of Air Pollution Models

Models vary considerably in their complexity, and may take account of different physical and chemical processes affecting the flow and transport. Different mathematical expressions can be derived to represent these atmospheric processes. Consequently, there is an enormous range of available atmospheric dispersion models. Comprehensive review of atmospheric dispersion methodology is given, e.g. by Holmes and Morawska (2006).

Box Models

This is a simple model, largely based on the concepts of conservation of mass and conservation of energy. The treatment of transport is simplified, but the model is capable to include complex chemistry. The model evaluates mass balance of a given system using the conservation laws, where the particles of pollutant are transferred from one domain of the environment to another. Inside a domain, the air mass is assumed to be well mixed and concentration of the pollutant is assumed to be homogeneous. Boundaries of the domains are boxes. For every pollutant, we can write the mass balance equation:

$$\text{Input rate} = \text{Output rate} + \text{Transformation rate} + \text{Accumulation rate}$$

Depending on the physical and chemical interactions, some of the pollutants may pass through the system unchanged, some may accumulate within the system, while some may undergo chemical transformation or radioactive decay.

The simplicity of the model implies that it requires simple meteorological inputs and simple parametrization of the emission source. As it provides area-wide averages of concentration for a given region, the box model is a useful tool for screening purposes, where we need quick answers without any stress on accuracy. However, well-mixed and homogeneous conditions are sometimes unrealistic and the box models should not be used to calculate concentration in large areas, where the local changes must be reflected. For more detailed modeling we need more complex models continuously tracking the plume through the environment as it is advected by the wind, spread by diffusion, mixed by turbulence and reflected or channeled by surfaces such as the ground and the buildings (Barratt, 2001).

Lagrangian and Eulerian Models

Both the *Lagrangian* and the *Eulerian* models solve the same advection-diffusion equation. The difference between Lagrangian and Eulerian approach to modeling consists in the different treatment of the frame of reference. The Lagrangian approach is based on studying the property of a particular fluid by following its trajectory. Lagrangian models are similar to the box models, where the region of air containing an initial concentration of pollutants is considered as a box (Gurjar, 2008). The box is considered to be advected with the flow and the model follows the trajectory of the box. It is said that an observer of a Lagrangian model follows along with the plume. The motion of air parcels is modeled as a superposition of the mean wind speed and a random perturbations simulating chaotic nature of the atmosphere. It is a random walk process indeed. Concentration in the Lagrangian models is evaluated in partial volumes (boxes) forming a 3-dimensional grid. Average concentration in a given grid cell is evaluated in a way that we sum up all the elemental concentrations associated with the particles in the cell. The main advantage of Lagrangian models is the capability to account for many physical processes in a natural way. They work well both for homogeneous and stationary conditions over the flat terrain and for inhomogeneous and unstable media conditions for the complex terrain. Particle dispersion model is an example of practical implementation of a Lagrangian model (Zheng et al., 2007).

In Eulerian modeling, we also track the movement of a hypothetical parcel of air, but we use a fixed frame of reference. The Eulerian approach is based on studying fluid property in a control volume at a fixed point in space, that is, the control volume is stationary and fluid moves through the control volume (Gurjar, 2008). It is said that an observer of an Eulerian model watches the plume go by. Eulerian models use 2-dimensional and 3-dimensional grids for solving the differential equations, e.g. (2.1.9), where diffusion, transport, and removal of pollutant emission is simulated in each cell.

Gaussian Models

Gaussian models are widely used in atmospheric dispersion modeling, and are often “nested” within Lagrangian and Eulerian models. They are based on a Gaussian dis-

tribution of concentration in the plume in vertical and horizontal directions under the steady state conditions (Zannetti, 1990; Holmes and Morawska, 2006). Gaussian models are popular, particularly for the following reasons:

- The Gaussian models represent a solution of (2.1.9) under some simplifying assumptions (e.g., constant wind and eddy diffusivity coefficients) and they are consistent with the random nature of the turbulence.
- Their simplicity allows for fast evaluation even with small computational resources. This is an essential property when we attempt to employ assimilation techniques based on Monte Carlo approach, when the model must be repeatedly run for many times.
- The analytical form of the Gaussian models allows for a good insight and a transparent evaluation of experimental results.
- The Gaussian models are easy to implement and they can be embedded into various forecasting and assimilation systems.
- Validity of the Gaussian models was satisfactorily verified for different meteorological conditions via comparison to the results of field tests with tracer releases, when the agreement of measured and modeled concentration was assessed, e.g. (Carruthers et al., 1995).

Gaussian models are not designed to model dispersion under low wind conditions or at sites close to the source, i.e., at distances closer than 100m. It was found that these models over-predict concentrations in low wind conditions (Hanna et al., 1982).

Gaussian models—in their basic form—assume just the diffusion and advection of the pollutants. Modified versions of the Gaussian models are capable to include physical processes such as dry and wet deposition and radioactive decay (Hofman et al., 2008). We can distinguish two main variants of the Gaussian models. The *Gaussian plume model* assumes a continuous release when a plume in the downwind direction is formed under stationary conditions. The *Gaussian puff model* assumes a sudden instantaneous release when an expanding puff is formed.

Computational Fluid Dynamics Models

Computational fluid dynamics models are able to deal with the fluid flux in a complex geometry by solving the Navier-Stokes equation and the continuity equation when the flow is idealized as a laminar flow (Gurjar, 2008). These two equations can be solved simultaneously using finite difference or finite volume methods. If the flow is turbulent, the Reynolds Navier-Stokes equation with the continuity and turbulence closure models is used for this case (Tennekes and Lumley, 1972).

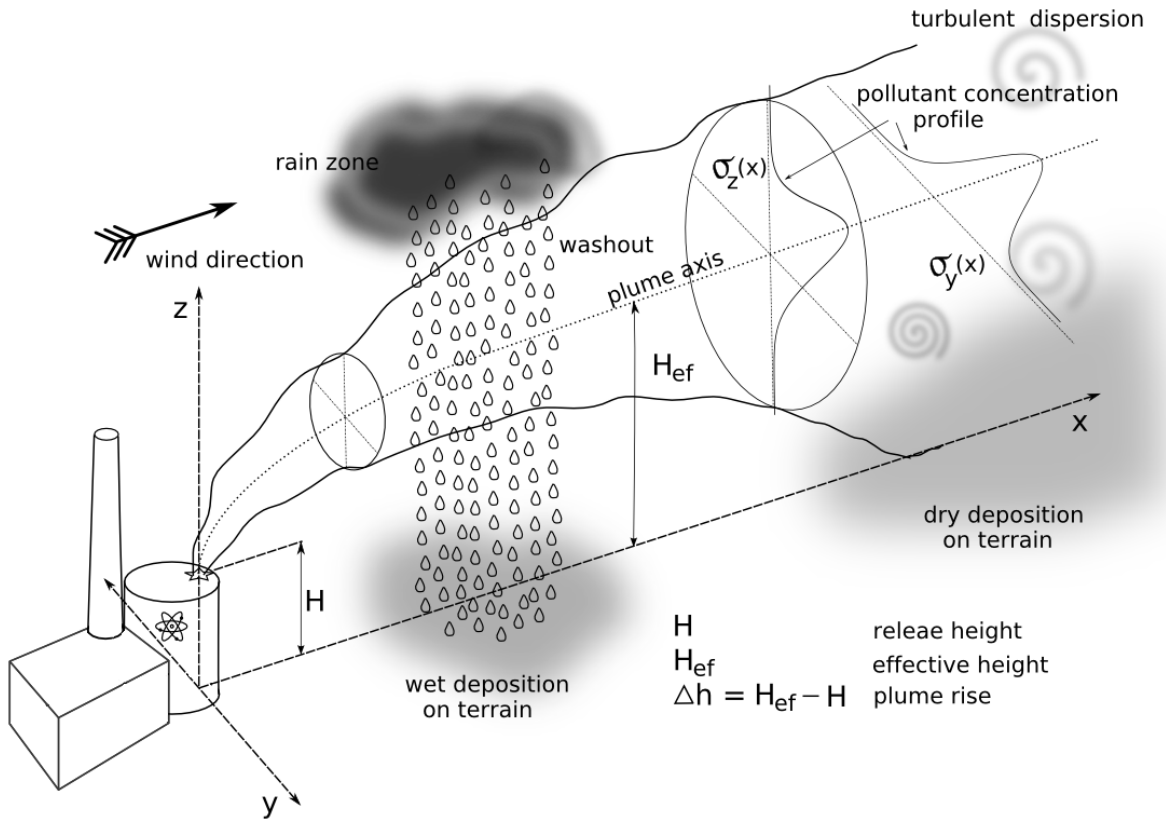


Figure 2.1.1: Illustration of the Gaussian plume model.

Summary

In this work, we focus on parametrized Gaussian models which are discussed in more detail in the following section.

2.1.3 Gaussian Models

To simplify the notion, we omit the overbars denoting the average values of C and u_i in the following text.

Gaussian Plume Model

Gaussian plume model is obtained as a 3-dimensional, time independent solution of (2.1.9) for a continuous source at the ground level, constant u_i and K_i , and a flat terrain. Gaussian plume models gives us a steady-state solution, i.e., the model does not take into account the time required for the pollutant to travel to the receptor and describes concentration in a fully established plume under stationary meteorological conditions.

Let us assume a continuous point-source ground-based release of mass Q with time constant coefficients K_i and wind speed components u_i . The wind is assumed to blow along the direction of s_1 -axis ($\mathbf{u} = (u_1, 0, 0)$) of an Eulerian coordinate system with the origin aligned with the source location. We can assume that the advection dominates diffusion in the downwind direction,

$$u_1 \frac{\partial C}{\partial s_1} \gg \frac{\partial}{\partial s_1} \left(K_1 \frac{\partial C}{\partial s_1} \right).$$

The diffusion in this direction can be then neglected and the basic equation (2.1.9) modified for the steady-state conditions is

$$u_1 \frac{\partial C}{\partial s_1} = \frac{\partial}{\partial s_2} \left(K_2 \frac{\partial C}{\partial s_2} \right) + \frac{\partial}{\partial s_3} \left(K_3 \frac{\partial C}{\partial s_3} \right). \quad (2.1.10)$$

The boundary conditions for solution of (2.1.10) are:

1. $C \rightarrow 0$ for $r = \sqrt{s_1^2 + s_2^2 + s_3^2} \rightarrow +\infty$,
2. $C \rightarrow +\infty$ for $r \rightarrow 0$,
3. $K_3 \frac{\partial C}{\partial s_3} \rightarrow 0$ for $s_3 \rightarrow 0$,
4. $\int_0^{+\infty} \int_{-\infty}^{+\infty} u_1 C \, ds_2 ds_3 = Q$.

Here, Q defines a continuous point-source in terms of released mass per time (activity per time in the case of a radioactive release). The first two conditions represent our requirements on the concentration values at zero and infinite distances from the source. Condition 3 expresses the fact that we assume no sedimentation on the ground and condition 4 is the formalization of the law of conservation of the released mass (activity). The appropriate solution for constant wind and diffusivity coefficients is

$$C(\mathbf{s}) = \frac{Q}{4\pi s_1 \sqrt{K_2 K_3}} \exp \left[-\frac{u_1}{4s_1} \left(\frac{s_2^2}{K_2} + \frac{s_3^2}{K_3} \right) \right]. \quad (2.1.11)$$

Since the values of diffusion coefficients is difficult to measure, we use *dispersion coefficients* defined as

$$\sigma_i = \sqrt{2K_i \tau}. \quad (2.1.12)$$

The dispersion coefficients are usually functions of the atmospheric stability category and the downwind distance from the source. Substitution of (2.1.12) into (2.1.11) gives us a time independent formula for concentration in a developed Gaussian plume

$$C(\mathbf{s}) = \frac{Q}{2\pi u_1 \sigma_2 \sigma_3} \exp \left(-\frac{s_2^2}{2\sigma_2^2} \right) \exp \left(-\frac{s_3^2}{2\sigma_3^2} \right). \quad (2.1.13)$$

The coefficients σ_2 and σ_3 represent the standard deviations of the concentration in the cross-wind (s_2) and vertical (s_3) planes, respectively. Larger values of the coefficients mean broader distribution and consequently higher dilution of pollutant and smaller concentration.

Gaussian Puff Model

Contrary to the plume models, the puff models are applicable when mean wind vector transporting the puff is variable in space and time. Using the puff model, these variations can be directly incorporated in a numerical scheme whereby they are used to transport the center of the puff. Dispersion of the puff (Gaussian distribution) is evaluated using the concept of *virtual source* at each time step. The characteristic feature of these models is that the calculation of pollutant diffusion, transportation, and removal is performed in the Lagrangian frame of reference attached to a number of parcels as they are transported around the geographical region of interest. Approximation of a continuous release is reached by simultaneous propagation of multiple puffs. Under assumption of stationarity, spatially homogeneous flow of multiple puffs over the flat terrain represents the Gaussian plume model, which is demonstrated in (Jung et al., 2003). The overall concentration is evaluated as a superposition of the puffs (Ludwig et al., 1977; Zannetti, 1986).

The form of (2.1.9) describing advection and diffusion of a single puff is

$$\frac{\partial C}{\partial \tau} + u_1 \frac{\partial C}{\partial s_1} = \frac{\partial}{\partial s_1} \left(K_1 \frac{\partial C}{\partial s_1} \right) + \frac{\partial}{\partial s_2} \left(K_2 \frac{\partial C}{\partial s_2} \right) + \frac{\partial}{\partial s_3} \left(K_3 \frac{\partial C}{\partial s_3} \right). \quad (2.1.14)$$

We solve (2.1.14) with the following boundary conditions:

1. $C \rightarrow 0$ for $r = \sqrt{s_1^2 + s_2^2 + s_3^2} \rightarrow +\infty$,
2. $C \rightarrow +\infty$ for $r \rightarrow 0$,
3. $K_3 \frac{\partial C}{\partial s_3} \rightarrow 0$ for $s_3 \rightarrow 0$,
4. $\int_0^{+\infty} \int_{-\infty}^{+\infty} \int_{-\infty}^{+\infty} C \, ds_1 ds_2 ds_3 = Q^i$.

Here, Q^i defines an instantaneous point-source in terms of released mass (activity in the case of a radioactive release). Analytical solution for the given case describing the concentration of pollutant everywhere in space is

$$C(\mathbf{s}, \tau) = \frac{Q^i}{8(\pi\tau)^{3/2} \sqrt{K_1 K_2 K_3}} \exp \left\{ -\frac{1}{4\tau} \left[\frac{(s_1 - u_1\tau)^2}{K_1} + \frac{s_2^2}{K_2} + \frac{s_3^2}{K_3} \right] \right\}. \quad (2.1.15)$$

After substitution of dispersion coefficients σ_i for the eddy diffusivity coefficients K_i we obtain equation of the Gaussian puff. Under general conditions, a puff located in $\mathbf{s}^P = (s_1^P, s_2^P, s_3^P)$ in time τ generates the concentration field

$$C(\mathbf{s}, \tau) = \frac{Q^i}{(2\pi)^{3/2} \sigma_1 \sigma_2 \sigma_3} \exp \left\{ -\frac{1}{2} \left[\frac{(s_1^R - s_1^P)^2}{\sigma_1^2} + \frac{(s_2^R - s_2^P)^2}{\sigma_2^2} + \frac{(s_3^R - s_3^P)^2}{\sigma_3^2} \right] \right\}, \quad (2.1.16)$$

at a receptor located at $\mathbf{s}^R = (s_1^R, s_2^R, s_3^R)$. Similarly to the plume model, coefficients σ_1 , σ_2 and σ_3 represent the standard deviations of the concentration in the downwind (s_1), cross-wind (s_2), and vertical (s_3) planes, respectively.

Parametrization of Dispersion Coefficients

Variability of temperature with altitude influences the turbulence characteristics and thus the dispersion of pollutants. The temperature in the atmosphere is governed by incident solar radiation, prevailing wind velocity, and percentage of cloud cover. Depending on the magnitude of these parameters, Pasquill (1961) introduced the six stability classes named A, B, C, D, E, and F of the atmospheric turbulence. Class A denotes the most unstable or most turbulent conditions (the dispersion is higher), and class F the most stable or the least turbulent class (very low dispersion).

Besides the atmospheric stability category, dispersion coefficients are also dependent on travel time from the source and the type of terrain (urban, rural, etc.), e.g. (Gifford, 1976). The comprehensive review can be found in (Hanna et al., 1982). More advanced models apply Monin-Obukhov similarity theory and use the surface roughness length and the Monin-Obukhov length to determine the magnitude of dispersion, see (Cheremisinoff, 2002; Cimorelli et al., 2004).

Elevated Sources and Reflections

The last exponential terms in (2.1.16) and (2.1.13) stand for exponential concentration profiles in the vertical direction. Let the terms be denoted as V ,

$$V = \exp \left[-\frac{s_3^2}{2\sigma_3^2} \right]. \quad (2.1.17)$$

In the most of real situations we assume, that the source is elevated over terrain in a height H . Moreover, if the effluent has a heat capacity or an initial vertical momentum, the height of the plume reaches so called *effective height* H_{ef} . It is a sum of the release height H and the height change due to the plume rise or subsidence ΔH ,

$$H_{\text{ef}} = H + \Delta H.$$

Vertical dispersion is usually assumed to be a growing function of the downwind distance, $\sigma_3 = \sigma_3(r)$. The form of (2.1.17) suggests that the vertical expansion of a puff or plume can be infinite. This is, of course, not possible in reality. The Gaussian distribution of the concentration is modified at greater distances from the source due to the effects of turbulent reflections from the surface. When the pollutant reaches the ground due to the vertical dispersion, the further spreading in vertical direction is not possible and it is assumed that at the surface is the pollutant reflected without any loss. Reflection on the ground is modeled as a virtual source at the effective height H_{ef} below the ground. To account for the elevated source and the ground reflection we

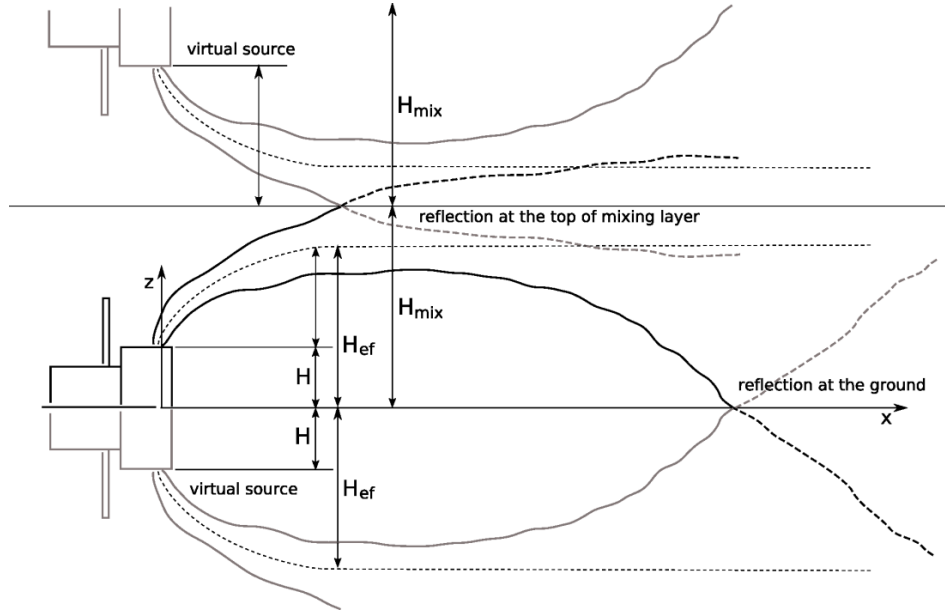


Figure 2.1.2: Illustration of the principle used for modeling of the reflections as a superposition of multiple plumes released from virtual sources below the ground and above the top of mixing layer .

modify the vertical dispersion term as follows,

$$V_1 = \exp \left[-\frac{(s_3 - H_{ef})^2}{2\sigma_3^2} \right] + \exp \left[-\frac{(s_3 + H_{ef})^2}{2\sigma_3^2} \right].$$

Puff or plume can be also reflected from the top of *mixing layer*. In such a case, the vertical profile of the plume is bounded by the ground and the top of mixing layer at height H_{mix} . Theoretically, the number of reflections can be infinite. However, multiple reflections on the ground and at the top of mixing layer lead to vertical homogenization of concentration and numerical experiments proved that one virtual source below ground and one at the top of the boundary layer gives sufficient accuracy (Barratt, 2001),

$$\begin{aligned} V_2 = & \exp \left[-\frac{(s_3 - H_{ef})^2}{2\sigma_3^2} \right] + \exp \left[-\frac{(s_3 + H_{ef})^2}{2\sigma_3^2} \right] \\ & + \exp \left[-\frac{(s_3 - 2H_{mix} - H_{ef})^2}{2\sigma_3^2} \right] + \exp \left[-\frac{(s_3 + 2H_{mix} - H_{ef})^2}{2\sigma_3^2} \right] \\ & + \exp \left[-\frac{(s_3 - 2H_{mix} + H_{ef})^2}{2\sigma_3^2} \right] + \exp \left[-\frac{(s_3 + 2H_{mix} + H_{ef})^2}{2\sigma_3^2} \right]. \end{aligned} \quad (2.1.18)$$

The principle used for modeling of the reflections as a superposition of multiple plumes released from virtual sources is illustrated in Figure 2.1.2.

2.2 Radiological Quantities

In this section we briefly describe some essential radiological quantities used in this work and their relations.

2.2.1 Radioactive Decay and Radioactivity

Radioactive decay is a spontaneous nuclear transformation followed by an emission of ionizing particles. As the decay of an unstable nucleus is entirely random and it is not possible to predict when a particular atom will decay, it is described in terms of a continuous quantity $N(\tau)$, mean value of radioactive (undecayed) atoms in time τ .

Given a sample of a particular radioisotope, the number of decay events ($-dN(\tau)$) expected to occur in a small interval of time dt is proportional to the number of atoms present:

$$-\frac{dN(\tau)}{d\tau} = \lambda N(\tau). \quad (2.2.1)$$

The negative sign indicates that the mean value of radioactive atoms $N(\tau)$ decreases with each decay event and λ is the proportionality constant known as the *decay constant*. Particular radionuclides decay at different rates, each having its own λ (there are more than 500 different nuclides). Solution of the first order differential equation (2.2.1) is a function

$$N(\tau) = N_0 \exp(-\lambda \tau), \quad (2.2.2)$$

where N_0 is the number of radioactive atoms in time $t = 0$.

The decay rate is denoted as *activity*, $A(\tau)$, which is a basic physical unit quantitatively describing physical phenomena *radioactivity*. Activity is a measure of the expected number of disintegrations per unit time (Choppin et al., 2002),

$$A(t) = -\frac{dN(\tau)}{d\tau}.$$

Since $A(\tau)$ is proportional to the mean number of atoms $N(\tau)$, we can write

$$A(\tau) = A_0 \exp(-\lambda \tau), \quad (2.2.3)$$

where A_0 , analogously to N_0 , is the activity in time $\tau = 0$. Although the radioactive decay is a discrete random process, the continuous exponential functions (2.2.2) and (2.2.3) are for large numbers of atoms (comparable to Avogadro's number in magnitude) a good approximation.

Mean lifetime τ^m of an atom before it undergoes the decay is inversely proportional to λ ,

$$\tau^m = \frac{1}{\lambda}.$$

Even more common is the use of physical half-life, $T_{1/2}$, which is the time needed to reduce the amount of radioactive material by a factor of 2. The formula

$$\frac{N(\tau)}{N_0} = \frac{1}{2} = \exp(-\lambda T_{1/2})$$

yields

$$T_{1/2} = \frac{\ln 2}{\lambda}. \quad (2.2.4)$$

Introducing the physical half-life (2.2.4) into (2.2.3), we get the *decay law*

$$A(\tau) = A_0 \exp\left(-\ln 2 \frac{\tau}{T_{1/2}}\right). \quad (2.2.5)$$

The SI unit for radioactivity is *Becquerel* (Bq) and the activity is given in reciprocal seconds, s^{-1} ,

$$1 \text{ Becquerel (Bq)} = 1 \text{ (disintegration) } s^{-1}.$$

In the field of dispersion modeling of radionuclides, we evaluate *activity concentration in air*, which is a number of disintegration of a dispersed radionuclide in a unit volume per unit time, i.e., its unit is $Bq m^{-3}$. It is a quantity of particular importance because it can be used for evaluation other radiological quantities like deposition and doses.

2.2.2 Calculation of Absorbed Doses

The *absorbed dose* (also known as the total ionizing dose) is a measure of the energy deposited in a medium by ionizing radiation. It is equal to the energy deposited per unit mass of medium. Its unit $J kg^{-1}$ was given the special name Gray (*Gy*).

Absorbed Dose from Cloudshine

The *cloudshine* is external gamma radiation from a radioactive plume passing over the terrain. The simplest way of cloudshine dose rate calculation is based on approximation of the plume as a semi-infinite hemisphere with homogeneous concentration of radionuclides (Raza et al., 2001; Thykier-Nielsen et al., 1995). Resulting formula for the gamma dose rate at a receptor R located at $\mathbf{s}^R = (s_1^R, s_2^R, s_3^R)$ is

$$D_c(\mathbf{s}^R, \tau) = K \frac{E C(\mathbf{s}, \tau)}{2\rho}, \quad (2.2.6)$$

where $\mathbf{s} = (s_1, s_2, s_3)$ is a spatial location; K is the dose rate conversion factor [$Gy kg eV$]; E is the gamma energy produced by decay of assumed radionuclide; $C(\mathbf{s}, \tau)$ is radionuclide concentration [$Bq m^{-3}$] in spatial location \mathbf{s} ; and ρ is the air density. This formula

assumes an equilibrium between the gamma energy released in the plume and that absorbed in the air. Approximation of a non-homogeneous plume (e.g. Gaussian) using the semi-infinite approach may lead to large errors. What is more, if the receptor point is not immersed in the radioactive cloud, the application of (2.2.6) is not well-founded at all.

The general expression for the effective flux of gamma rays at a receptor point \mathbf{s}^R from a source of ionizing radiation dispersed in air is according to Thykier-Nielsen et al. (1995), as follows,

$$\Phi(\mathbf{s}^R, \tau, E) = \int_{\Omega} \frac{f(E) C(\mathbf{s}, \tau) B(E, \mu r) \exp(-\mu r)}{4\pi r^2} d\mathbf{s}, \quad (2.2.7)$$

where $f(E)$ is the branching ratio to the specific energy E ; B is the build up factor; μ is the linear attenuation coefficient; Ω is a spatial domain of integration; and $r = \|\mathbf{s}^R - \mathbf{s}\|$ is the distance of spatial locations \mathbf{s}^R and \mathbf{s} . The build-up factor can be calculated from Berger's analytical formula

$$B(E, \mu r) = 1 + a \mu r \exp(b \mu r),$$

where coefficients μ , a and b depend on E . Energy dependent absorption coefficient μ_a is calculated using

$$\mu_a = \frac{\mu}{1 + \frac{a}{(1-b)^2}}.$$

The gamma dose rate from a mixture of nuclides emitting gamma radiation on different energy levels E^i , $i = 1, \dots, N_E$, is

$$D_c(\mathbf{s}^R, \tau) = \sum_i^{N_E} \frac{K^i \mu E^i \Phi^i}{\rho}.$$

For a plume of a mono-energetic radionuclide dispersed in air emitting gamma radiation on a single energy level E , i.e. $f(E) = 1$, we obtain

$$D_c(\mathbf{s}^R, \tau) = \frac{K E \mu_a}{\rho} \int_{\Omega} \frac{C(\mathbf{s}, \tau) B(E, \mu r) \exp(-\mu r)}{4\pi r^2} d\mathbf{s}. \quad (2.2.8)$$

The time integrated gamma dose rate $\mathcal{D}_c(\mathbf{s}^R, \tau_1, \tau_2)$ integrated over the time interval (τ_1, τ_2) is defined as

$$\mathcal{D}_c(\mathbf{s}^R, \tau_1, \tau_2) = \int_{\tau_1}^{\tau_2} D_c(\mathbf{s}^R, \tau) d\tau. \quad (2.2.9)$$

In the case of Gaussian models, concentration $C(\mathbf{s})$ is given by the analytical formulas (2.1.16) and (2.1.13). Specifically, the simplicity of the Gaussian puff model (2.1.16) allows for numerical evaluation of the integral in (2.2.8) on a compact support where the activity concentration is not negligible.

Absorbed Dose from Groundshine

The *groundshine* is the external gamma radiation from radioactive material deposited on the ground, trees, buildings etc. (Golikov et al., 1999). Given deposition $SD(\mathbf{s}, \tau)$ in location \mathbf{s} and time τ , the groundshine dose rate $D_g(\mathbf{s}, \tau)$ is calculated as follows,

$$D_g(\mathbf{s}, \tau) = DF_g SD(\mathbf{s}, \tau) SF, \quad (2.2.10)$$

where the coefficient of proportionality DF_g is the radionuclide-dependent integrated *dose rate conversion factor* for groundshine in units $Sv s^{-1}$ per $Bq m^{-2}$. Unit-less *shielding factor* SF is defined as

$$SF = \sum_i f_i SF_i,$$

where f_i is i th fraction of time spent in different places (indoor, outdoor, etc.) and $SF_i \in [0, 1]$ is the shielding factor at each place.

The time evolution of the deposition is modeled according to the standard formula

$$SD(\mathbf{s}, \tau) = SD(\mathbf{s}, 0) f_R(\tau) f_E(\tau), \quad (2.2.11)$$

where $SD(\mathbf{s}, 0)$ is initial deposition in time $\tau = 0$; $f_R(\tau)$ is a function taking into account *radioactive decay* (2.2.5) in terms on relative amount of undecayed material in time τ ; and $f_E(\tau)$ a function taking into account decrease of radioactivity due to the environmental removal processes. Environmental removal is a general term referring to different processes causing radioactivity removal from terrain, e.g., radionuclide migration deeper into the soil, weathering, leaching.

An adequate description of the long term dynamics of radionuclides in soil is the most important factor in the correct estimation of the radioactive contamination of local agricultural and forest products, which has a major contribution to the exposure of the local population. There exist several computer codes implementing formulas (2.2.10) and (2.2.11). Their comprehensive review can be found in (Thiessen et al., 2005). In calculation of the groundshine dose, the main difference among the codes consists in different descriptions of $f_E(\tau)$ and in application of different numerical values of SF and DF_g (IAEA, 2003).

We adopt groundshine dose model from Japanese code OSCAAR (Off-Site Consequence Analysis Code for Atmospheric Releases in reactor accidents) (Homma, 2002). Environmental removal is in (2.2.11) modeled using

$$f_E(t) = d^f \exp\left(-\ln 2 \frac{t}{T^f}\right) + d^s \exp\left(-\ln 2 \frac{t}{T^s}\right), \quad (2.2.12)$$

where the rate of environmental decay is modeled as a superposition of two exponentials, fast and slow components with fractions $d^f, d^s > 0$; $d^f + d^s = 1$, and removal half-times T^f, T^s .

Illustration of the relative decrease of goudnshine dose from deposition of ^{134}Cs in time due to the radioactive decay and the environmental removal is in Figure 2.2.1.

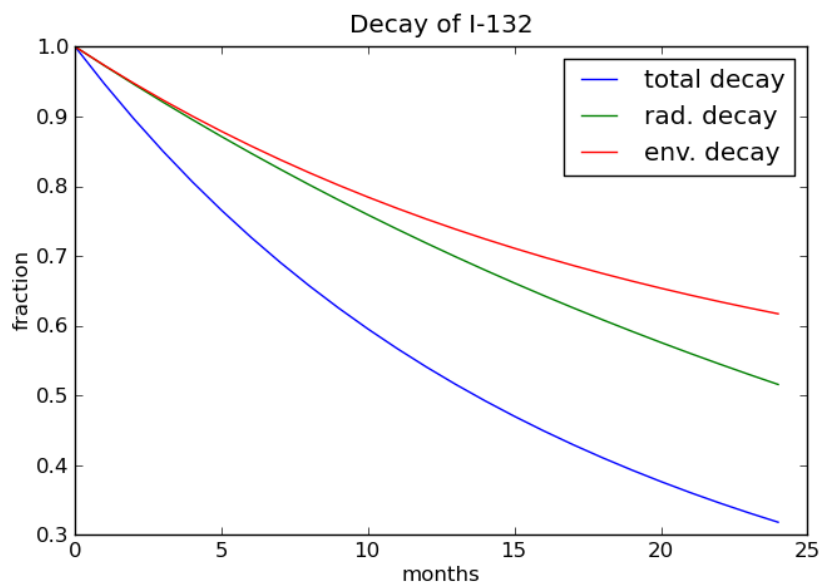


Figure 2.2.1: Illustration of the relative decrease of groundshine dose from deposition of ^{134}Cs in time due to the radioactive decay and the environmental removal.

Radionuclide ^{134}Cs has the half-life of radioactive decay $T_{1/2} = 2.0648$ years. We see, that after 24 months, the exponential function describing the radioactive decay (green line) falls approximately to 0.5 of the initial value. The blue line represents the total ^{134}Cs removal due to the environmental removal (red line) and the radioactive decay. Values of coefficients in (2.2.12) were set to some reference values.

2.3 Developed Atmospheric Dispersion Model

For purposes of testing of assimilation algorithms developed in subsequent chapters, we implemented a simple Gaussian puff model. In this chapter, we describe the model and numerical schemes used for calculation of the activity concentration in air under variable meteorological conditions and the corresponding cloudshine at a ground based receptor.

2.3.1 Model Inputs and Outputs

The implemented model has the following meteorological and radiological inputs:

1. wind speed [$m s^{-1}$]
2. wind direction [deg]
3. Pasquill atmospheric stability category $\in \{A, B, C, D, E, F\}$ for determination of the dispersion rate and the height of mixing layer

4. magnitude of release [Bq]
5. radionuclide dependent half-life of decay [s]
6. effective height of release [m]
7. type of radionuclide parameterizing the dry deposition

The wind speed and the wind direction are valid for the whole computational domain at a time. During the puff propagation, we assume the terrain flat. Given the inputs, the model calculates following radiological quantities on an arbitrary computational grid:

1. activity concentration in air [$Bq m^{-3}$],
2. time integral of activity concentration in air [$Bq s m^{-3}$],
3. surface deposition [$Bq m^{-2}$],
4. time integral of surface deposition [$Bq s m^{-2}$],
5. gamma dose rate [$Gy s^{-1}$],
6. time integral of gamma dose rate [Gy].

2.3.2 Numerical Evaluation of Gaussian Puff Model under Variable Meteorological Conditions

Activity concentration in air is calculated using (2.1.16) in a consecutive time steps. Between discrete time steps t and $t + 1$, the time integral of activity concentration in air in a spatial location \mathbf{s} is approximated using the difference equation

$$C(\mathbf{s}, k + 1) = C(\mathbf{s}, k) \frac{\sigma_1(k)\sigma_2(k)\sigma_3(k)}{\sigma_1(k+1)\sigma_2(k+1)\sigma_3(k+1)} \frac{G(k+1)}{G(k)} \frac{V_2(k+1)}{V_2(k)} \Delta f^{k \rightarrow k+1}, \quad (2.3.1)$$

$$G(k) = \exp \left[-\frac{(s_1 - s_1^P(k))^2}{2\sigma_1^2(k)} - \frac{(s_2 - s_2^P(k))^2}{2\sigma_2^2(k)} \right].$$

Here, $k = 1, \dots, N_k$, are indices of partial integration steps between time instances t and $t + 1$; $\mathbf{s}^P(k) = (s_1^P(k), s_2^P(k), s_3^P(k))$ are coordinates of the puff center in time k ; $\sigma_i(k)$ are values of dispersion coefficients in time k ; $G(k)$ is a term accounting for horizontal dispersion in time k ; $V_2(k)$ is a term given by (2.1.18) accounting for vertical dispersion of the puff in time k ; and $\Delta f^{k \rightarrow k+1}$ stands for removing of activity from the puff during elemental shifts. The last term is given as follows,

$$\Delta f^{k \rightarrow k+1} = f_R^{k \rightarrow k+1} f_D^{k \rightarrow k+1},$$

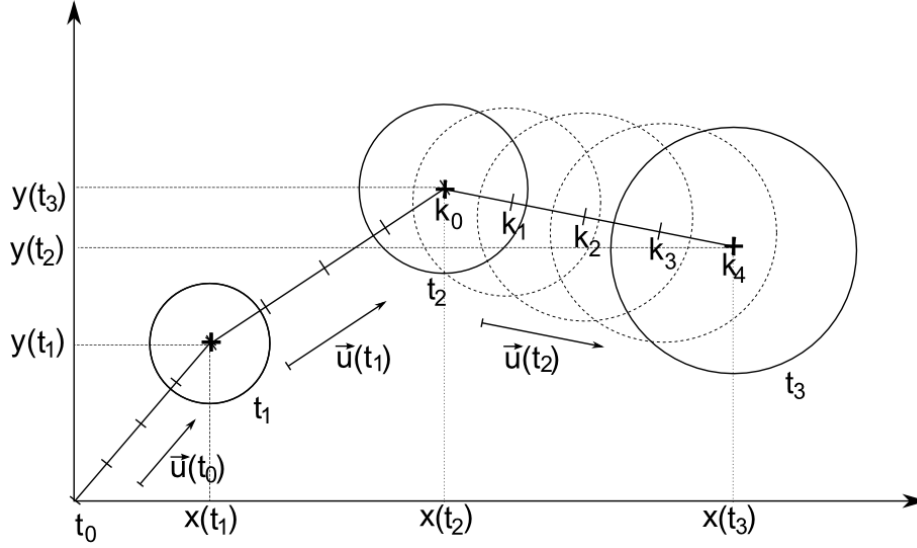


Figure 2.3.1: Illustration of numerical integration scheme of the Gaussian puff propagation. Between time steps t and $t + 1$, the puff is integrated forward in using elemental shifts k .

where the factors $\Delta f_R^{k \rightarrow k+1}$ and $\Delta f_D^{k \rightarrow k+1}$ stand for magnitude of radioactive decay of the considered isotope and the puff depletion due to the dry deposition, respectively. The decay factor $\Delta f^{k \rightarrow k+1} < 1$ is evaluated using (2.2.3). In the case that the assumed radionuclide is a noble gas, the puff is not depleted during elemental shifts.

Generally, the time integrated concentration of activity in air is given by

$$C(\tau_1, \tau_2, \mathbf{s}) = \int_{\tau_1}^{\tau_2} C(\mathbf{s}, \tau) d\tau, \quad (2.3.2)$$

where $\tau_1, \tau_2, \tau_2 > \tau_1$, are arbitrary time instances. It can be approximated with forward differences using (2.3.1) as

$$C(\tau_1, \tau_2, \mathbf{s}) \approx \sum_{k=1}^{N_k} \frac{C(\mathbf{s}, \tau_1 + \Delta_k k) + C(\mathbf{s}, \tau_1 + \Delta_k (k + 1))}{2} \Delta_k, \quad (2.3.3)$$

where N_k is the number of partial steps of length Δ_k between τ_1 and τ_2 , i.e., $\tau_2 - \tau_1 = N_k \Delta_k$. If the time difference Δ_k is small enough, (2.3.3) gives us a good approximation of (2.3.2). The numerical integration scheme is illustrated in Figure 2.3.1.

The main advantages of this step-wise approach consist in the fact, that the puff can be propagated using different meteorology in each time step t . Besides the radioactive decay and the dry deposition, it is possible to include more physical and chemicals processes affecting the inventory of the plume, e.g., the wet deposition, buildup of daughter decay products, (Pecha et al., 2007).

parameter	description	range	step	unit
$\sigma_1 = \sigma_2$	horizontal dispersion coefficients	10-1000	20	<i>m</i>
σ_3	vertical dispersion coefficient	10-1000	20	<i>m</i>
r	distance of the puff center to receptor	50-10000	50, 100, 500	<i>m</i>

Table 2.1: Discretization of parameters for evaluation of pre-calculated values of gamma dose rate from a radionuclide ^{41}Ar dispersed in air.

2.3.3 Numerical Evaluation of Cloudshine Dose Rate

Evaluation of (2.2.9) is not straightforward. From (2.2.7)–(2.2.9) is obvious, that the integration must be performed over both time and space domains. For the time integration of effective flux of gamma rays in (2.2.9), we use a numerical scheme similar to (2.3.3) based on a difference equation (2.3.1) ,

$$\int_{\tau_1}^{\tau_2} \Phi(\mathbf{s}^R, \tau, E) d\tau \approx \sum_{k=1}^{N_k} \frac{\Phi(\mathbf{s}^R, \tau_1 + \Delta_k k, E) + \Phi(\mathbf{s}^R, \tau_1 + \Delta_k(k+1), E)}{2} \Delta_k, \quad (2.3.4)$$

where N_k is the number of partial steps of length Δ_k between τ_1 and τ_2 , i.e., $\tau_2 - \tau_1 = N_k \Delta_k$. In the formula, we have to calculate the effective flux of gamma rays (2.2.7) in each partial step $k = 1, \dots, N_k$. It is a function of the activity concentration in air C integrated over a spatial domain Ω .

Since a single evaluation of (2.2.7) is time consuming, its values were pre-calculated for a selected set of discretized inputs and stored in a multidimensional field. Function $C(\mathbf{s}, \tau)$ in (2.2.7) is given by the Gaussian puff model. We exploit its simplicity. Since we assume an instantaneous release, the coefficient Q^i describing the amount of released material is time independent. Spatial distribution of activity concentration in air is in this case linearly dependent on Q^i . It means, given a reference value Φ_{ref} of (2.2.7) calculated with the nominal value $Q_{\text{ref}}^i = 1Bq$, corresponding value for an arbitrary Q^i can be simply obtained by multiplying Φ_{ref} with Q^i as follows,

$$\Phi(\mathbf{s}^R, E, Q^i) = Q^i \Phi_{\text{ref}}(\mathbf{s}^R, E, 1Bq).$$

During the puff propagation, values of Φ depend on the concentration profile given by dispersion coefficients $\sigma_1, \sigma_2, \sigma_3$, and the distance r of the receptor point to the puff (measured as a distance of the receptor to the puff center). We discretized these three parameters and pre-calculated values of Φ_{ref} for a set of their reasonable combinations. The list of discretized parameters together with their ranges and discretization steps are in Table 2.1. Simplicity of the Gaussian puff model (2.1.16) allows for numerical evaluation of integral (2.2.7) on a finite support where the concentration is not negligible. Due to exponential functions involved in concentration profiles, the values of activity concentration in air are theoretically positive everywhere in space, but they

fall dramatically to zero. If the spatial integration in (2.2.7) is performed over a box Ω centered at the puff center $\mathbf{s}^P = (s_1^P, s_2^P, s_3^P)$,

$$\Omega = (s_1^P - 3\sigma_1, s_1^P + 3\sigma_1) \times (s_2^P - 3\sigma_2, s_2^P + 3\sigma_2) \times (s_3^{\min}, s_3^{\max}),$$

we account for approximately 94% of the released material, which is for our purposes sufficient. The last interval (s_3^{\min}, s_3^{\max}) providing the integration limits in the vertical direction must be chosen with respect to limitations given by the ground and the height of the mixing layer H_{mix} :

$$\begin{aligned} s_3^{\min} &= \max\{0, s_3^P - 3\sigma_3\}, \\ s_3^{\max} &= \min\{H_{\text{mix}}, s_3^P + 3\sigma_3\}. \end{aligned}$$

Definite integrals $\Phi_{\text{ref}}(\mathbf{s}^R, \tau_1 + \Delta_k k, E)$, $k = 1, \dots, N_k$, are approximated using the Gaussian quadrature method. We use the implementation contained in numerical module Integrate of the scientific extension SciPy of the Python scripting language. During the model propagation, the pre-calculated values Φ_{ref} are used for fast calculation of the gamma dose rates approximated by the difference equation

$$\mathcal{D}^c(\tau_1, \tau_2, \mathbf{s}^R) \approx Q^i \frac{K \mu_a E}{\rho} \sum_{k=1}^{N_k} \frac{\Phi_{\text{ref}}(\mathbf{s}^R, \tau_1 + \Delta_k k, E) + \Phi_{\text{ref}}(\mathbf{s}^R, \tau_1 + \Delta_k (k+1), E)}{2} \Delta_k, \quad (2.3.5)$$

where $\tau_2 - \tau_1 = N_k \Delta_k$.

If the radioactive plume is large compared to the mean free path of the gamma rays, then the semi-infinite cloud approximation of the effective flux can be successfully used. See (Overcamp and Fjeld, 1987) for more details.

Chapter 3

Data Assimilation

3.1 Introduction and Terminology

Data assimilation results from the methods of objective analysis introduced in the middle of the 20th century in order to eliminate a subjective human factor in numerical weather prediction (Daley, 1993). It refers to a group of mathematical methods for estimation of a state of a dynamic system by the means of combining multiple sources of information, typically observational data with a numerical model of the system under investigation. We are concerned with 4-D data assimilation, where the assimilation is performed in time and space.

3.1.1 Data Assimilation Cycle

Data assimilation is performed in cycles, where each the assimilation cycle has two steps. Adopting the generally accepted data assimilation terminology unified in (Ide et al., 1997), the first step, the *data update*, can be described as follows: Given the model *forecast* (so called *background field*) and the observations, the data update produces their statistically optimal combination called *analysis*. It is an estimate of the current system state considered to be better both the standalone model forecast and the observations. Essentially, the analysis step tries to balance the uncertainty in the data and in the forecast. In the second step, the *time update*, the analysis is integrated forward in time using the model equations. This becomes the new forecast in the next assimilation cycle. Periodic updating of the model with observations should ensure that the model will not diverge from the physical truth.

Illustration of the sequential data assimilation process is in Figure 3.1.1: Let the system state be a one-dimensional continuous random variable estimated in discrete time steps. Observations available in discrete time steps represent a connection with the physical reality and can be understood as a noisy samples from the true state represented by the blue curve. Observations are denoted with squares and the green circles represent their uncertainty. In each time instance, the best state estimate—analysis denoted by asterisk—is produced on basis of current model forecast (plus sign)

and observations. The red and yellow circles represent the uncertainties of forecast and analysis, respectively. In the figure is schematically depicted that the forecast error is reduced in each time step after the data update (yellow dashed line). The red dashed line represents the time update step, when the analysis is advanced via the model forward in time.

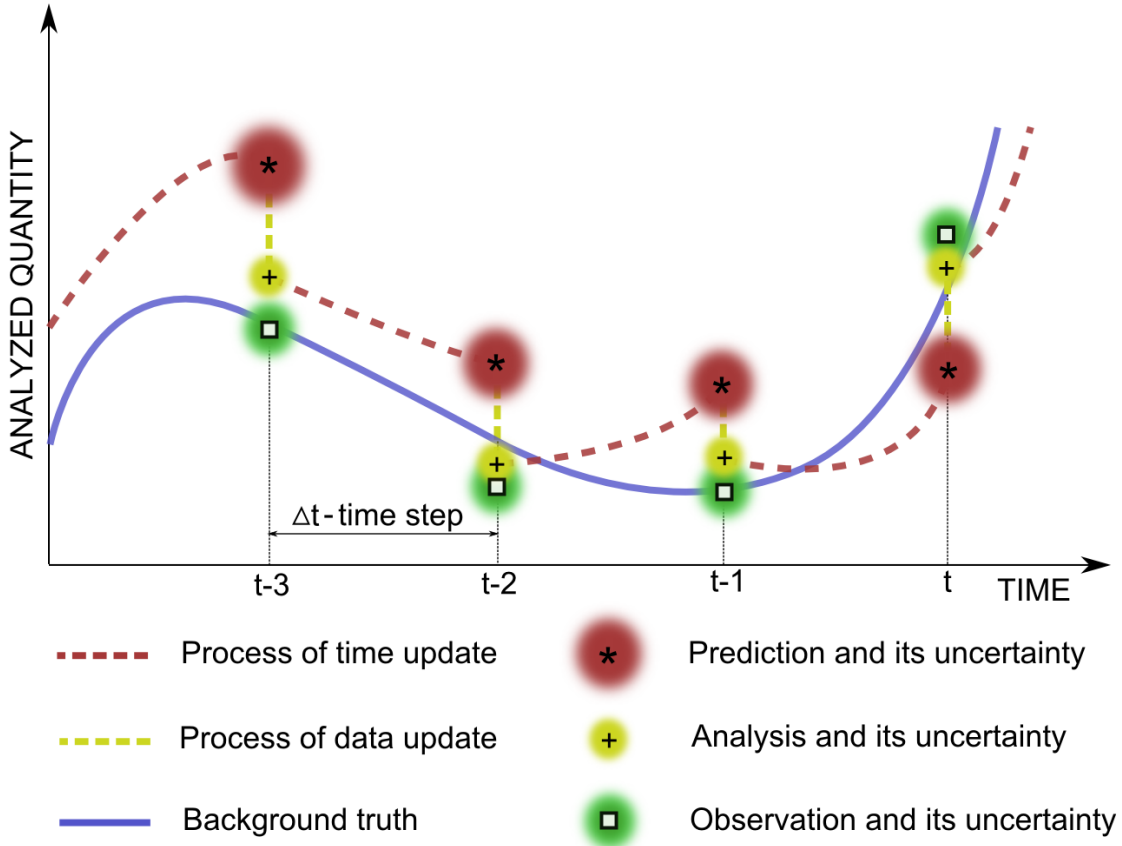


Figure 3.1.1: Illustration of basic principle of sequential data assimilation.

3.1.2 Identification of Data Assimilation with Bayesian Estimation

Bayesian approach is based on quantifying uncertainty in statistical inference via probability density functions (pdfs). The importance of such approach is justified by the fact, that it facilitates a common-sense interpretation of statistical conclusions (Gelman, 2004).

If we think of the forecast and the analysis as of pdfs, the data assimilation can be understood as a particular case of recursive Bayesian estimation (Peterka, 1981). In the Bayesian framework, the forecast and the analysis are represented by the *prior* pdf and *posterior* pdf, respectively. When no measurements are available, the pdf

of the considered state must be rather wide to cover all possible realizations of the state. Each incoming measurement brings information about the “true” state, reducing the original uncertainty. In effect, with increasing measurements, the posterior pdf is narrowing down around the best possible estimate. From the Bayesian point of view, data assimilation is analogical to the problem of filtering, i.e., characterizing the distribution of the state of the hidden Markov model at the present time, given the information provided by all of the observations received up to the present time. Data update step of the assimilation cycle is implemented using *Bayes formula*.

3.2 Recursive Bayesian Filtering

The task of data assimilation can be interpreted as a problem of *inference* of a discrete-time *stochastic process*:

$$\mathbf{x}_t \sim p(\mathbf{x}_t | \mathbf{x}_{t-1}), \quad (3.2.1)$$

$$\mathbf{y}_t \sim p(\mathbf{y}_t | \mathbf{x}_t). \quad (3.2.2)$$

Here, $\mathbf{x}_t \in \mathbb{R}^{N_x}$ is a vector known as the state variable, $\mathbf{y}_t \in \mathbb{R}^{N_y}$ is a vector of observations, t is the time index, and $p(\cdot | \cdot)$ denotes the conditional pdf of the variable. State evolution model (3.2.1) describes the evolution of the state variables \mathbf{x}_t over time, whereas the measurement model (3.2.2) explains how the measurements \mathbf{y}_t relate to the state variables.

System given by (3.2.1)–(3.2.2) is rather general. It represents a *Markov process* of the first order, where realization of the process at time t contains all the information about the past, which is necessary to calculate its future behavior. In data assimilation we often restrict to its special case, where the explicit expressions for both the state model and the measurement model exist. This results in a discrete-time state-space models with additive noise represented by a set of difference equations (Jazwinski, 1970):

$$\mathbf{x}_t = \mathcal{M}_t(\mathbf{x}_{t-1}) + \mathbf{w}_t, \quad (3.2.3)$$

$$\mathbf{y}_t = \mathcal{H}_t(\mathbf{x}_t) + \mathbf{v}_t. \quad (3.2.4)$$

The state transition operator $\mathcal{M}_t : \mathbb{R}^{N_x} \rightarrow \mathbb{R}^{N_x}$ integrates the state forward to the next time step. The observation operator $\mathcal{H}_t : \mathbb{R}^{N_x} \rightarrow \mathbb{R}^{N_y}$ transforms vectors from the state-space to the space of observations and makes them thus comparable with the observations. In environmental modeling, these operators represent our mathematical conceptualization of the physical reality under investigation. Vectors \mathbf{w}_t and \mathbf{v}_t with appropriate dimensions represent mutually independent noise processes of the model and the observations, respectively.

Formally, the prior distribution $p(\mathbf{x}_0)$ representing uncertainty of the forecast in time $t = 0$ is transformed into the posterior pdf $p(\mathbf{x}_t|\mathbf{y}_{1:t})$ using measurements $\mathbf{y}_{1:t} = [\mathbf{y}_1, \dots, \mathbf{y}_t]$ by recursive application of the data update and the time update:

1. Data update:

$$p(\mathbf{x}_t|\mathbf{y}_{1:t}) = \frac{p(\mathbf{y}_t|\mathbf{x}_t)p(\mathbf{x}_t|\mathbf{y}_{1:t-1})}{p(\mathbf{y}_t|\mathbf{y}_{1:t-1})} = \frac{p(\mathbf{y}_t|\mathbf{x}_t)p(\mathbf{x}_t|\mathbf{y}_{1:t-1})}{\int p(\mathbf{y}_t|\mathbf{x}_t)p(\mathbf{x}_t|\mathbf{y}_{1:t-1})d\mathbf{x}_t}, \quad (3.2.5)$$

2. Time update:

$$p(\mathbf{x}_{t+1}|\mathbf{y}_{1:t}) = \int p(\mathbf{x}_{t+1}|\mathbf{x}_t)p(\mathbf{x}_t|\mathbf{y}_{1:t})d\mathbf{x}_t. \quad (3.2.6)$$

Given the prior pdf $p(\mathbf{x}_t|\mathbf{y}_{1:t-1})$ representing uncertainty in the forecast in time t , we use Bayes formula (3.2.5) and evaluate the posterior pdf $p(\mathbf{x}_t|\mathbf{y}_{1:t})$ representing uncertainty in the analysis in time t . Likelihood function $p(\mathbf{y}_t|\mathbf{x}_t)$ is defined by the observation model (3.2.4). In recursive Bayesian filtering, we exploit the fact that if the prior pdf is properly chosen from a class *conjugate* to (3.2.2), the formula (3.2.5) yields a posterior pdf of the same type.

Chapman–Kolmogorov equation (3.2.6) (Jazwinski, 1970) advances the the posterior $p(\mathbf{x}_t|\mathbf{y}_{1:t})$ in time and produces the forecast in time $t + 1$ represented by the prior $p(\mathbf{x}_{t+1}|\mathbf{y}_{1:t})$. Pdf $p(\mathbf{x}_{t+1}|\mathbf{x}_t)$ is called the *state transition pdf* and represents model dynamics given by (3.2.3). Integration in (3.2.5)–(3.2.6) and everywhere else in this work is performed over the maximum support of the integrand, if not stated otherwise.

Using posterior $p(\mathbf{x}_t|\mathbf{y}_{1:t})$, we can evaluate the expected value of a function $f(\cdot)$ of \mathbf{x}_t integrable with respect to $p(\mathbf{x}_t|\mathbf{y}_{1:t})$, (Doucet et al., 2001):

$$\mathbb{E}[f(\mathbf{x}_t)|\mathbf{y}_{1:t}] = \int f(\mathbf{x}_t)p(\mathbf{x}_t|\mathbf{y}_{1:t})d\mathbf{x}_t. \quad (3.2.7)$$

Evaluation of (3.2.5) and (3.2.6) may involve integration over complex spaces and in the most cases it is computationally infeasible. Thats the reason why were developed methods for solution of the problem under simplifying conditions or methods providing some sub-optimal, but still satisfactory, solution. In the following text we briefly review the basic approaches to solution of the sequential data assimilation problem.

3.3 Kalman Filter

Kalman Filter (KF) (Kalman, 1960) gives us the optimal solution for the system (3.2.3)–(3.2.4) with linear dynamics (operators \mathcal{M}_t and \mathcal{H}_t are linear) and zero mean Gaussian white noise processes \mathbf{w}_t and \mathbf{v}_t . The state transition pdf $p(\mathbf{x}_t|\mathbf{x}_{t-1})$ and the likelihood function $p(\mathbf{y}_t|\mathbf{x}_t)$ then become of the Gaussian type:

$$p(\mathbf{x}_t|\mathbf{x}_{t-1}) = \mathcal{N}(\mathbf{M}_t\mathbf{x}_{t-1}, \mathbf{Q}_t), \quad p(\mathbf{y}_t|\mathbf{x}_t) = \mathcal{N}(\mathbf{H}_t\mathbf{x}_t, \mathbf{R}_t).$$

Here, $\mathcal{N}(\boldsymbol{\mu}, \boldsymbol{\Sigma})$ is a Gaussian pdf with mean value $\boldsymbol{\mu}$ and covariance matrix $\boldsymbol{\Sigma}$. Matrices $\mathbf{M}_t \in \mathbb{R}^{N_x \times N_x}$ and $\mathbf{H}_t \in \mathbb{R}^{N_y \times N_x}$ are matrices of linear operators \mathcal{M}_t and \mathcal{H}_t , respectively. Matrices \mathbf{Q}_t and \mathbf{R}_t are known covariance matrices of model error and measurement error, respectively, with appropriate dimensions:

$$\mathbf{Q}_t = \mathbb{E} [\mathbf{v}_t \mathbf{v}_t^T], \quad \mathbf{R}_t = \mathbb{E} [\mathbf{w}_t \mathbf{w}_t^T].$$

The analysis (posterior state estimate) is in the Kalman filter represented by mean value $\bar{\mathbf{x}}_{t|t}$ and covariance matrix $\mathbf{P}_{t|t}$ of the estimated filtering Gaussian distribution:

$$\bar{\mathbf{x}}_{t|t} = \mathbb{E} [\mathbf{x}_t | \mathbf{y}_{1:t}], \quad \mathbf{P}_{t|t} = \mathbb{E} [(\mathbf{x}_t - \bar{\mathbf{x}}_{t|t})(\mathbf{x}_t - \bar{\mathbf{x}}_{t|t})^T | \mathbf{y}_{1:t}]. \quad (3.3.1)$$

Similarly, the forecast (prior state estimate) is represented with mean value $\bar{\mathbf{x}}_{t+1|t}$ and its covariance $\mathbf{P}_{t+1|t}$ of estimated predictive Gaussian distribution:

$$\bar{\mathbf{x}}_{t+1|t} = \mathbb{E} [\mathbf{x}_{t+1} | \mathbf{y}_{1:t}], \quad \mathbf{P}_{t+1|t} = \mathbb{E} [(\mathbf{x}_{t+1} - \bar{\mathbf{x}}_{t+1|t})(\mathbf{x}_{t+1} - \bar{\mathbf{x}}_{t+1|t})^T | \mathbf{y}_{1:t}]. \quad (3.3.2)$$

The data update step of the KF assimilation cycled is given by the following equations:

$$\mathbf{K}_t = \mathbf{P}_{t|t-1} \mathbf{H}_t^T (\mathbf{H}_t \mathbf{P}_{t|t-1} \mathbf{H}_t^T + \mathbf{R}_t)^{-1}, \quad (3.3.3)$$

$$\bar{\mathbf{x}}_{t|t} = \bar{\mathbf{x}}_{t|t-1} + \mathbf{K}_t (\mathbf{y}_{1:t} - \mathbf{H}_t \bar{\mathbf{x}}_{t|t-1}), \quad (3.3.4)$$

$$\mathbf{P}_{t|t} = (\mathbf{I} - \mathbf{K}_t \mathbf{H}_t) \mathbf{P}_{t|t-1} (\mathbf{I} - \mathbf{K}_t \mathbf{H}_t)^T + \mathbf{K}_t \mathbf{R}_t \mathbf{K}_t^T \quad (3.3.5)$$

$$= (\mathbf{I} - \mathbf{K}_t \mathbf{H}_t) \mathbf{P}_{t|t-1}, \quad (3.3.6)$$

where $\mathbf{I} \in \mathbb{R}^{N_x \times N_x}$ is the identity matrix. We use the Kalman gain matrix $\mathbf{K}_t \in \mathbb{R}^{N_x \times N_y}$ for linear weighing of contributions given by the current observations \mathbf{y}_t and the forecast to the resulting analysis. The analysis $\bar{\mathbf{x}}_{t|t}$ together with the posterior error covariance matrix $\mathbf{P}_{t|t}$ represent the sufficient statistics of the estimated posterior Gaussian pdf,

$$p(\mathbf{x}_t | \mathbf{y}_{1:t}) = \mathcal{N}(\bar{\mathbf{x}}_{t|t}, \mathbf{P}_{t|t}).$$

The time update given by (3.3.7)–(3.3.8)

$$\bar{\mathbf{x}}_{t+1|t} = \mathbf{M} \bar{\mathbf{x}}_{t|t}, \quad (3.3.7)$$

$$\mathbf{P}_{t+1|t} = \mathbf{M}_t \mathbf{P}_{t|t} \mathbf{M}_t^T + \mathbf{Q}_{t+1}, \quad (3.3.8)$$

evaluates new prior pdf given by the forecast $\bar{\mathbf{x}}_{t+1|t}$ and its error covariance matrix $\mathbf{P}_{t+1|t}$,

$$p(\mathbf{x}_{t+1} | \mathbf{y}_{1:t}) = \mathcal{N}(\bar{\mathbf{x}}_{t+1|t}, \mathbf{P}_{t+1|t}).$$

The algorithm is initialized with prior estimates of the mean value $\bar{\mathbf{x}}_{0|-1}$ and covariance matrix $\mathbf{P}_{0|-1}$.

Generally, violation of assumptions on linearity of the model and normality of the noise terms leads to a suboptimal solution. The computationally cheaper form of the posterior error covariance matrix (3.3.6) should be used only for the optimal gain \mathbf{K}_t , otherwise it can cause a numerical instability.

3.3.1 Suboptimal Solution for Nonlinear Model

Suboptimal modification of the KF algorithm for nonlinear \mathcal{M}_t and \mathcal{H}_t is called the *Extended Kalman Filter* (EKF) (Welch and Bishop, 1995). The EKF is based on assumption that local linearization of (3.2.3)–(3.2.4) may be sufficient description of nonlinearity. Given the \mathcal{M}_t and \mathcal{H}_t are differentiable functions, we can linearize them around the current estimates using the first terms in their Taylor series expansions:

$$\mathbf{M}_t \approx \left. \frac{\partial \mathcal{M}_t}{\partial \mathbf{x}} \right|_{\mathbf{x}=\bar{\mathbf{x}}_t|t}, \quad \mathbf{H}_t \approx \left. \frac{\partial \mathcal{H}_t}{\partial \mathbf{x}} \right|_{\mathbf{x}=\bar{\mathbf{x}}_{t+1}|t}. \quad (3.3.9)$$

Matrices \mathbf{M}_t and \mathbf{H}_t are used in the Kalman filter equations for advancing the posterior covariance matrix and during the data update step, respectively. Since the *Jacobians* (3.3.9) are dependent on the current state estimates, they must be recalculated at each time step.

If the functions \mathcal{M}_t and \mathcal{H}_t are highly nonlinear, the results of the EKF are rather poor. We can use expansions of higher orders or choose an alternative filtering methodology, e.g., the Unscented Kalman Filter (Julier and Uhlmann, 1997) or an ensemble filter.

3.4 Ensemble Filters

Since the propagation and storing of large covariance matrices is computationally demanding, formally correct KF and its variants are not suitable for high-dimensional problems commonly occurring in different geoscience applications, for instance, in meteorology (Houtekamer et al., 2005). The idea of ensemble filtering was introduced by Evensen (1994). Ensemble filters avoid explicit evolution of covariance by approximating the estimated pdf with an ensemble of states. It can be understood as a Monte Carlo approximation of the traditional KF.

3.4.1 Ensemble Kalman Filter

In *Ensemble Kalman Filter* (EnKF), a small random ensemble of states is used to represent the estimated pdf. Similarly to the KF, the EnKF makes the assumption that all probability density functions involved are Gaussian.

Let $\mathbf{X}_{t|t-1}$ denote prior ensemble in time t ,

$$\mathbf{X}_{t|t-1} = [\mathbf{x}_{t|t-1}^1, \mathbf{x}_{t|t-1}^2, \dots, \mathbf{x}_{t|t-1}^M].$$

The prior estimate $\bar{\mathbf{x}}_{t|t-1}$ and prior covariance matrix $\mathbf{P}_{t|t-1}$ are approximated as sample mean and sample variance of $\mathbf{X}_{t|t-1}$, respectively:

$$\bar{\mathbf{x}}_{t|t-1} \equiv \frac{1}{M} \sum_{i=1}^M \mathbf{x}_{t|t-1}^i, \quad (3.4.1)$$

$$\mathbf{P}_{t|t-1} \equiv \frac{1}{M-1} \sum_{i=1}^M (\mathbf{x}_{t|t-1}^i - \bar{\mathbf{x}}_{t|t-1}) (\mathbf{x}_{t|t-1}^i - \bar{\mathbf{x}}_{t|t-1})^\top. \quad (3.4.2)$$

The posterior ensemble

$$\mathbf{X}_{t|t} = [\mathbf{x}_{t|t}^1, \mathbf{x}_{t|t}^2, \dots, \mathbf{x}_{t|t}^M]$$

is given by the Bayesian data update, where each ensemble member is updated separately:

$$\mathbf{K}_t = \mathbf{P}_{t|t-1} \mathbf{H}_t^\top (\mathbf{H}_t \mathbf{P}_{t|t-1} \mathbf{H}_t^\top + \mathbf{R}_t)^{-1}, \quad (3.4.3)$$

$$\mathbf{x}_{t|t}^i = \mathbf{x}_{t|t-1}^i + \mathbf{K}_t (\mathbf{y}_{1:t}^i - \mathbf{H}_t \mathbf{x}_{t|t-1}^i), \quad i = 1, \dots, M. \quad (3.4.4)$$

A set of perturbed observation vectors $\mathbf{y}_t^i \sim \mathcal{N}(\mathbf{y}_t, \mathbf{R}_t)$, $i = 1, \dots, M$, must be used to update the ensemble members in order to fulfill (3.3.5). It can be shown that if all the ensemble members were updated with the same observation vector \mathbf{y}_t and the same gain \mathbf{K}_t , the posterior covariance will be

$$\mathbf{P}_{t|t} = (\mathbf{I} - \mathbf{K}_t \mathbf{H}_t) \mathbf{P}_{t|t-1} (\mathbf{I} - \mathbf{K}_t \mathbf{H}_t)^\top. \quad (3.4.5)$$

Without the term $\mathbf{K}_t \mathbf{R}_t \mathbf{K}_t^\top$ is the posterior covariance systematically underestimated.

Using posterior ensemble $\mathbf{X}_{t|t}$, posterior estimate $\bar{\mathbf{x}}_{t|t}$ and covariance $\mathbf{P}_{t|t}$ are approximated with its sample mean and variance:

$$\bar{\mathbf{x}}_{t|t} \equiv \frac{1}{M} \sum_{i=1}^M \mathbf{x}_{t|t}^i, \quad (3.4.6)$$

$$\mathbf{P}_{t|t} \equiv \frac{1}{M-1} \sum_{i=1}^M (\mathbf{x}_{t|t}^i - \bar{\mathbf{x}}_{t|t}) (\mathbf{x}_{t|t}^i - \bar{\mathbf{x}}_{t|t})^\top. \quad (3.4.7)$$

Advancing of the estimated Gaussian pdf approximated with the ensemble in time is achieved by simply advancing each ensemble member with the nonlinear forecast model \mathcal{M}_t :

$$\mathbf{x}_{t+1|t}^i = \mathcal{M}_t(\mathbf{x}_{t|t}^i), \quad i = 1, \dots, M.$$

Since the time evolution of the posterior covariance is performed by evolution of an ensemble, the posterior covariance itself does not have to be stored.

What is more, since only $\mathbf{P}_{t|t-1}\mathbf{H}^\top$ and $\mathbf{H}\mathbf{P}_{t|t-1}\mathbf{H}^\top$ are required during filter evaluation, the full prior covariance matrix $\mathbf{P}_{t|t-1}$ needs never to be calculated (Evensen, 1994). We can directly calculate the terms occurring in the expression for the Kalman gain,

$$\begin{aligned}\mathbf{P}_{t|t-1}\mathbf{H}_t^\top &= \frac{1}{M-1} \sum_{i=1}^M (\mathbf{x}_{t|t-1}^i - \bar{\mathbf{x}}_{t|t-1}) (\mathbf{H}_t\mathbf{x}_{t|t-1}^i - \mathbf{H}_t\bar{\mathbf{x}}_{t|t-1})^\top, \\ \mathbf{H}_t\mathbf{P}_{t|t-1}\mathbf{H}_t^\top &= \frac{1}{M-1} \sum_{i=1}^M (\mathbf{H}_t\mathbf{x}_{t|t-1}^i - \mathbf{H}_t\bar{\mathbf{x}}_{t|t-1}) (\mathbf{H}_t\mathbf{x}_{t|t-1}^i - \mathbf{H}_t\bar{\mathbf{x}}_{t|t-1})^\top.\end{aligned}$$

Covariance $\mathbf{P}_{t|t-1}$ is also used in the formula for predictive density of the observations,

$$p(\mathbf{y}_t|\mathbf{y}_{1:t-1}) = \mathcal{N}(\mathbf{H}_t\bar{\mathbf{x}}_{t|t-1}, \mathbf{Z}_t), \quad \mathbf{Z}_t = \mathbf{H}_t\mathbf{P}_{t|t-1}\mathbf{H}_t^\top + \mathbf{R}_t, \quad (3.4.8)$$

which corresponds to the standard predictive density of the Kalman filter (Peterka, 1981). This quantity is often called *marginal likelihood* (marginalization is with respect to \mathbf{x}_t) and plays an important role in statistical model selection (Jeffreys, 1961).

Efficient Implementation of EnKF

Following (Mandel, 2006), let $\tilde{\mathbf{X}}_t = [\tilde{\mathbf{x}}_t^1, \dots, \tilde{\mathbf{x}}_t^M] = [\mathbf{x}_t^1 - \bar{\mathbf{x}}_t, \dots, \mathbf{x}_t^M - \bar{\mathbf{x}}_t]$ be an ensemble of deviations from the ensemble mean. $\tilde{\mathbf{X}}_t$ can be easily calculated using

$$\tilde{\mathbf{X}}_t = \mathbf{X}_t - \frac{1}{M}(\mathbf{X}_t\boldsymbol{\Psi}_{N_x \times 1})\boldsymbol{\Psi}_{N_x \times 1}^\top,$$

where matrix $\boldsymbol{\Psi}_{N_x \times 1}$ is a matrix of all ones of dimension $N_x \times 1$ and the expression $\frac{1}{M}(\mathbf{X}_t\boldsymbol{\Psi}_{N_x \times 1})\boldsymbol{\Psi}_{N_x \times 1}^\top$ stands for the ensemble, where all the members are equal to the mean values $\bar{\mathbf{x}}_t$ of the original ensemble \mathbf{X}_t . Covariance of \mathbf{X}_t can be then evaluated using

$$\mathbf{P}_t = \frac{1}{M-1}\tilde{\mathbf{X}}_t\tilde{\mathbf{X}}_t^\top. \quad (3.4.9)$$

If we rewrite (3.4.9) as follows,

$$\mathbf{P}_t = \frac{1}{\sqrt{M-1}}\tilde{\mathbf{X}}_t \frac{1}{\sqrt{M-1}}\tilde{\mathbf{X}}_t^\top = \mathbf{S}_t\mathbf{S}_t^\top,$$

the matrix \mathbf{S}_t can be thought of as a square root of \mathbf{P}_t .

Bayesian update can be then formulated in a matrix form, where all the ensemble members are updated simultaneously and the square root $\mathbf{S}_{t|t-1}$ of $\mathbf{P}_{t|t-1}$ is used,

Algorithm 3.1 EnKF with perturbed observations.

1. Initialization. Generate a prior ensemble (background field):

$$\mathbf{X}_{0|-1} = [\mathbf{x}_{0|-1}^1, \dots, \mathbf{x}_{0|-1}^M], \quad \mathbf{x}_{0|-1}^i \sim \mathcal{N}(\bar{\mathbf{x}}_0, \mathbf{P}_0), \quad i = 1, \dots, M.$$

2. EnKF data update:

- (a) Generate perturbed measurements:

$$\mathbf{D}_t = [\mathbf{y}_t^1, \dots, \mathbf{y}_t^M], \quad \mathbf{y}_t^i \sim \mathcal{N}(\mathbf{y}_t, \mathbf{R}_t), \quad i = 1, \dots, N_y.$$

- (b) Calculate Kalman gain \mathbf{K}_t for update of ensemble:

$$\begin{aligned} \mathbf{S}_{t|t-1} &= \frac{1}{\sqrt{M-1}} \left(\mathbf{X}_{t|t-1} - \frac{1}{M} (\mathbf{X}_{t|t-1} \boldsymbol{\Psi}_{N_x \times 1}) \boldsymbol{\Psi}_{N_x \times 1}^\top \right), \\ \mathbf{Z}_t^{-1} &= \mathbf{R}_t^{-1} \left[\mathbf{I} - \mathbf{H}_t \mathbf{S}_{t|t-1} (\mathbf{I} + (\mathbf{H}_t \mathbf{S}_{t|t-1})^\top \mathbf{R}_t^{-1} \mathbf{H}_t \mathbf{S}_{t|t-1})^{-1} (\mathbf{H}_t \mathbf{S}_{t|t-1})^\top \mathbf{R}_t^{-1} \right], \\ \mathbf{K}_t &= \mathbf{S}_t (\mathbf{H}_t \mathbf{S}_t)^\top \mathbf{Z}_t^{-1}. \end{aligned}$$

- (c) Update the ensemble:

$$\mathbf{X}_{t|t} = \mathbf{X}_{t|t-1} + \mathbf{K}_t (\mathbf{D}_t - \mathbf{H}_t \mathbf{X}_{t|t-1}).$$

3. EnKF time update. Predict new ensemble:

$$\mathbf{x}_{t+1|t}^i = \mathcal{M}(\mathbf{x}_{t|t}^i), \quad i = 1, \dots, M.$$

4. Set $t := t + 1$ and iterate from step 2.
-

$$\mathbf{X}_{t|t} = \mathbf{X}_{t|t-1} + \mathbf{S}_{t|t-1} (\mathbf{H}_t \mathbf{S}_{t|t-1})^\top (\mathbf{H}_t \mathbf{S}_{t|t-1} (\mathbf{H}_t \mathbf{S}_{t|t-1})^\top + \mathbf{R}_t)^{-1} (\mathbf{D}_t - \mathbf{H}_t \mathbf{X}_{t|t-1}).$$

Here, $\mathbf{D}_t = [\mathbf{y}_t^1, \dots, \mathbf{y}_t^M]$ is the ensemble of perturbed observation vectors.

For a large number of data points, the inversion of the term $\mathbf{Z}_t = \mathbf{H}_t \mathbf{P}_{t|t-1} \mathbf{H}_t^\top + \mathbf{R}_t$ in (3.4.3) can be computationally demanding or even numerically unstable (Mandel, 2006). Given that the observations error covariance matrix \mathbf{R}_t is diagonal, i.e, the observations are uncorrelated, we can use *Sherman–Morrison–Woodbury formula* (Hager, 1989) for computation of \mathbf{Z}_t^{-1} :

$$(\mathbf{A} + \mathbf{UCV})^{-1} = \mathbf{A}^{-1} - \mathbf{A}^{-1} \mathbf{U} (\mathbf{C}^{-1} + \mathbf{VA}^{-1} \mathbf{U})^{-1} \mathbf{VA}^{-1}. \quad (3.4.10)$$

Substituting $\mathbf{A} = \mathbf{R}_t$, $\mathbf{U} = \mathbf{H}_t \mathbf{S}_{t|t-1}$, $\mathbf{C} = \mathbf{I}$, $\mathbf{V} = \mathbf{H}_t \mathbf{S}_{t|t-1}$ into (3.4.10) yields formula for \mathbf{Z}_t^{-1} , where only the diagonal matrix \mathbf{R}_t must be inverted:

$$\begin{aligned} \mathbf{Z}_t^{-1} &= [\mathbf{R}_t + \mathbf{H}_t \mathbf{S}_{t|t-1} (\mathbf{H}_t \mathbf{S}_{t|t-1})^\top]^{-1} \\ &= \mathbf{R}_t^{-1} \left[\mathbf{I} - \mathbf{H}_t \mathbf{S}_{t|t-1} (\mathbf{I} + (\mathbf{H}_t \mathbf{S}_{t|t-1})^\top \mathbf{R}_t^{-1} \mathbf{H}_t \mathbf{S}_{t|t-1})^{-1} (\mathbf{H}_t \mathbf{S}_{t|t-1})^\top \mathbf{R}_t^{-1} \right]. \end{aligned}$$

3.4.2 Ensemble Square Root Filter

The *Ensemble square root filter* (EnSRF) is a revised version of the EnKF that eliminates the necessity to perturb the observations (Whitaker and Hamill, 2002) and the posterior ensemble is formed deterministically. Deterministic methods were developed to address the problems related to sampling errors associated with the use of perturbed observations in stochastic analysis ensemble update methods (Tippett et al., 2003). Whitaker and Hamill (2002) demonstrated that for an ensemble of a given size, the EnSRF is more accurate than the EnKF.

In the EnSRF, the data update step (3.4.4) is expressed as $N + 1$ equations for separate update of the ensemble mean $\bar{\mathbf{x}}_{t|t-1}$ and the deviations $\tilde{\mathbf{x}}_{t|t-1}^i$:

$$\begin{aligned}\bar{\mathbf{x}}_{t|t} &= \bar{\mathbf{x}}_{t|t-1} + \mathbf{K}_t (\mathbf{y}_t - \mathbf{H}\bar{\mathbf{x}}_{t|t-1}), \\ \tilde{\mathbf{x}}_{t|t}^i &= \tilde{\mathbf{x}}_{t|t-1}^i - \tilde{\mathbf{K}}_t \mathbf{H} \tilde{\mathbf{x}}_{t|t-1}^i = \left(\mathbf{I} - \tilde{\mathbf{K}}_t \mathbf{H} \right) \tilde{\mathbf{x}}_{t|t-1}^i, \quad i = 1, \dots, M.\end{aligned}$$

Here, \mathbf{K}_t is the traditional Kalman gain (3.4.3) and $\tilde{\mathbf{K}}_t$ is the gain used to update the deviations. In the EnKF, $\mathbf{K}_t = \tilde{\mathbf{K}}_t$ and deviations $\tilde{\mathbf{x}}_{t|t-1}$ are updated using

$$\tilde{\mathbf{x}}_{t|t}^i = \tilde{\mathbf{x}}_{t|t-1}^i - \mathbf{K}_t (\tilde{\mathbf{y}}_t^i - \mathbf{H}\tilde{\mathbf{x}}_{t|t-1}^i), \quad i = 1, \dots, M, \quad (3.4.11)$$

where $\tilde{\mathbf{y}}_t^i \sim \mathcal{N}(\mathbf{0}, \mathbf{R}_t)$ are the deviations of perturbed measurements from the mean \mathbf{y}_t (Burgers et al., 1998).

Whitaker and Hamill (2002) derived a formula for $\tilde{\mathbf{K}}_t$ that will result in an ensemble whose posterior error covariance satisfies (3.3.5). Substituting $\tilde{\mathbf{K}}_t$ into (3.4.5) and requiring the expression to be equal to the correct $\mathbf{P}_{t|t}$, we obtain the following equation for $\tilde{\mathbf{K}}_t$,

$$(\mathbf{I} - \tilde{\mathbf{K}}_t \mathbf{H}) \mathbf{P}_{t|t-1} (\mathbf{I} - \tilde{\mathbf{K}}_t \mathbf{H})^T = (\mathbf{I} - \tilde{\mathbf{K}}_t \mathbf{H}) \mathbf{P}_{t|t-1} (\mathbf{I} - \tilde{\mathbf{K}}_t \mathbf{H})^T + \tilde{\mathbf{K}}_t \mathbf{R}_t \tilde{\mathbf{K}}_t^T, \quad (3.4.12)$$

which has a solution

$$\tilde{\mathbf{K}}_t = \mathbf{P}_{t|t-1} \mathbf{H}^T \left[\left(\sqrt{\mathbf{H} \mathbf{P}_{t|t-1} \mathbf{H}^T + \mathbf{R}_t} \right)^{-1} \right]^T \left[\sqrt{\mathbf{H} \mathbf{P}_{t|t-1} \mathbf{H}^T + \mathbf{R}_t} + \sqrt{\mathbf{R}_t} \right]^{-1}. \quad (3.4.13)$$

The fact that the evaluation of (3.4.13) involves square roots of error covariance matrices is the reason why the algorithm implementing the deterministic version of data update is called the ensemble square root filter. The matrix square roots in (3.4.13) are not unique and can be calculated by a commonly used factorization methods, e.g., Cholesky or singular value decomposition.

Given that the state evolution operator \mathcal{M}_t is linear, the posterior ensemble mean $\bar{\mathbf{x}}_{t|t}$ and the posterior deviations from the mean $\tilde{\mathbf{x}}_{t|t}^i$ can be evolved separately

$$\begin{aligned}\bar{\mathbf{x}}_{t+1|t} &= \mathbf{M}_t \bar{\mathbf{x}}_{t|t}, \\ \tilde{\mathbf{X}}_{t+1|t} &= \mathbf{M}_t \tilde{\mathbf{X}}_{t|t}.\end{aligned}$$

Otherwise, the full ensemble \mathbf{X}_t must be formed before the time update.

Sequential Processing of Observations

For an individual observation, i.e., when $\mathbf{H} \in \mathbb{R}^{1 \times N_x}$ and $\mathbf{R}_t \in \mathbb{R}$, the terms $\mathbf{HP}_{t|t-1}\mathbf{H}^\mathbf{T}$ and \mathbf{R}_t reduce to scalars and (3.4.12) may be written as follows,

$$\frac{\mathbf{HP}_{t|t-1}\mathbf{H}^\mathbf{T}}{\mathbf{HP}_{t|t-1}\mathbf{H}^\mathbf{T} + \mathbf{R}_t} \tilde{\mathbf{K}}_t \tilde{\mathbf{K}}_t - \mathbf{K}_t \tilde{\mathbf{K}}_t - \tilde{\mathbf{K}}_t \mathbf{K}_t + \mathbf{K}_t \mathbf{K}_t = \mathbf{0}. \quad (3.4.14)$$

If the desired gain $\tilde{\mathbf{K}}_t$ is assumed to be linearly proportional to the original gain \mathbf{K} ,

$$\tilde{\mathbf{K}}_t = \alpha_t \mathbf{K}_t, \quad (3.4.15)$$

where $\alpha \in \mathbb{R}$ is a constant, we obtain

$$\frac{\mathbf{HP}_{t|t-1}\mathbf{H}^\mathbf{T}}{\mathbf{HP}_{t|t-1}\mathbf{H}^\mathbf{T} + \mathbf{R}_t} \alpha^2 \mathbf{K}_t \mathbf{K}_t - 2\alpha \mathbf{K}_t \mathbf{K}_t - \mathbf{K}_t \mathbf{K}_t = \mathbf{0}. \quad (3.4.16)$$

This yields a quadratic equation for α

$$\frac{\mathbf{HP}_{t|t-1}\mathbf{H}^\mathbf{T}}{\mathbf{HP}_{t|t-1}\mathbf{H}^\mathbf{T} + \mathbf{R}_t} \alpha^2 - 2\alpha \mathbf{K}_t \mathbf{K}_t + 1 = 0. \quad (3.4.17)$$

The equation has two roots. Since we want the deviations from the ensemble mean to be reduced in magnitude, i.e., to decrease posterior variance of the ensemble, and to maintain the same sign, the appropriate solution is

$$\alpha_t = \left(1 + \sqrt{\frac{\mathbf{R}_t}{\mathbf{HP}_{t|t-1}\mathbf{H}^\mathbf{T} + \mathbf{R}_t}} \right)^{-1}, \quad (3.4.18)$$

which is always between 0 and 1 (Whitaker and Hamill, 2002).

In the case of non-correlated observations, when the observation error covariance matrix \mathbf{R}_t is diagonal, the observations \mathbf{y}_t can be processed sequentially, one at a time. Updating the deviations from ensemble mean with $\tilde{\mathbf{K}}_t$ given by (3.4.15) and (3.4.18) ensures the posterior error covariance to be equal to (3.3.5). Algorithm of EnSRF with sequential processing of observations is summarized in Algorithm 3.2.

Algorithm 3.2 EnSRF with sequential processing of observations.

1. Initialization. Generate a prior ensemble (background field):

$$\mathbf{X}_{0|-1} = [\mathbf{x}_{0|-1}^1, \dots, \mathbf{x}_{0|-1}^M], \quad \mathbf{x}_t^i \sim \mathcal{N}(\bar{\mathbf{x}}_0, \mathbf{P}_0), \quad i = 1, \dots, M,$$

and set $t := 0$.

2. EnSRF data update. For $j = 1, \dots, N_y$:

- (a) Calculate Kalman gain $\mathbf{K}_{j;t}$ for update of ensemble mean with j th observation

$$\begin{aligned} \mathbf{S}_{t|t-1} &= \frac{1}{\sqrt{M-1}} \left(\mathbf{X}_t - \frac{1}{M} (\mathbf{X}_t \boldsymbol{\Psi}_{N_x \times 1}) \boldsymbol{\Psi}_{N_x \times 1}^\top \right), \\ \mathbf{K}_{j;t} &= \frac{\mathbf{S}_{t|t-1} (\mathbf{H}_j \mathbf{S}_{t|t-1})^\top}{\mathbf{H}_j \mathbf{S}_{t|t-1} (\mathbf{H}_j \mathbf{S}_{t|t-1})^\top + \mathbf{R}_{j;t}}, \end{aligned}$$

where $\mathbf{R}_{j;t}$ is variance of j -th observation and $\mathbf{H}_j \in \mathbb{R}^{1 \times n}$ is the corresponding observation operator.

- (b) Calculate Kalman gain $\tilde{\mathbf{K}}_{j;t}$ for update of deviations from the mean with j -th observation:

$$\begin{aligned} \tilde{\mathbf{K}}_{j;t} &= \alpha_{j;t} \mathbf{K}_{j;t}, \\ \alpha_{j;t} &= \left[1 + \sqrt{\frac{\mathbf{R}_{j;t}}{(\mathbf{H}_j \mathbf{S}_{t|t-1}) (\mathbf{H}_j \mathbf{S}_{t|t-1})^\top + \mathbf{R}_{j;t}}} \right]^{-1}. \end{aligned}$$

- (c) Update of ensemble mean $\bar{\mathbf{x}}_{t|t-1}$ and departures from the mean $\tilde{\mathbf{X}}_{t|t-1}$

$$\begin{aligned} \bar{\mathbf{x}}_{t|t} &= \bar{\mathbf{x}}_{t|t-1} + \mathbf{K}_t (\mathbf{y}_t - \mathbf{H} \bar{\mathbf{x}}_{t|t-1}) \\ \tilde{\mathbf{x}}_{t|t}^i &= \tilde{\mathbf{x}}_{t|t-1}^i - \tilde{\mathbf{K}}_t \mathbf{H} \tilde{\mathbf{x}}_{t|t-1}^i, \quad i = 1, \dots, M. \end{aligned}$$

3. EnSRF time update. Predict new ensemble according to:

$$\mathbf{x}_{t+1|t}^i = \mathcal{M}(\mathbf{x}_{t|t}^i), \quad i = 1, \dots, M.$$

4. Set $t := t + 1$ and iterate from step 2.
-

3.4.3 Sampling Error Issues in Ensemble Filtering

Ensemble Inflation

For a finite-sized ensemble, there is a sampling error in the estimation of forecast error covariance matrix (3.4.2). The theoretical exact forecast error covariance obtained from an infinite-sized ensemble differs from any obtained from a finite-sized ensemble of $M \in \mathbb{N}$ members (Whitaker and Hamill, 2002). Implication of this fact is, that in ensemble-based assimilation systems, the forecast error is systematically underestimated. Information brought by new measurements is then penalized because the measurement error seems to be relatively higher to the underestimated forecast error.

Filter becomes too confident in the forecast and the divergence may occur. This effect can be observed particularly in small ensembles. Multiplicative *ensemble inflation* is a method for artificial increase of the model forecast error variance (Anderson and Anderson, 1999). The inflation is used to replace the forecast ensemble according to:

$$\mathbf{x}^i \rightarrow \Delta (\mathbf{x}^i - \bar{\mathbf{x}}^i) + \bar{\mathbf{x}}^i, \quad i = 1, \dots, M \quad (3.4.19)$$

with *inflation factor* Δ slightly greater than 1. From (3.4.19) is obvious that the mean value of the ensemble remains unchanged but its variance is increased.

Localization of Covariance

The sampling error introduced by the finite ensemble size also causes *spurious covariances* in the estimated forecast error covariance matrix. Techniques of *covariance localization* filter out the small and noisy covariances and reduce the impact of the observations on remote state variables. In spatial data assimilation, where the state vector usually represent values of a quantity on a computational grid, the distance between states and observation simply denotes the real geographical distance between the grid points and the place of observation. Localization of a covariance matrix can be performed by using the *Schur product* of a localization matrix with the covariance matrix (Gaspari and Cohn, 1999). Schur product is an element-by-element matrix multiplication: the Schur product $\mathbf{A} \circ \mathbf{B}$ of matrices $\mathbf{A} \in \mathbb{R}^{m \times n}$ and $\mathbf{B} \in \mathbb{R}^{m \times n}$ is matrix $\mathbf{C} \in \mathbb{R}^{m \times n}$, where $C_{ij} = A_{ij}B_{ij}$, $i = 1, \dots, n$, $j = 1, \dots, m$.

More specifically, we modify the formula for the Kalman gain (3.4.3) to be

$$\mathbf{K}_t = (\boldsymbol{\rho} \circ \mathbf{P}_{t|t-1})\mathbf{H}_t^T (\mathbf{H}_t(\boldsymbol{\rho} \circ \mathbf{P}_{t|t-1})\mathbf{H}_t^T + \mathbf{R}_t)^{-1}, \quad (3.4.20)$$

where $\boldsymbol{\rho}$ is a localization matrix (Houtekamer and Mitchell, 2001). Localization matrices are constructed by the means of correlation functions. Maximum of such a function reached at the observation location is 1 and the function typically decreases monotonically to zero at some finite distance from the observation location. The rate of correlation decrease with distance is given by the *length-scale parameter* l . Let $\|D_{ij}\|$ be the Euclidean distance between the observation location i and the grid points j . Then the example of a localization function is the compactly supported, 5th order piecewise rational function $\Omega(\sqrt{10/3}l, \|D_{ij}\|)$ suggested by Gaspari and Cohn (1999):

$$\Omega(a, b) = \begin{cases} -\frac{1}{4} \left(\frac{b}{a}\right)^5 + \frac{1}{2} \left(\frac{b}{a}\right)^4 + \frac{5}{8} \left(\frac{b}{a}\right)^3 - \frac{5}{3} \left(\frac{b}{a}\right)^2 + 1, & \text{if } 0 \leq b \leq a; \\ \frac{1}{12} \left(\frac{b}{a}\right)^5 - \frac{1}{2} \left(\frac{b}{a}\right)^4 + \frac{5}{8} \left(\frac{b}{a}\right)^3 + \frac{5}{3} \left(\frac{b}{a}\right)^2 - 5 \left(\frac{b}{a}\right) + 4 - \frac{2}{3} \left(\frac{a}{b}\right), & \text{if } a < b \leq 2a; \\ 0, & \text{if } b > 2a, \end{cases} \quad (3.4.21)$$

where a and b correspond to $\sqrt{10/3}l$ and $\|D_{ij}\|$, respectively. Function given by (3.4.21) is similar to the Gaussian distribution in shape but is has a compact support. It is a homogeneous and isotropic correlation function, it means that it has the same behavior in all direction and the rate of correlation decrease is also invariant to translation of

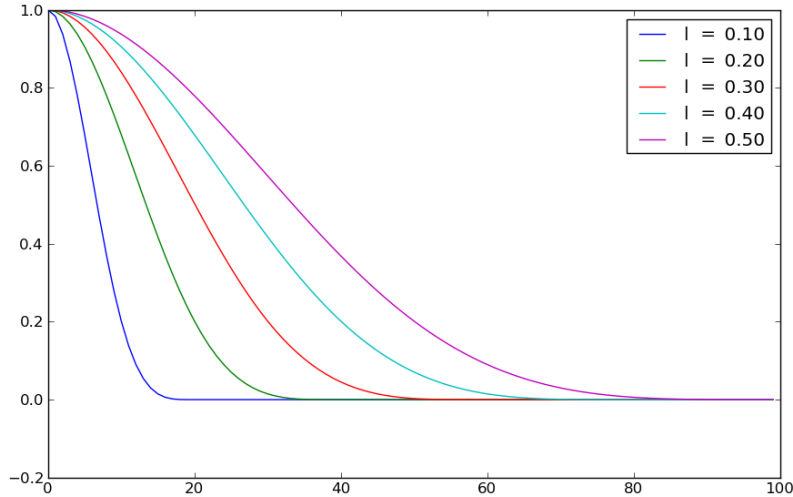


Figure 3.4.1: Correlation function given by (3.4.21) with different values of the length-scale parameter l .

observation location in space. Correlation function given by (3.4.21) with different values of l is visualized in Figure 3.4.1.

Illustration of localization effect on spatial data is illustrated in Figure 3.4.2. In Figure 3.4.2 (a), a contour plot of spatial covariance of a point denoted with the red circle with the rest of the polar computational grid is visualized. In Figures 3.4.2 (b)–(d), we see the resulting covariance after application of the localization using a localization matrices given by (3.4.21) with different values of the length-scale parameter l .

3.5 Particle Filter

Particle filtering (PF) refers to a group of methods further generalizing the Bayesian update problem for non-Gaussian pdfs. It includes a range of Monte Carlo techniques for generating an empirical approximation of posterior $p(\mathbf{x}_{1:t}|\mathbf{y}_{1:t})$ of a state trajectory $\mathbf{x}_{1:t} = (\mathbf{x}_1, \dots, \mathbf{x}_t)$,

$$p(\mathbf{x}_{1:t}|\mathbf{y}_{1:t}) \approx \frac{1}{N} \sum_{i=1}^N \delta(\mathbf{x}_{1:t} - \mathbf{x}_{1:t}^{(i)}). \quad (3.5.1)$$

Here, $\mathbf{x}_{1:t}^{(i)}$, $i = 1, \dots, N$, are i.i.d. samples from the posterior $p(\mathbf{x}_{1:t}|\mathbf{y}_{1:t})$ and $\delta(\cdot)$ is the Dirac δ -function. It comes out from the method of Monte Carlo integration. Expected value of an arbitrary function $f(\cdot)$ of $\mathbf{x}_{1:t}$ integrable with respect to $p(\mathbf{x}_{1:t}|\mathbf{y}_{1:t})$ can be

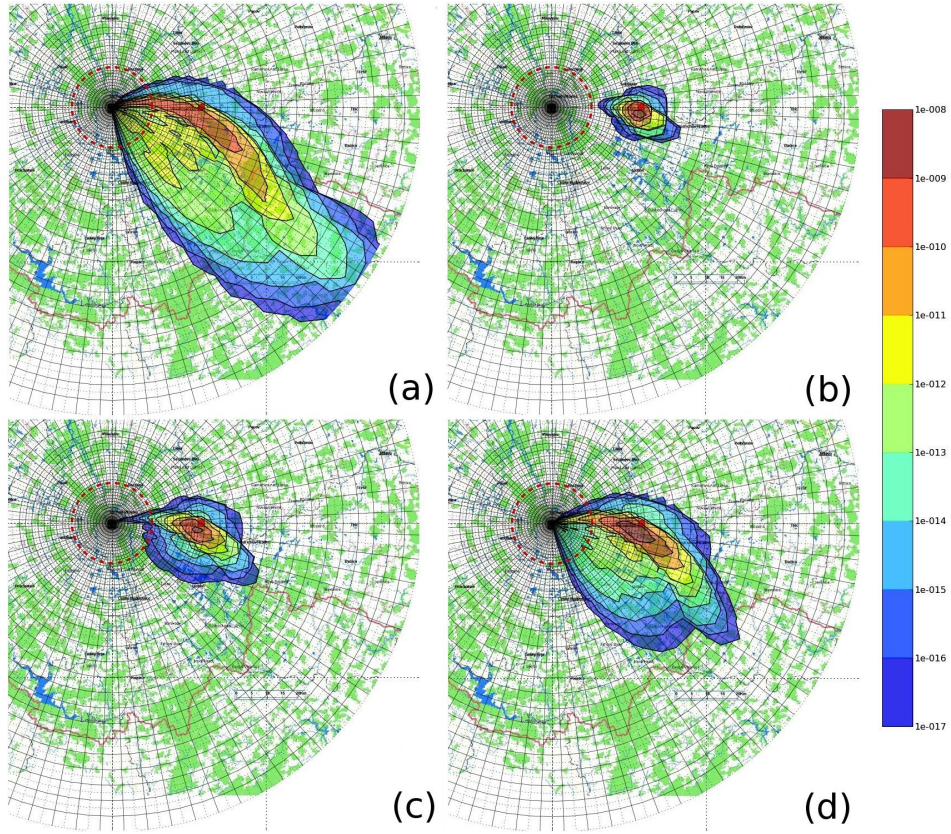


Figure 3.4.2: Illustration of the effect of covariance localization; (a) contour plot of spatial covariance (without localization) of a point denoted with the red circle with the rest of the polar computational grid; (b)–(d) resulting covariance after application of the localization using localization matrices given by (3.4.21) with increasing value of the length-scale parameter l .

then approximated as

$$\mathbb{E}[f(\mathbf{x}_{1:t})|\mathbf{y}_{1:t}] = \int f(\mathbf{x}_{1:t})p(\mathbf{x}_{1:t}|\mathbf{y}_{1:t})d\mathbf{x}_{1:t} \approx \frac{1}{N} \sum_{i=1}^N f(\mathbf{x}_{1:t}^{(i)}), \quad (3.5.2)$$

and the rate of convergence of this approximation is independent of the dimension of the integrand (Doucet et al., 2001).

In most of real applications we are not able to sample directly from the exact posterior, however, we can draw samples from a chosen *proposal density* (importance function) $q(\mathbf{x}_{1:t}|\mathbf{y}_{1:t})$:

$$\begin{aligned} p(\mathbf{x}_{1:t}|\mathbf{y}_{1:t}) &= \frac{p(\mathbf{x}_{1:t}|\mathbf{y}_{1:t})}{q(\mathbf{x}_{1:t}|\mathbf{y}_{1:t})}q(\mathbf{x}_{1:t}|\mathbf{y}_{1:t}) \\ &\approx \frac{p(\mathbf{x}_{1:t}|\mathbf{y}_{1:t})}{q(\mathbf{x}_{1:t}|\mathbf{y}_{1:t})} \frac{1}{N} \sum_{i=1}^N \delta(\mathbf{x}_{1:t} - \mathbf{x}_{1:t}^{(i)}). \end{aligned} \quad (3.5.3)$$

Approximation (3.5.3) can be written in a form of the *weighted* empirical distribution,

$$p(\mathbf{x}_{1:t}|\mathbf{y}_{1:t}) \approx \sum_{i=1}^N w_t^{(i)} \delta(\mathbf{x}_{1:t} - \mathbf{x}_{1:t}^{(i)}), \quad (3.5.4)$$

$$w_t^{(i)} \propto \frac{p(\mathbf{x}_{1:t}^{(i)}|\mathbf{y}_{1:t})}{q(\mathbf{x}_{1:t}^{(i)}|\mathbf{y}_{1:t})}. \quad (3.5.5)$$

Under this *importance sampling* procedure (Rubinstein and Kroese, 2008), the true posterior distribution needs to be evaluated point-wise only, since (3.5.4) can be normalized trivially via a constant $c = \sum_{i=1}^N w_t^{(i)}$.

In the following text, we will show how to recursively update a pdf given as a weighted empirical distribution. Following Ristic et al. (2004), suppose we have a set of samples approximating posterior $p(\mathbf{x}_{1:t-1}|\mathbf{y}_{1:t-1})$ at time $t-1$ and a new vector of measurements \mathbf{y}_t . We wish to approximate $p(\mathbf{x}_{1:t}|\mathbf{y}_{1:t})$ with a new set of samples. If the proposal density is chosen to factorize such that

$$q(\mathbf{x}_{1:t}|\mathbf{y}_{1:t}) = q(\mathbf{x}_t|\mathbf{x}_{1:t-1}, \mathbf{y}_{1:t})q(\mathbf{x}_{1:t-1}|\mathbf{y}_{1:t-1}), \quad (3.5.6)$$

then the new samples $\mathbf{x}_{1:t}^{(i)} \sim q(\mathbf{x}_{1:t}|\mathbf{y}_{1:t})$ can be obtained by augmenting each of the existing samples $\mathbf{x}_{1:t-1}^{(i)} \sim q(\mathbf{x}_{1:t-1}|\mathbf{y}_{1:t-1})$ with the new state $\mathbf{x}_t^{(i)} \sim q(\mathbf{x}_t|\mathbf{x}_{1:t-1}, \mathbf{y}_{1:t})$. Using the chain rule and the Bayes formula, $p(\mathbf{x}_{1:t}|\mathbf{y}_{1:t})$ can be written in terms of $p(\mathbf{x}_{1:t-1}|\mathbf{y}_{1:t-1})$, $p(\mathbf{x}_t|\mathbf{x}_{t-1})$ and $p(\mathbf{y}_t|\mathbf{x}_t)$, as follows:

$$\begin{aligned} p(\mathbf{x}_{1:t}|\mathbf{y}_{1:t}) &= \frac{p(\mathbf{y}_t|\mathbf{x}_{1:t}, \mathbf{y}_{1:t-1})p(\mathbf{x}_{1:t}|\mathbf{y}_{1:t-1})}{p(\mathbf{y}_t|\mathbf{y}_{1:t-1})} \\ &= \frac{p(\mathbf{y}_t|\mathbf{x}_{1:t}, \mathbf{y}_{1:t-1})p(\mathbf{x}_t|\mathbf{x}_{1:t-1}, \mathbf{y}_{1:t-1})p(\mathbf{x}_{1:t-1}|\mathbf{y}_{1:t-1})}{p(\mathbf{y}_t|\mathbf{y}_{1:t-1})} \\ &= \frac{p(\mathbf{y}_t|\mathbf{x}_t)p(\mathbf{x}_t|\mathbf{x}_{t-1})p(\mathbf{x}_{1:t-1}|\mathbf{y}_{1:t-1})}{p(\mathbf{y}_t|\mathbf{y}_{1:t-1})} \end{aligned} \quad (3.5.7)$$

$$\propto p(\mathbf{y}_t|\mathbf{x}_t)p(\mathbf{x}_t|\mathbf{x}_{t-1})p(\mathbf{x}_{1:t-1}|\mathbf{y}_{1:t-1}) \quad (3.5.8)$$

By substituting (3.5.6) and (3.5.7) into (3.5.5), (3.5.5) may be written in the following recursive form:

$$\begin{aligned} w_t^{(i)} &\propto \frac{p(\mathbf{y}_t|\mathbf{x}_t^{(i)})p(\mathbf{x}_t^{(i)}|\mathbf{x}_{t-1}^{(i)})p(\mathbf{x}_{1:t-1}^{(i)}|\mathbf{y}_{1:t-1})}{q(\mathbf{x}_t^{(i)}|\mathbf{x}_{1:t-1}^{(i)}, \mathbf{y}_{1:t})q(\mathbf{x}_{1:t-1}^{(i)}|\mathbf{y}_{1:t-1})} \\ &\propto w_{t-1}^{(i)} \frac{p(\mathbf{y}_t|\mathbf{x}_t^{(i)})p(\mathbf{x}_t^{(i)}|\mathbf{x}_{t-1}^{(i)})}{q(\mathbf{x}_t^{(i)}|\mathbf{x}_{1:t-1}^{(i)}, \mathbf{y}_{1:t})}. \end{aligned} \quad (3.5.9)$$

Furthermore, if the proposal density is chosen as follows,

$$q(\mathbf{x}_t|\mathbf{x}_{1:t-1}, \mathbf{y}_{1:t}) = q(\mathbf{x}_t|\mathbf{x}_{t-1}, \mathbf{y}_t) \quad (3.5.10)$$

then the proposal density becomes only dependent on the \mathbf{x}_{t-1} and \mathbf{y}_t . This is particularly useful in the common case when only an estimate of the marginal posterior $p(\mathbf{x}_t|\mathbf{y}_{1:t})$ is required at each time step. It means, that only samples $\mathbf{x}_t^{(i)}$ need to be stored (Ristic et al., 2004) and the marginal posterior density $p(\mathbf{x}_t|\mathbf{y}_{1:t})$ can be approximated as

$$p(\mathbf{x}_t|\mathbf{y}_{1:t}) \approx \sum_{i=1}^N w_t^{(i)} \delta(\mathbf{x}_t - \mathbf{x}_t^{(i)}), \quad (3.5.11)$$

$$w_t^{(i)} \propto w_{t-1}^{(i)} \frac{p(\mathbf{y}_t|\mathbf{x}_t^{(i)})p(\mathbf{x}_t^{(i)}|\mathbf{x}_{t-1}^{(i)})}{q(\mathbf{x}_t^{(i)}|\mathbf{x}_{t-1}^{(i)}, \mathbf{y}_t)}. \quad (3.5.12)$$

Using the particles, the mean value $\bar{\mathbf{x}}_{1:t}$ and the covariance $\Sigma_{1:t}$ of the posterior approximation (3.5.4) can be calculated as follows,

$$\bar{\mathbf{x}}_{1:t} = \sum_{i=1}^N w_t^{(i)} \mathbf{x}_{1:t}^{(i)}, \quad (3.5.13)$$

$$\Sigma_{1:t} = \sum_{i=1}^N w_t^{(i)} \left[\left(\mathbf{x}_{1:t}^{(i)} - \bar{\mathbf{x}}_{1:t} \right) \left(\mathbf{x}_{1:t}^{(i)} - \bar{\mathbf{x}}_{1:t} \right)^T \right]. \quad (3.5.14)$$

The scheme for sequential evaluation of the weight with incoming observations is referred to as *sampling-importance-sampling* (SIS) (Andrieu et al., 2003). Besides the appropriate choice of the proposal density, successful application of the PF requires more steps, namely implementation of a re-sampling algorithm, which avoids degeneracy of the weights.

3.5.1 Degeneracy Problem and Re-sampling

The variance of weights (3.5.9) increases during their recursive evaluation. The increase has a harmful effect on the accuracy and leads to the weights degeneracy, which is a common problems with the SIS particle filter (Ristic et al., 2004). The weights degeneracy means, that after certain number of recursive steps, all but one particle have negligible normalized weight which implies sample impoverishment and loss of diversity of the particles. In the SIS framework, weight degeneracy is unavoidable and has negative effects. Computational time must be spent on propagation of particles with negligible weights whose contribution to the approximation of $p(\mathbf{x}_t|\mathbf{y}_{1:t})$ is small.

A suitable measure of degeneracy of an algorithm is the effective sample size N_{eff} (Ristic et al., 2004), which can be estimated using normalized weights $w_t^{(i)}$ as follows:

$$\overline{N_{\text{eff}}} = \frac{1}{\sum_{i=1}^N (w_t^{(i)})^2}, \quad (3.5.15)$$

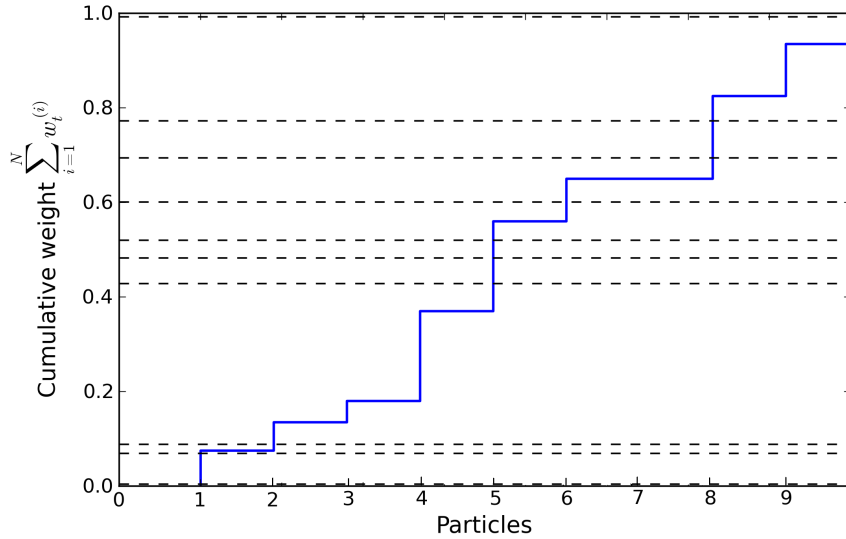


Figure 3.5.1: Illustration of basic principle of re-sampling in PF. The piecewise-constant blue line denotes the cumulative weight $\sum_i w_t^{(i)}$ of $N = 10$ particles. The higher the weight $w_t^{(i)}$, the longer the interval I (3.5.17) and the higher the probability that random samples $u_i \sim \mathcal{U}[0, 1)$, denoted with dashed lines, are from I . Particle 1 was copied twice, particle 2 once, particle 5 for three times, particle 6 once, particle 8 twice and particle 10 once.

When all the weight are approximately of the same value—ideally $w_t^{(i)} = 1/N$, $i = 1, \dots, N$ —then $\overline{N}_{\text{eff}} = N$. If there is a particle j such that $w_t^{(j)} = 1$, and $w_t^{(i)} = 0$ for all $i \neq j$, then $\overline{N}_{\text{eff}} = 1$. Small values of $\overline{N}_{\text{eff}}$ indicate a severe degeneracy of particle weights and the particles should be re-sampled.

Re-sampling is a method for elimination of the particles with low importance weights and copying of those samples with high importance weights. Reproduction of the best particles brings more focus on the promising parts of the state-space. During re-sampling, a random measure $\{\mathbf{x}_t^{(i)}, w_t^{(i)}\}_{i=1}^N$ is replaced with $\{\mathbf{x}_t^{(i)*}, 1/N\}_{i=1}^N$ with uniform weights (Ristic et al., 2004). Re-sampling is not deterministic. The new set of particles and weights is generated in a way that the probability of sampling a particle $\mathbf{x}_t^{(j)}$ from discrete approximation of $p(\mathbf{x}_t|\mathbf{y}_{1:t})$ is given by its normalized importance weight $w_t^{(j)}$:

$$\Pr(\mathbf{x}_t^{(i)*} = \mathbf{x}_t^{(j)}) = w_t^{(j)}, \quad i = 1, \dots, N. \quad (3.5.16)$$

The resulting sample is an i.i.d. sample from the discrete approximation of density $p(\mathbf{x}_t|\mathbf{y}_{1:t})$, where the weights of all the particles are uniform.

Illustration of the basic idea behind the re-sampling is in Figure 3.5.1. The piecewise-constant blue line denotes the cumulative weight $\sum_i w_t^{(i)}$ of $N = 10$ particles. Particles with high weights have a high probability being re-sampled. The higher the weight $w_t^{(i)}$,

Algorithm 3.3 Systematic re-sampling.

1. Generate N increasingly ordered numbers

$$u_j = \frac{(j-1) + \tilde{u}}{N}, \quad j = 1, \dots, N,$$

where \tilde{u} is sampled from uniform distribution $\mathcal{U}(0,1)$.

2. Produce new set of particles. Particle $\mathbf{x}_t^{(i)}$ is copied n_i -times, where

$$n_i \text{ is the number of } u_k \in \left[\sum_{s=1}^{i-1} w_t^{(s)}, \sum_{s=1}^i w_t^{(s)} \right).$$

the longer the interval

$$I = \left[\sum_{s=1}^{i-1} w_t^{(s)}, \sum_{s=1}^i w_t^{(s)} \right), \quad i = 1, \dots, N, \quad (3.5.17)$$

and the higher the probability that random samples $u_i \sim \mathcal{U}[0,1)$, denoted with dashed lines, will be from I . In the figure, particle 1 was copied twice, particle 2 once, particle 5 for three times, particle 6 once, particle 8 twice and particle 10 once. These 10 samples with uniform weights represent the re-sampled empirical density.

Example of a re-sampling algorithm is the *systematic re-sampling* given in Algorithm 3.3, where we have to sample only one number from $\mathcal{U}[0,1)$. Modification of the SIS algorithm with re-sampling is called *sampling-importance-resampling* (SIR), see Algorithm 3.4. More on re-sampling algorithms can be found, e.g., in (Douc and Cappé, 2005).

3.5.2 Choice of Proposal Density

The choice of proposal density $q(\mathbf{x}_{1:t}|\mathbf{y}_{1:t})$ plays a crucial role in particle filtering. There is no easy prescription for choosing a good proposal density, nevertheless, we can summarize its typically desirable properties (Oh and Berger, 1992):

- It should have convenient Monte Carlo properties, i.e., it should be easy to draw random samples from it.
- The tails of $q(\cdot)$ should not be sharper than the tails of $p(\cdot)$. Otherwise, approximation of $p(\cdot)$ may have a large variance or even fail to converge.
- Proposal density $q(\cdot)$ should mimic $p(\cdot)$ well.

The most straightforward choice of the proposal density in the recursive scheme (3.5.9) is the state transition pdf

$$q(\mathbf{x}_t^{(i)}|\mathbf{x}_{t-1}^{(i)}, \mathbf{y}_t) = p(\mathbf{x}_t|\mathbf{x}_{t-1}). \quad (3.5.18)$$

Algorithm 3.4 Sampling–importance–re-sampling algorithm (particle filter).

1. Initialization. For $i = 1, \dots, N$ initialize particles $\mathbf{x}_{0|-1}^{(i)} \sim p(\mathbf{x}_0)$ and set $t := 0$.

2. PF data update: Evaluate the importance weights

$$\tilde{w}_t^{(i)} = w_{t-1}^{(i)} p(\mathbf{y}_t | \mathbf{x}_{t|t-1}^{(i)}), \quad i = 1, \dots, N,$$

and normalize $w_t^{(i)} = \tilde{w}_t^{(i)} / \sum_{j=1}^N \tilde{w}_t^{(j)}$.

3. Re-sampling: Evaluate estimate of effective sample size $\overline{N}_{\text{eff}}$. If $\overline{N}_{\text{eff}} < N_{\text{Thr}}$, where N_{Thr} is a given threshold, sample N particles, with replacement, according to

$$\Pr(\mathbf{x}_{t|t}^{(i)} = \mathbf{x}_{t|t-1}^{(j)}) = w_t^{(j)}, \quad i = 1, \dots, N,$$

and set uniform weights $w_t^{(i)} = \frac{1}{N}$, $i = 1, \dots, N$.

4. PF time update: Predict new particles according to

$$\mathbf{x}_{t+1|t}^{(i)} \sim p(\mathbf{x}_{t+1|t} | \mathbf{x}_{t|t}^{(i)}), \quad i = 1, \dots, N.$$

5. Set $t := t + 1$ and iterate from step 2.

Under the choice (3.5.18), the recursion of weights (3.5.11) is given by

$$w_t^{(i)} \propto w_{t-1}^{(i)} p(\mathbf{y}_t | \mathbf{x}_t^{(i)}). \quad (3.5.19)$$

However, this popular choice is rather sub-optimal.

More advanced approaches are based on adaptive selection of the proposal, where we assume a parameterized form of the proposal in time t and estimate its parameters using weights $w_t^{(i)}$ (Andrieu et al., 2003, 2010). The approach can be extended for estimation of the proposal of the whole state trajectory up to time t . From the re-estimated proposal $q(\mathbf{x}_{1:t} | \mathbf{y}_{1:t})$ we can generate new population of trajectories $\mathbf{x}_{1:t}^{(i)}$ and recompute the weights from the beginning up to time t . For instance, given that the proposal density is assumed to be a multidimensional Gaussian pdf, we use the weights for estimation of its mean and covariance matrix. This example is a simple choice and more elaborated proposal densities can be constructed, e.g., a parametrized proposal in the form of a Gaussian mixture estimated using the EM algorithm (Dempster et al., 1977).

The PF algorithm with an adaptive selection of the proposal density is summarized in Algorithm 3.5. In Step 2, weights $w_t^{(i)}$ are computed using up-to-now observation $\mathbf{y}_{1:t}$. The weights are used for re-estimation of the proposal density $q(\mathbf{x}_{1:t} | \mathbf{y}_{1:t})$ in Step 3. Up-to-now trajectories of particles are discarded and new trajectories are sampled from the corrected proposal in Step 4. The new trajectories are augmented with the forecasts of the state values for the next time step evaluated using the state transition density. In Step 5, we increment the time index and proceed to Step 2, where the

Algorithm 3.5 Particle filter with adaptive selection of proposal density.

1. Initialization. For $i = 1, \dots, N$ initialize particles $\mathbf{x}_0^{(i)} \sim p(\mathbf{x}_0)$ and set $t := 0$.

2. Evaluation of normalized weights $w_t^{(i)}$

$$w_t^{(i)} \propto \frac{p(\mathbf{x}_{1:t}^{(i)} | \mathbf{y}_{1:t})}{q(\mathbf{x}_{1:t}^{(i)} | \mathbf{y}_{1:t})}.$$

3. Adaptive selection of proposal density $q(\mathbf{x}_{1:t} | \mathbf{y}_{1:t})$ for the next time step using weights $w_t^{(i)}$ and particle trajectories $\mathbf{x}_{1:t}^{(i)}$.

4. Sample new trajectories from for the next time step:

(a) $\mathbf{x}_{1:t+1}^{(i)} \sim q(\mathbf{x}_{1:t+1} | \mathbf{y}_{1:t})$, where $q(\mathbf{x}_{1:t+1} | \mathbf{y}_{1:t}) = q(\mathbf{x}_{1:t} | \mathbf{y}_{1:t})p(\mathbf{x}_{t+1} | \mathbf{x}_t)$.

(b) Reset particle weights $w_t^{(i)} = 1/N$, $i = 1, \dots, N$.

5. Set $t := t + 1$ and iterate from step 2.

weights are recomputed using the new state trajectories.

3.5.3 Practical Evaluation of Weights

Evaluation of Weights in Logarithmic Scale

In practice, it is beneficial to evaluate non-normalized weights $\tilde{w}_t^{(i)}$ in a logarithmic scale. In the following text, let

$$\ln \tilde{w}_t^{(i)} = \ln(\tilde{w}_t^{(i)}), \quad i = 1, \dots, N.$$

Before normalization, we subtract the value of the maximum weight \tilde{w}_t^{\max} from all the weights, as follows,

$$\ln \tilde{w}_t^{(i)*} = \ln \tilde{w}_t^{(i)} - \ln \tilde{w}_t^{\max} = \ln \left(\frac{\tilde{w}_t^{(i)}}{\tilde{w}_t^{\max}} \right),$$

where $\ln \tilde{w}_t^{\max} = \max_{i \in N} \ln \tilde{w}_t^{(i)}$.

This procedure ensures, that the weights are better scaled and the overall algorithm is numerically more stable. After exponentiation, the maximum weight is equal to 1 and there is always at least one particle which has a reasonable weight after normalization. The procedure does not affect the resulting normalized weights:

$$w_t^{(i)*} = \frac{\tilde{w}_t^{(i)*}}{\sum_{j=1}^N \tilde{w}_t^{(j)*}} = \frac{\frac{\tilde{w}_t^{(i)}}{\tilde{w}_t^{\max}}}{\sum_{j=1}^N \frac{\tilde{w}_t^{(j)}}{\tilde{w}_t^{\max}}} = \frac{\tilde{w}_t^{(i)}}{\frac{1}{\tilde{w}_t^{\max}} \sum_{j=1}^N \tilde{w}_t^{(j)}} = \frac{\tilde{w}_t^{(i)}}{\sum_{j=1}^N \tilde{w}_t^{(j)}} = w_t^{(i)}.$$

Effective Evaluation of Gaussian Likelihood

Let the likelihood function given by the observation model (3.2.4) be of a multidimensional Gaussian type, $p(\mathbf{y}_t|\mathbf{x}_t) = \mathcal{N}(\mathcal{H}_t(\mathbf{x}_t), \mathbf{Z}_t)$, more specifically

$$p(\mathbf{y}_t|\mathbf{x}_t) = (2\pi)^{-\frac{N_y}{2}} (\det \mathbf{Z}_t)^{-\frac{1}{2}} \exp \left[-\frac{1}{2} \left((\mathbf{y}_t - \mathcal{H}_t(\mathbf{x}_t))^T \mathbf{Z}_t^{-1} (\mathbf{y}_t - \mathcal{H}_t(\mathbf{x}_t)) \right) \right].$$

A logarithmic weight is then

$$\ln \tilde{w}_t = -0.5 \left(\ln \det \mathbf{Z}_t + \mathbf{v}_t^T \mathbf{Z}_t^{-1} \mathbf{v}_t \right).$$

Let \mathbf{F}_t be the lower triangular Cholesky factor of \mathbf{Z}_t . It can be shown (Golub and Van Loan, 1996), that it holds

$$\ln \tilde{w}_t = \ln \prod_{i=1}^{N_y} (\mathbf{F}_t[i, i])^2 + \|\mathbf{F}_t^{-1} \mathbf{v}_t\|^2, \quad (3.5.20)$$

where $\mathbf{F}_t[i, i]$, $i = 1, \dots, N_y$, are diagonal elements of \mathbf{F}_t and $\|\cdot\|$ denotes the Euclidean 2-norm.

3.6 Marginalized Particle Filter

The main advantage of importance sampling is its generality. Particle filters are capable of approximating an arbitrary density via empirical density at the price of high computational cost, which is prohibitive in high-dimensional problems. This obstacle can be overcome in the cases, where the structure of the model (3.2.3)–(3.2.4) allows analytical marginalization over a subset, \mathbf{x}_t^c , of the full state vector

$$\mathbf{x}_t = \begin{bmatrix} \mathbf{x}_t^c \\ \mathbf{x}_t^p \end{bmatrix}. \quad (3.6.1)$$

Using the chain rule and the factorization (3.6.1), the posterior $p(\mathbf{x}_{1:t}|\mathbf{y}_{1:t})$ has the form

$$p(\mathbf{x}_{1:t}|\mathbf{y}_{1:t}) = \underbrace{p(\mathbf{x}_{1:t}^c|\mathbf{x}_{1:t}^p, \mathbf{y}_{1:t})}_{\text{analytical filter}} \underbrace{p(\mathbf{x}_{1:t}^p|\mathbf{y}_{1:t})}_{\text{PF}}, \quad (3.6.2)$$

where $p(\mathbf{x}_t^c|\mathbf{x}_{1:t}^p, \mathbf{y}_{1:t})$ is analytically tractable, while $p(\mathbf{x}_{1:t}^p|\mathbf{y}_{1:t})$ is not (Doucet et al., 2001; Schön et al., 2005), and we use particle filter for its approximation. This technique is referred as Rao-Blackwellization (Doucet et al., 2001). We replace the term

$p(\mathbf{x}_{1:t}^p | \mathbf{y}_{1:t})$ in (3.6.2) by a weighted empirical distribution, in analogy to (3.5.3), yielding

$$p(\mathbf{x}_{1:t} | \mathbf{y}_{1:t}) \approx \sum_{i=1}^n w_t^{(i)} p(\mathbf{x}_{1:t}^c | \mathbf{x}_{1:t}^{p,(i)}, \mathbf{y}_{1:t}) \delta(\mathbf{x}_{1:t}^p - \mathbf{x}_{1:t}^{p,(i)}), \quad (3.6.3)$$

$$w_t^{(i)} \propto \frac{p(\mathbf{x}_{1:t}^{p,(i)} | \mathbf{y}_{1:t})}{q(\mathbf{x}_{1:t}^{p,(i)} | \mathbf{y}_{1:t})}. \quad (3.6.4)$$

Note that now we only have to sample from the space of \mathbf{x}_t^p . Recursive evaluation is achieved by application of the Bayes rule

$$p(\mathbf{x}_{1:t} | \mathbf{y}_{1:t}) \propto p(\mathbf{y}_t | \mathbf{x}_t) p(\mathbf{x}_t | \mathbf{x}_{t-1}) p(\mathbf{x}_{1:t-1} | \mathbf{y}_{1:t-1}), \quad (3.6.5)$$

and substitution of (3.6.3) in place of $p(\mathbf{x}_{1:t} | \mathbf{y}_{1:t})$ and $p(\mathbf{x}_{1:t-1} | \mathbf{y}_{1:t-1})$. Comparing elements in the summations on both sides of equation (3.6.5), we obtain:

$$w_t^{(i)} \propto \frac{p(\mathbf{y}_t, \mathbf{x}_t^{p,(i)} | \mathbf{x}_{1:t-1}^{p,(i)}, \mathbf{y}_{1:t-1})}{q(\mathbf{x}_t^{p,(i)} | \mathbf{x}_{1:t-1}^{p,(i)}, \mathbf{y}_{1:t})} w_{t-1}^{(i)}, \quad (3.6.6)$$

$$p(\mathbf{y}_t, \mathbf{x}_t^{p,(i)} | \mathbf{x}_{1:t-1}^{p,(i)}, \mathbf{y}_{1:t-1}) = \int p(\mathbf{y}_t | \mathbf{x}_t) p(\mathbf{x}_t | \mathbf{x}_{t-1}) p(\mathbf{x}_{t-1}^c | \mathbf{x}_{1:t-1}^{p,(i)}, \mathbf{y}_{1:t-1}) d\mathbf{x}_t^c d\mathbf{x}_{t-1}^c. \quad (3.6.7)$$

The requirement of analytical tractability of integrations in (3.6.7) is always fulfilled when (3.2.1) contains a linear-Gaussian part, (Schön et al., 2005), giving rise to the marginalized particle filter (MPF) with the Kalman filter. Resulting approximation of the posterior pdf (3.6.3) then becomes a weighted sum of Gaussian pdfs

$$p(\mathbf{x}_{1:t} | \mathbf{y}_{1:t}) \approx \sum_{i=1}^n w_t^{(i)} \mathcal{N}(\mathbf{x}_t^c; \bar{\mathbf{x}}_t^{c,(i)}, \mathbf{P}_t^{(i)}) \delta(\mathbf{x}_{1:t}^p - \mathbf{x}_{1:t}^{p,(i)}),$$

where $\bar{\mathbf{x}}_t^{c,(i)}$ and $\mathbf{P}_t^{(i)}$ are mean values and covariance matrices of Gaussian distributions $\mathcal{N}(\mathbf{x}_t^c; \bar{\mathbf{x}}_t^{c,(i)}, \mathbf{P}_t^{(i)})$ attached to particles $\mathbf{x}_t^{p,(i)}$.

Using the results from Appendix A, the minimum mean square error estimates of the expected value $\hat{\mathbf{x}}_t^c$ and covariance \mathbf{P}_t of the resulting posterior mixture $p(\mathbf{x}_t^c | \mathbf{x}_{1:t}^p, \mathbf{y}_{1:t})$ are given, as follows:

$$\hat{\mathbf{x}}_t^c = \sum_{i=1}^N w_t^{(i)} \bar{\mathbf{x}}_t^{c,(i)}, \quad (3.6.8)$$

$$\mathbf{P}_t = \sum_{i=1}^N w_t^{(i)} \left[\mathbf{P}_t^{(i)} + \left(\bar{\mathbf{x}}_t^{c,(i)} - \hat{\mathbf{x}}_t^c \right) \left(\bar{\mathbf{x}}_t^{c,(i)} - \hat{\mathbf{x}}_t^c \right)^\top \right]. \quad (3.6.9)$$

Illustration of a 2-dimensional state $\mathbf{x} = [x_1, x_2]^\top$ estimated using MPF is in Figure (3.6.1). Resulting joint estimate of the posterior pdf is in the linear-Gaussian part

of the state, x_1 , estimated using the optimal Kalman filter and approximated using a particle filter in the non-linear and/or non-Gaussian part of the full state vector, x_2 .

Tractable solution also exists for discrete-variable models (Thrun et al., 2005) and models based on conjugate statistics (Saha et al., 2010). However, the range of models amenable to this approach is still rather small and does not contain any models suitable for large-scale and non-linear problems.

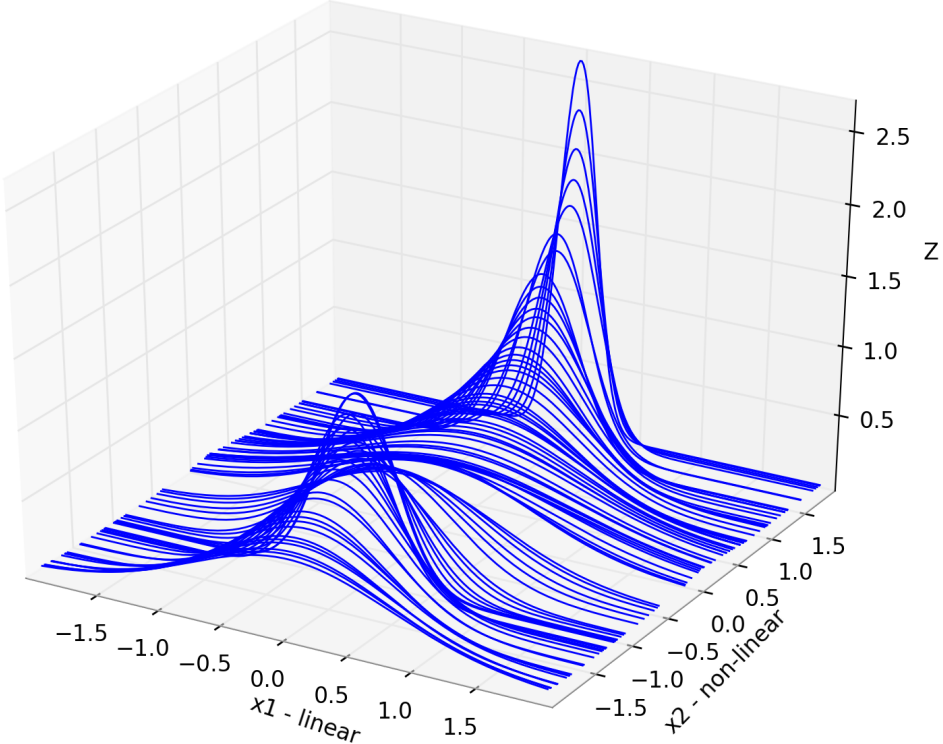


Figure 3.6.1: Illustration of a 2-dimensional state $\mathbf{x} = [x_1, x_2]^T$ estimated using MPF. Resulting joint estimate of the posterior pdf is in the linear-Gaussian part of the state, x_1 , estimated using the optimal Kalman filter and approximated using a particle filter in the non-linear and/or non-Gaussian part of the full state vector, x_2 .

Chapter 4

MPF Framework for Tuning of Ensemble Filters

4.1 Modification of MPF Algorithm for Suboptimal Conditional Filters

Since the optimal Kalman filter is not suitable for large scale and non-linear problems, it would be advantageous to substitute it with an approximate filter within MPF. We propose to relax the requirement of exact marginalization in (3.6.6) and replace it by an approximation. We note that given numerical values of $\mathbf{x}_t^{p,(i)}, \mathbf{x}_{t-1}^{p,(i)}$, equation (3.6.7) is equivalent to the normalizing constant of a Bayesian filter (3.2.5). Hence, any Bayesian filter that is capable of evaluating its normalizing constant can be used to approximate (3.6.7). What results is an algorithm equivalent to marginalized particle filtering where the analytical Kalman filters are replaced by approximate conditional filters. Specifically, the following filters interact via Algorithm 4.1:

1. Conditional filter on variable \mathbf{x}_t^c , treating \mathbf{x}_t^p as an observation, i.e.,

$$p(\mathbf{x}_t^c | \mathbf{x}_{1:t}^p, \mathbf{y}_{1:t}) = \frac{p(\mathbf{y}_t, \mathbf{x}_t^p | \mathbf{x}_t^c, \mathbf{x}_{1:t}^p) p(\mathbf{x}_t^c | \mathbf{x}_{1:t-1}^p, \mathbf{y}_{1:t-1})}{p(\mathbf{y}_t, \mathbf{x}_t^p | \mathbf{x}_{1:t-1}^p, \mathbf{y}_{1:t-1})}. \quad (4.1.1)$$

2. Particle filter on variable \mathbf{x}^p , that handles sampling from the proposal density $q(\mathbf{x}_t^p | \mathbf{x}_{t-1}^p, \mathbf{y}_{1:t})$ and re-sampling. Each particle is attached to one conditional filter.

In this general form, the algorithm is rather unspecific. This is due to the fact that arbitrary conditional filters can be combined with arbitrary particle filtering approaches. Therefore, we consider Algorithm 4.1 to represent a framework for designing specific filtering variants. The word framework is used to distinguish this approach from the analytical MPF.

Algorithm 4.1 General MPF framework.

1. Generate initial particles $\mathbf{x}_0^{p,(i)}$, $i = 1, \dots, N$, and set initial statistics of all associated conditional filters.
 2. For each new data record \mathbf{y}_t do:
 - (a) Sample new value of particles $\mathbf{x}_t^{p,(i)}$, $i = 1, \dots, N$, and update statistics of all associated conditional filters via (4.1.1).
 - (b) Compute weights (3.6.6) of all particles and their associated conditional filters.
 - (c) If the number of efficient particles, $\overline{N_{\text{eff}}}$, is lower than the chosen threshold, re-sample the particles.
-

The key property of the MPF is partitioning of the state variable into two parts. In the original exact formulation, the choice of partitioning is fully determined by tractability of the Bayes rule (3.2.5). Finding a partitioning in the context of environmental modeling where the state variables typically obey the same equations is harder. However, the relaxed formalization of Section 3.6 allows to interpret \mathbf{x}_t^p not as a partition of the full state but rather as an augmentation of the original state \mathbf{x}_t^c by nuisance parameters. What results is a framework for on-line tuning of existing filters.

The general algorithm of tuning is described in Algorithm 4.1, specific variants arise for the following choices:

1. Choose a preferred variant of the conditional filter (e.g. a variant of ensemble filter) estimating \mathbf{x}_t^c ,
2. Choose tuning parameters of interest, \mathbf{x}_t^p , use them to augment the original state \mathbf{x}_t^c via the chosen model of their evolution, $p(\mathbf{x}_t^p|\cdot)$,
3. Choose a proposal density $q(\mathbf{x}_t^p|\cdot)$, e.g., the evolution model, $q(\mathbf{x}_t^p|\cdot) \equiv p(\mathbf{x}_t^p|\cdot)$.

Different choices in each of the points above will lead to different properties of the resulting filter. The number of possible combinations of these choices is enormous, and finding guidelines for the best option in a given application context is a task for further research. In some applications, a physically motivated evolution model of \mathbf{x}_t^p may be found, while heuristic or expert-chosen models may be more appropriate in others.

4.2 Estimation of Inflation Factor, Observation Error Variance, and Length-scale Parameter

We focus on ensemble filters, which are suitable for large-scale problems arising in spatial data analysis. Generally, ensemble methods tend to underestimate model error, which can significantly decrease filtering performance or even result in divergence. The

techniques for compensating small ensemble issues described in Section 3.4.3 have tuning parameters that typically need to be set-up experimentally. Substantial effort has been put into on-line estimation of the inflation factor alone, (Anderson, 2007a), or in tandem with the observation error (Li et al., 2009). In this Section, we approach the same problem using the MPF framework with the following specific choices.

1. We have chosen the EnSRF with multiplicative inflation (3.4.19) as our conditional filter.
2. The unknown tuning parameters regarding model error are: the time-variant inflation factor Δ_t and the time-varying length-scale parameter l_t of the covariance localization function. We can include also different types of parameters like magnitude of observation error, r_t , for all observations, i.e., $\mathbf{R}_t = r_t \mathbf{I}$. The augmentation of the state vector is then $\mathbf{x}_t^p = [\Delta_t, r_t, l_t]^T$.
3. The proposal density is chosen as $p(\mathbf{x}_t^p | \mathbf{x}_{t-1}^p)$.

Augmentation \mathbf{x}_t^p is evolved using

$$p(\mathbf{x}_t^p | \mathbf{x}_{t-1}^p) = p(\Delta_t | \Delta_{t-1}) p(r_t | r_{t-1}) p(l_t | l_{t-1}),$$

where, evolution of the parameters is modeled by truncated Gaussian random walks,

$$\begin{aligned} p(\Delta_t | \Delta_{t-1}) &= t\mathcal{N}(\Delta_{t-1}, \sigma_\Delta^2, [1, \infty]), \\ p(r_t | r_{t-1}) &= t\mathcal{N}(r_{t-1}, \sigma_r^2, [0, \infty]), \\ p(l_t | l_{t-1}) &= t\mathcal{N}(l_{t-1}, \sigma_l^2, [0, \infty]). \end{aligned} \tag{4.2.1}$$

Scalar parameters σ_Δ , σ_r , and σ_l denote the spread of the random walks, respectively. Non-negativity of all considered parameters motivates truncation of support of the random walks.

Under the choice of proposal density (3.6.6) reduces to

$$w_t^{(i)} = w_{t-1}^{(i)} p(\mathbf{y}_t | \mathbf{y}_{1:t-1}, \mathbf{x}_t^{p,(i)}), \tag{4.2.2}$$

where $p(\mathbf{y}_t | \mathbf{y}_{1:t-1}, \mathbf{x}_t^{p,(i)})$ defined by (3.4.8) is now explicitly conditioned on the unknown parameters:

$$\begin{aligned} p(\mathbf{y}_t | \mathbf{y}_{1:t-1}, \mathbf{x}_t^{p,(i)}) &\propto \det \left(\mathbf{Z}_t(\mathbf{x}_t^{p,(i)}) \right)^{-\frac{1}{2}} \times \\ &\times \exp \left[-\frac{1}{2} \left(\mathbf{y}_t - \mathbf{H} \bar{\mathbf{x}}_{t|t-1}^{c,(i)} \right)^T \mathbf{Z}_t^{-1}(\mathbf{x}_t^{p,(i)}) \left(\mathbf{y}_t - \mathbf{H} \bar{\mathbf{x}}_{t|t-1}^{c,(i)} \right) \right]. \end{aligned} \tag{4.2.3}$$

Resulting algorithm defines an adaptation scheme related to other approaches used in the literature. Specifically, (4.2.3) is the same equation that was used for maximum

likelihood estimation of covariance parameters (Dee, 1995). Maximization of this function is achieved, e.g., via simplex methods (Mitchell and Houtekamer, 2000). In our approach, (4.2.3) serves as a likelihood function for Bayesian estimation of the tuning parameters, $\mathbf{x}_{p,t}$. The variance of the random walk then models our belief in time-variability of the tuning parameters. In the special case of stationary parameters, (i.e., $\sigma_\Delta = \sigma_r = \sigma_l = 0$), Algorithm 4.1 is reduced to a parallel run of N ensemble filters, each of which is accumulating the product of $p(\mathbf{y}_t | \mathbf{y}_{1:t-1}, \mathbf{x}_t^{p,(i)})$ in each step. After several hundreds of steps, majority of the weights will converge to zeros and one of them will converge to one. Such behavior is known as sample impoverishment in the particle filtering literature. The convergence of probability mass to a single point may be useful for finding the best tuned values in off-line phase. However, this degeneracy is undesirable for on-line application, and non-zero variances of random walks (4.2.1) have to be used.

For non-stationary parameters, each of the N filters follows a random walk of the tuning parameters. The re-sampling operation removes filters that diverged into unlikely regions, and replaces them by copies of the filters with parameters that are more likely. The area of higher likelihood is then explored by more filters in detail. This of course requires to run N ensemble filters in parallel which is computationally expensive. However, the key advantage of this approach is that it is able to optimize non-convex and multi-modal likelihood functions.

4.3 Simulation Studies

4.3.1 Lorenz-96 Model

To demonstrate versatility of the method, we test the MPF approach in the Lorenz-96 model by Lorenz and Emanuel (1998) which has been widely used in simulation studies. The model is given by

$$\frac{dx_j}{dt} = x_{j-1}(x_{j+1} - x_{j-2}) - x_j + F, \quad (4.3.1)$$

where F is the model forcing and x_j are variables forming a cyclic chain. We define $x_{-1} = x_{J-1}$, $x_0 = x_J$ and $x_{J+1} = x_1$ to make (4.3.1) meaningful for all values of $j = 1 \dots J$. We use 40 variables, and $F = 8$ for the strength of forcing. The model (4.3.1) can be integrated forward with the fourth-order Runge-Kutta scheme. The system is computationally stable for step of 0.05 non-dimensional units, which is also the step of the analysis. All the experiments are performed as twin experiments.

4.3.2 Stationary Parameters

To create a baseline for comparison of adaptive tuning strategies, we performed parallel run of EnSRFs for fixed values of Δ, l selected on a rectangular grid, as in (Whitaker

rank	RMSE			marginalized log-likelihood		
	inflation	localization	mean value	inflation	localization	sum
#1	1.04	7.0	0.2074	1.05	7.0	-2079401
#2	1.04	6.0	0.2075	1.05	8.0	-2079483
#3	1.05	8.0	0.2076	1.04	6.0	-2079513

Table 4.1: Best stationary choices of nuisance parameters for EnSRF according to two criteria.

and Hamill, 2002). From Bayesian point of view, this setup corresponds to estimation of stationary parameters:

$$p(\Delta, l | \mathbf{y}_{1:t}) \propto p(\Delta, l) \prod_{j=1}^t p(\mathbf{y}_j | \mathbf{y}_{1:j-1}, \Delta, l) \quad (4.3.2)$$

where $p(\Delta, l)$ is a prior probability density on discrete values of Δ, l at the grid points, which is uniform, and $p(\mathbf{y}_j | \mathbf{y}_{1:j-1}, \Delta, l)$ is given by (4.2.3). For numerical stability, (4.3.2) is often computed in logarithmic scale where the product is replaced by the sum of marginal log-likelihoods.

The observation data are generated from the perfect model scenario where the “true” state was generated by integrating the Lorenz-96 model (4.3.1) for 100000 steps and observations are generated from the true state by addition of zero-mean Gaussian noise with variance $r = 1$. The analysis was performed by the EnSRF with covariance localization constructed using a compactly supported fifth-order piecewise rational function given by (3.4.21) with length-scale parameter l . The results of a simulation experiment with 132 EnSRFs with 15 ensemble members, $r = 1$, $\Delta = [1.0, 1.1, \dots, 1.10]$, and $l = [0, 1, \dots, 11]$ are displayed in Figure 4.3.1 in two modalities. First, the traditional RMSE is computed for each couple of parameters,

$$\text{RMSE} = \frac{1}{99000} \sum_{t=1000}^{100000} \sqrt{\frac{1}{40} (\mathbf{x}_t - \hat{\mathbf{x}}_t^c)^T (\mathbf{x}_t - \hat{\mathbf{x}}_t^c)}, \quad (4.3.3)$$

for the MPF algorithm. Second, the sum of marginal log-likelihoods (4.3.2) within the same time intervals is displayed for illustration.

Note that the contours of the marginal log-likelihood (4.3.2) correspond closely to the contours of the RMSE. This suggests that the marginal likelihood $p(y_\tau | y_{1:\tau-1}, \Delta, l)$ is a good measure to optimize for the best RMSE in the cases where the true state values are not known. The three best choices within each modality are given in Table 4.1. Note that two choices— $\Delta = 1.05, l = 8$ and $\Delta = 1.04, l = 6$ —are in the top three for both criteria. The relative differences are rather small, however, in terms of normalized posterior probability (4.3.2) the best parameters in Table 4.1 are e^{82} times more likely than the second best.

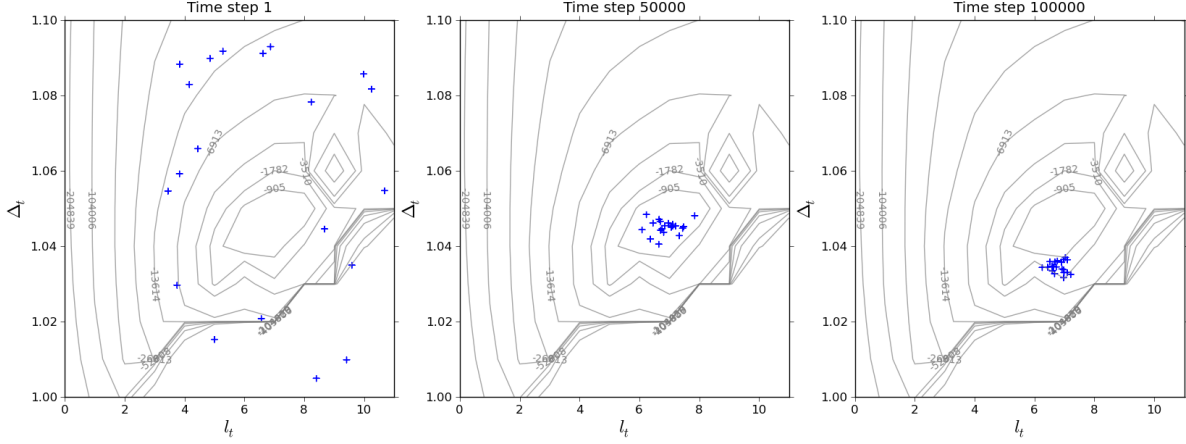


Figure 4.3.2: Position of the particles $\Delta_t^{(i)}, l_t^{(i)}$ denoted by '+' on the background of stationary contours of marginal log-likelihood.

The particle filter is using multinomial re-sampling (Gordon et al., 2002) and $\overline{N}_{\text{eff}} = 0.8N$. The variances of random walks (4.2.1) for the MPF algorithm were chosen as

$$\begin{aligned}
 \sigma_{\Delta} &= 0.01\Delta_{t-1}^{(i)} + 0.0001, \\
 \sigma_l &= 0.01l_{t-1}^{(i)} + 0.0001, \\
 \sigma_r &= 0.005r_{t-1}^{(i)} + 0.0001,
 \end{aligned}
 \tag{4.3.4}$$

The prior density of the tuning parameters is chosen as uniform on support $p(\sigma_{y,0}) = U(0.1, 4)$, $p(\Delta_0) = U(1.0, 1.10)$, $p(l_0) = U(0.11, 11.11)$.

Results of simulations for different number of particles and both scenarios are displayed in Tables 4.2 and 4.3, respectively. Using particles and their weights, estimates of the parameters are evaluated using

$$\bar{\mathbf{x}}_t^p = \sum_{i=1}^n w_t^{(i)} \mathbf{x}_t^{p,(i)}.$$

In accordance with (Whitaker and Hamill, 2002; Li et al., 2009), we ignore the first 1000 steps and report the results only for the subsequent steps. Spatial distribution of the particles for Δ_t, l_t in scenario (i) at time steps $t = 1, 50000, 100000$ is displayed in Figure 4.3.2 on the background of contours for the stationary marginal log-likelihood from Fig 4.3.1. We note that alignment of the particles in the middle of the stationary contour at $t = 50000$ is a coincidence, in majority of all other time steps the cloud is a bit off the stationary optimum.

As expected, the RMSE is steadily decreasing with increasing number of particles for both considered scenarios. Note that for $N = 10$ and higher, the MPF filter achieves better performance than the best-tuned filter. In the more complex scenario of tuning

Results for scenario (i)								
N	mean RMSE	std RMSE	mean $\bar{\Delta}_t$	std $\bar{\Delta}_t$	mean \bar{l}_t	std \bar{l}_t	mean \bar{r}_t	std \bar{r}_t
5	0.2089	0.0521	1.0334	0.0080	5.6942	0.9072	1.0	0.0
10	0.2071	0.0510	1.0337	0.0064	6.3431	0.9229	1.0	0.0
20	0.2065	0.0523	1.0331	0.0061	6.2933	0.5005	1.0	0.0

Table 4.2: Adaptive tuning of $\mathbf{x}_t^p = [\Delta_t, l_t]^T$ and the resulting analysis RMSE error, averaged over assimilation steps between $t = 1000$ and $t = 100000$, std denotes standard deviation of the estimates from the mean over time.

Results for scenario (ii)								
N	mean RMSE	std RMSE	mean $\bar{\Delta}_t$	std $\bar{\Delta}_t$	mean \bar{l}_t	std \bar{l}_t	mean \bar{r}_t	std \bar{r}_t
5	0.2094	0.0521	1.0317	0.0075	5.6154	0.7289	1.0059	0.0215
10	0.2072	0.0509	1.0354	0.0058	6.7455	0.9541	1.0031	0.0230
20	0.2064	0.0511	1.0355	0.0055	6.7182	0.9202	1.0018	0.0193

Table 4.3: Adaptive tuning of $\mathbf{x}_t^p = [\Delta_t, r_t, l_t]^T$ and the resulting analysis RMSE error, averaged over assimilation steps between $t = 1000$ and $t = 100000$, std denotes standard deviation of the estimates from the mean over time.

all three parameters, Table 4.3 the MPF algorithm achieves only negligible increase of the RMSE over the scenario with known observation variance r .

We note that good performance of the adaptive tuning was achieved for as low as 10 particles. This result is especially promising since it suggests that even more challenging assimilation scenarios can be handled at comparable computational complexity. Addition of one extra tuning parameter in second scenario had negligible impact on the performance.

4.3.4 Model with Random Perturbations

For comparison with (Li et al., 2009), we tested the MPF algorithms on data simulated with model (4.3.1) with additive random perturbations

$$\frac{dx_j}{dt} = x_{j-1}(x_{j+1} - x_{j-2}) - x_j + F + \alpha e_t, \quad (4.3.5)$$

where e_t is Gaussian distributed noise with zero-mean and unit variance. The observed data were generated using model (4.3.5) with $\alpha = 4$ for 100000 steps. The same setup of the EnSRF as in the previous experiments was used, including the same initial conditions. Results for estimation for the 100000 steps are displayed in Table 4.4. Since parameter α is stationary, the time evolution of the parameter estimates $\bar{\Delta}_t, \bar{l}_t$ using MPF is reaching the stationary values in Table 4.4 after the initial convergence period.

Results for imperfect model scenario, $\alpha = 4$							
mean RMSE	std RMSE	mean Δ_t	std $\bar{\Delta}_t$	mean \bar{l}_t	std \bar{l}_t	mean \bar{r}_t	std \bar{r}_t
0.3563	0.0542	1.1944	0.0230	3.0810	0.8198	1.0055	0.0618

Table 4.4: Adaptive tuning of $\mathbf{x}_t^p = [\Delta_t, l_t, r_t]^T$ for system with random model errors (4.3.5) with variance $\alpha = 4$. The resulting analysis RMSE error is averaged over assimilation steps between $t = 1000$ and $t = 100000$, time averages of parameter estimates are displayed in tandem with standard deviation of the estimates from the mean over time. Both algorithms were run with $N = 10$ and $\bar{N}_{\text{eff}} = 0.8N$.

Note that the additive noise was compensated by higher values of $\bar{\Delta}_t$ and lower values of \bar{l}_t than that of the perfect model, Table 4.3. This is in agreement with findings of Li et al. (2009) and also expected because α is increasing the background covariance (reflected by higher inflation) and decreasing correlation between elements of the state vector (reflected by lower length-scale).

For testing the tracking properties of the MPF algorithms, we have designed a scenario with time varying α_t according to a triangular profile. Posterior densities of the parameters obtained using the MPF algorithm are displayed in Fig. 4.3.3. For this experiment, we increased the variances of random walks (4.2.1) to

$$\begin{aligned}\sigma_\Delta &= 0.01\Delta_{t-1}^{(i)} + 0.001, \\ \sigma_l &= 0.01l_{t-1}^{(i)} + 0.001, \\ \sigma_r &= 0.01r_{t-1}^{(i)} + 0.01.\end{aligned}$$

This experiment confirms the trend of increasing Δ_t and decreasing l_t with increasing α_t . Note that when α returns to the stationary values, so do the estimates of the tuning parameters.

4.4 Summary

The purpose of this chapter is to present marginalized particle filtering (also known as Rao-Blackwellized filtering) as an attractive tool for research of data assimilation methods in environmental modeling and especially for tuning of ensemble filters.

The method is based on partitioning of the state (or unknown parameters) into two parts: (i) unknowns estimated by a conditional filter, and (ii) unknowns estimated by a particle filter. The original MPF assumes that the conditional filter is analytically tractable, which allows to prove advantages over a pure particle filter. In this chapter, we propose to replace analytical filters by ensemble filters. The resulting algorithm is loosing its theoretical advantages, however it allows to address the problem of tuning of ensemble filters. We have shown that the number of particles needed to achieve acceptable performance is rather low, for example 10 particles are sufficient to achieve on-line tuning of the inflation factor and the length-scale parameter in the EnSRF for

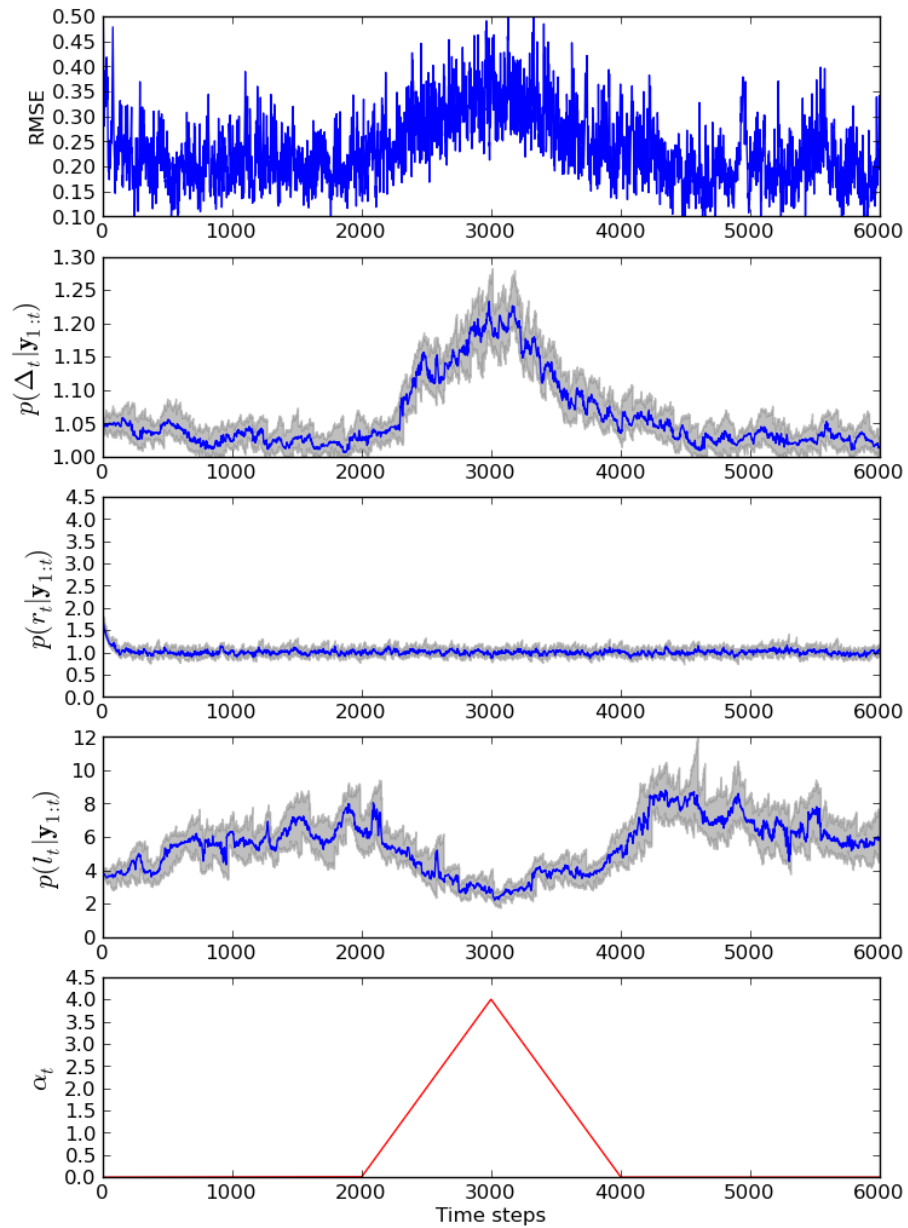


Figure 4.3.3: Estimation of system (4.3.5) with time-varying α_t of triangular profile displayed at the bottom. Posterior densities of the parameters are displayed via their mean value (blue line) and region between minimum and maximum value of the particles (gray area).

the 40-dimensional Lorenz-96 model. Furthermore, we have shown that the approach easily extends to estimation of unknown variance of the observation error and potentially any other tuning parameters. Once again, 10 particles were sufficient to achieve performance comparable to that of the best-tuned filter.

Computational cost of the MPF framework is high since it requires running N filters in parallel. We expect that advantages of parallel evaluation of ensemble filters over adaptation of a single ensemble filter will become apparent in even more demanding scenarios. Computational complexity may prevent its operational use, however, it may be an important tool for gaining insight into the ensemble filters in the same spirit as in (Anderson, 2007b).

The potential of the framework has been demonstrated on on-line tuning of the ensemble filters. However, it is not the only scenario where it can be used. Since posterior density of the MPF is a mixture of Gaussians, the approach may be adapted for estimation of Gaussian mixture filters that have been studied, e.g. by Bengtsson et al. (2003). More work is required to discover full potential of the method. The open problems include justified design of suitable models of parameter evolution and approximations reducing the computational cost of the MPF. However, the existence of the exact solution allows to design the necessary computational simplifications to resemble its behavior.

Chapter 5

Data Assimilation in the Early Phase

5.1 Problem Statement

Assume an accident in a nuclear power plant followed by an atmospheric release of radionuclides. After the release, there is a radioactive plume moving over the terrain. Urgent protective measures must be introduced as soon as possible to protect the public from the harmful effects of ionizing radiation. These are planned with regards to expected exceeding of regulatory radiation limits given by the law. Decision making regarding countermeasures is supported with radiological measurements from terrain. However, particularly in the first hours of the accident, the measurements are sparse and it is not possible to base prognoses of radiation situation just upon them solely. For determination of affected areas and estimation of radiation levels in a wider scale, atmospheric dispersion models (ADMs) are used. Given a meteorological forecast and values of other important control variables of an ADM, the model evaluates a *prediction* of spatial and temporal distribution of radionuclides on a computational grid in terms of activity concentration in air. It is an important radiological quantity which can be used for calculation of other quantities like deposition and doses. Under the term *control variables* we understand a set of inputs to the model, which parameterize initial conditions and important physical processes influencing the spreading of the pollutants, e.g., information on the source term (composition and magnitude of the release and its dynamics) and meteorological inputs.

In reality, our knowledge of the release conditions is limited. Typically, meteorological inputs are set using a numerical prediction model and other control variables are set with expert-provided values. This subjective choice can introduce significant errors into the resulting predictions. What is more, the chaotic nature of the atmosphere makes impossible to obtain accurate results using a model of a finite complexity and evaluated with finite computational resources. In other words, inaccurate model initialized with erroneous inputs can not provide reliable predictions. Relying on them can lead in fatal errors in the countermeasures planning. Inherent uncertainty of the problem is not the only factor making the forecasting in the early phase challenging. There are also strict time constraints caused by the problem dynamics and the urgent need of reliable

information. There must be made a compromise between the time spent on evaluation of the dispersion model and its accuracy.

Using data assimilation we can tune uncertain model inputs in a way that the model output fits the available measurements. The number of variables is potentially large but the most important subset can be identified for a specific scenario and a given ADM (Eleveld and Twenhöfel, 2004; Pecha et al., 2007). Recent advances in this field have shown great promise in improving model performance through optimal calculation of emission and meteorological inputs by a systematic comparison of observations and modeled concentrations. These improved estimates may in turn be used as inputs to long- and short-range atmospheric dispersion models, resulting in greatly improved efficiency of the countermeasures.

In this chapter, we describe a new data assimilation method based on particle filtering for estimation of important control variables of a parameterized ADM.

5.2 Proposed Data Assimilation Methodology

We propose a new data assimilation methodology based on particle filtering for reduction of uncertainty in atmospheric dispersion modeling during the early phase of a radiation accident. We focus on the parametrized ADMs, where selected control variables are treated as random and we attempt to select their most plausible values in consecutive time steps using available measurements.

5.2.1 State Evolution Model

Parametrized ADMs can be understood as deterministic functions of the control variables $\theta \in \mathbb{R}^{N_\theta}$. It means, that all the uncertainty is assumed to be in values of the variables, not in the parametrization itself. Trajectory $\theta_{1:t}$ represents values of control variables of the model up to time t and fully determines its propagation. Vector θ_t aggregates values of control variables used for model propagation between time instances t and $t+1$. Physics behind the dispersion modeling motivates us to distinguish between two types of control variables, where each type must be treated differently:

Mutable control variables: Values of mutable control variables can—and are expected to—change in respective time steps. Typically, control variables describing meteorological conditions must be treated as mutable in order to correctly simulate stochastic fluctuations of the wind field and other atmospheric phenomena.

Immutable control variables: Values of immutable control variables must be the same along the whole state trajectory. Typical representative is the magnitude of release in the case of an instantaneous releases. As the initial magnitude of release affects the deposition, doses and other radiological quantities during the whole propagation of the plume, its variation would violate the law of activity conservation. Neglecting the radioactive decay, the integral of activity over time and

space must be equal to the initial value in all time steps. In context of the classical estimation theory the immutable control variables denote the *stationary parameters*.

We want to estimate the state trajectory $\boldsymbol{\theta}_{1:t}$ —from the Bayesian point of view, evaluate the posterior $p(\boldsymbol{\theta}_{1:t}|\mathbf{y}_{1:t})$ —in successive time steps $t = 1, 2, \dots$. Let the state $\boldsymbol{\theta}_t$ be comprised of two parts, the immutable variables $\boldsymbol{\eta}_t$ and the mutable variables $\boldsymbol{\nu}_t$:

$$\boldsymbol{\theta}_t = \begin{bmatrix} \boldsymbol{\eta}_t \\ \boldsymbol{\nu}_t \end{bmatrix}. \quad (5.2.1)$$

We assume that $\boldsymbol{\eta}_t$ and $\boldsymbol{\nu}_t$ are mutually independent. Since the immutable variables are not allowed to change during the model propagation, we can evolve only the mutable part of $\boldsymbol{\theta}_t$ and the state transition pdf has then the form:

$$\begin{aligned} p(\boldsymbol{\theta}_t|\boldsymbol{\theta}_{t-1}) &= p(\boldsymbol{\eta}_t, \boldsymbol{\nu}_t|\boldsymbol{\eta}_{t-1}, \boldsymbol{\nu}_{t-1}) \\ &= p(\boldsymbol{\eta}_t|\boldsymbol{\eta}_{t-1})p(\boldsymbol{\nu}_t|\boldsymbol{\nu}_{t-1}) \end{aligned} \quad (5.2.2)$$

$$= \delta(\boldsymbol{\eta}_t - \boldsymbol{\eta}_{t-1})p(\boldsymbol{\nu}_t|\boldsymbol{\nu}_{t-1}). \quad (5.2.3)$$

5.2.2 Observation Operator

Measurements are assumed to be normally distributed with covariance matrix \mathbf{R}_t and mutually independent given the state trajectory $\boldsymbol{\theta}_{1:t}$,

$$\mathbf{y}_t \sim \mathcal{N}(\mathcal{H}(\boldsymbol{\theta}_{1:t}), \mathbf{R}_t), \quad (5.2.4)$$

where $\mathcal{H}(\cdot)$ is an observation operator. It performs two tasks. Firstly, the observation operator relates measured radiological quantity and an output quantity given by the dispersion model. Secondly, it performs spatial interpolation in the case that the computational and receptor grids are not aligned. Given a radiological quantity evaluated on a computational grid \mathcal{S}_t , observation operator yields a vector of measurements $\mathbf{y}_t \in \mathbb{R}^{N_y}$ evaluated in a set of receptor points $\mathcal{S}_t^R = \{\mathbf{s}_{1,t}^R, \dots, \mathbf{s}_{N_y,t}^R\}$. Generally, the set \mathcal{S}_t^R can vary between time steps. This would be of a particular importance in the case of measurements provided by the moving mobile groups. In the case of a stationary radiation monitoring network we can treat the observation operator as time invariant, i.e., $\mathcal{H}_t = \mathcal{H}$.

5.2.3 Data Assimilation Algorithm

The posterior pdf is approximated using particle filter,

$$p(\boldsymbol{\theta}_{1:t}|\mathbf{y}_{1:t}) \approx \sum_{i=1}^N w_t^{(i)} \delta(\boldsymbol{\theta}_{1:t} - \boldsymbol{\theta}_{1:t}^{(i)}), \quad w_t^{(i)} \propto \frac{p(\boldsymbol{\theta}_{1:t}^{(i)}|\mathbf{y}_{1:t})}{q(\boldsymbol{\theta}_{1:t}^{(i)}|\mathbf{y}_{1:t})}, \quad (5.2.5)$$

Particles are represented with trajectories $\boldsymbol{\theta}_{1:t}^{(i)}$ parameterizing N simultaneously propagated dispersion models.

If the proposal density

$$q\left(\boldsymbol{\theta}_{1:t}^{(i)}|\mathbf{y}_{1:t}\right) = q\left(\boldsymbol{\eta}_1^{(i)}|\mathbf{y}_{1:t}\right) q\left(\boldsymbol{\nu}_{1:t}^{(i)}|\mathbf{y}_{1:t}\right)$$

is badly chosen, the performance of the filter would be rather poor. Application of sequential evaluation of weights would result in a computationally ineffective scheme, where the computational resources would be wasted on propagation of particles with small weights. Enormous number of particles would be needed to achieve a good performance.

Significant improvements can be achieved by application of the adaptive proposal selection methodology described in Section 3.5.2, where the proposal density $q(\boldsymbol{\theta}_{1:t}^{(i)}|\mathbf{y}_{1:t})$ is re-estimated in respective time steps using the weights $w_t^{(i)}$. Drawbacks of this approach is the fact that the dispersion models and the weights $w_t^{(i)}$ must be always recomputed because of the immutable variables. However, this adaptive procedure guarantees that the trajectories with low weights are discarded and a new population of trajectories is sampled from the regions of the state-space determined by particles with high weights. In other words, the sequential update of the proposal pdf suppresses the effect of sample impoverishment. The resulting algorithm is summarized in Algorithm 3.5.

5.2.4 Evaluation of Radiological Quantities of Interest

Usually, we are not interested just in the estimates of control variables but also in radiological quantities evaluated by the dispersion model. Let the radiological quantity of interest be a continuous function $C(\mathbf{s}, \tau, \boldsymbol{\theta})$ of spatial coordinates $\mathbf{s} = (s_1, s_2, s_3)$; time since the release star τ ; and the control variables $\boldsymbol{\theta}$. For computational reasons, $C(\mathbf{s}, \tau, \boldsymbol{\theta})$ is discretized in both spatial and temporal domains. Let $\mathbf{c}_t \in \mathbb{R}^{N_c}$ be a vector aggregating values of $C(\mathbf{s}, \tau, \boldsymbol{\theta})$ evaluated in an ordered set of spatial location $\mathcal{S} = \{\mathbf{s}_1, \dots, \mathbf{s}_{N_c}\}$ forming a computational grid in time $\tau = \Delta_\tau t$:

$$\mathbf{c}_t = \begin{bmatrix} C(\mathbf{s}_1, \Delta_\tau t, \boldsymbol{\theta}_{1:t}) \\ \vdots \\ C(\mathbf{s}_{N_c}, \Delta_\tau t, \boldsymbol{\theta}_{1:t}) \end{bmatrix}.$$

Here, Δ_τ is the time step length and t is time step index. In the following text, $\mathbf{c}_t \equiv C(\boldsymbol{\theta}_{1:t})$.

Using the particles $\mathbf{c}_t^{(i)} = C(\boldsymbol{\theta}_{1:t}^{(i)})$, $i = 1, \dots, N$, the mean value $\bar{\mathbf{c}}_t$ and the covariance $\boldsymbol{\Sigma}_t^c$ of the radiological quantity evaluated by the dispersion models can be at each time step computed using the posterior (5.2.5), as follows,

$$\bar{\mathbf{c}}_t = \sum_{i=1}^N w_t^{(i)} \mathbf{c}_t^{(i)}, \quad \boldsymbol{\Sigma}_t^c = \sum_{i=1}^N w_t^{(i)} \left[\left(\mathbf{c}_t^{(i)} - \bar{\mathbf{c}}_t \right) \left(\mathbf{c}_t^{(i)} - \bar{\mathbf{c}}_t \right)^\top \right]. \quad (5.2.6)$$

5.3 Application to Gaussian Puff Model

In this section we describe application of the proposed methodology to the assimilation of the Gaussian puff model with the time integrated gamma dose rate measurements.

5.3.1 Parametrization of Gaussian Puff Model

The idea behind the methodology allows for estimation of an arbitrary set of control variables. However, we restrict to the parametrization of the following physical quantities identified as the most influencing the resulting dose rates: magnitude of instantaneous release Q^i , wind speed $u = |\mathbf{u}|$ and wind direction ϕ . Using location parameters $Q^{i,*}, u_t^*, \phi_t^*$ and control variables $\boldsymbol{\theta}_t = (\omega_t, \xi_t, \psi_t)^T$, the three physical quantities are parametrized:

1. Parametrization of magnitude of release Q^i :

The overall magnitude of release must be treated as time invariant. It is parametrized using multiplicative immutable control variable $\omega_t \in \mathbb{R}^+$ as follows:

$$Q = \omega_t Q^{i,*}. \quad (5.3.1)$$

2. Parametrization of wind speed u :

In contrast to the overall magnitude of release, the wind direction is assumed to be variable in time. This assumption is in agreement with the stochastic nature of the atmospheric flow. It is parametrized using control variable $\xi_t \in \mathbb{R}$ as follows:

$$u_t = (1 + 0.1\xi_t)u_t^* + 0.5\xi_t. \quad (5.3.2)$$

We can see, that $u_t = u_0$ given $\xi_t = 0$.

3. Parametrization of wind direction ϕ :

Wind direction is also assumed to be variable over time and homogeneous over the whole calculation domain at a time. It is parametrized using control variable $\psi_t \in \mathbb{R}$ as follows:

$$\phi_t = \phi_t^* + \psi_t. \quad (5.3.3)$$

From the parameterization is evident that the wind field is assumed to be homogeneous in the whole computational domain at a time. This simplifying assumption is reasonable in the case of a short-range dispersion modeling, where the wind field is not likely to change dramatically in space. Location parameters u_t^* and ϕ_t^* represent the wind speed and the wind direction given by a meteorological forecast and $Q^{i,*}$ is the initial estimate of source term based on the safety parameters of a NPP. Similar parameterizations can

be constructed for some other physical processes involved, e.g., magnitude of vertical and horizontal dispersion, dry and wet deposition.

The state vector $\boldsymbol{\theta}_t$ is evolved using a transitional pdf

$$p(\boldsymbol{\theta}_t|\boldsymbol{\theta}_{t-1}) = \delta(\omega_t - \omega_1)p(\xi_t|\xi_{t-1})p(\psi_t|\psi_{t-1}), \quad (5.3.4)$$

and the process is initialized with a prior pdf

$$p(\boldsymbol{\theta}_1) = p(\omega_1)p(\xi_1)p(\psi_1). \quad (5.3.5)$$

5.3.2 Observation Operator

Given the control variables and other inputs, the model (2.1.16) evaluates activity concentration in air in $Bq\ m^{-3}$. The observation operator converting the concentration to the time integrated gamma dose in Gy is defined by (2.2.8)–(2.2.9).

5.3.3 Evaluation of Weights

The weights are evaluated using

$$\begin{aligned} w_t^{(i)} &\propto \frac{p(\boldsymbol{\theta}_{1:t}^{(i)}|\mathbf{y}_{1:t})}{q(\boldsymbol{\theta}_{1:t}^{(i)}|\mathbf{y}_{1:t})} = \frac{p(\mathbf{y}_t|\boldsymbol{\theta}_t^{(i)})p(\boldsymbol{\theta}_t^{(i)}|\boldsymbol{\theta}_{t-1}^{(i)})p(\boldsymbol{\theta}_{1:t-1}^{(i)}|\mathbf{y}_{1:t-1})}{q(\boldsymbol{\theta}_{1:t}^{(i)}|\mathbf{y}_{1:t})} \\ &\propto \frac{\prod_{j=1}^t p(\mathbf{y}_j|\boldsymbol{\theta}_j^{(i)})p(\boldsymbol{\theta}_j^{(i)}|\boldsymbol{\theta}_{j-1}^{(i)})}{q(\boldsymbol{\theta}_{1:t}^{(i)}|\mathbf{y}_{1:t})}. \end{aligned} \quad (5.3.6)$$

For computational reasons, the weights are evaluated in the logarithmic scale according to Section 3.5.3 and the product in (5.3.6) becomes a sum of logarithms

$$\ln w_t^{(i)} = \sum_{j=1}^t \left[\ln p(\mathbf{y}_j|\boldsymbol{\theta}_j^{(i)}) + \ln p(\boldsymbol{\theta}_j^{(i)}|\boldsymbol{\theta}_{j-1}^{(i)}) \right] - \ln q(\boldsymbol{\theta}_{1:t}^{(i)}|\mathbf{y}_{1:t}).$$

The normality of the observation model (5.2.4) determines the likelihood functions $p(\mathbf{y}_j|\boldsymbol{\theta}_j^{(i)})$ to be

$$p(\mathbf{y}_j|\boldsymbol{\theta}_j^{(i)}) = (2\pi)^{-\frac{N_y}{2}} (\det \mathbf{R}_j)^{-\frac{1}{2}} \exp \left[-0.5 \left(\mathbf{y}_j - \mathcal{H}(\boldsymbol{\theta}_j^{(i)}) \right)^T \mathbf{R}_j^{-1} \left(\mathbf{y}_j - \mathcal{H}(\boldsymbol{\theta}_j^{(i)}) \right) \right].$$

Matrix \mathbf{R}_j is the covariance matrix of observations \mathbf{y}_j . Since the observations are assumed to be conditionally independent given $\boldsymbol{\theta}_j$, covariance matrix \mathbf{R}_j is diagonal and the observations can be processed sequentially using

$$p(\mathbf{y}_j|\boldsymbol{\theta}_j^{(i)}) = \prod_{k=1}^{N_y} p(y_{k,j}|\boldsymbol{\theta}_j^{(i)}) = (2\pi)^{-\frac{N_y}{2}} \prod_{k=1}^{N_y} \sigma_{k,j}^{-1} \exp \left[-0.5 \left(y_{k,j} - \mathcal{H}_k(\boldsymbol{\theta}_j^{(i)}) \right)^2 / \sigma_{k,j}^2 \right].$$

Here, \mathcal{H}_k is a reduced observation operator evaluating just time integrated gamma dose rate in location $\mathbf{s}_k^R \in \mathcal{S}^R$, and $\sigma_{k,j}^2 = \mathbf{R}_j[k, k]$, $k = 1, \dots, N_y$, is the k th diagonal element of \mathbf{R}_j .

5.3.4 Adaptive Selection of Proposal Density

We apply the adaptive proposal selection procedure described in Section 3.5.2. Let the proposal density be normally distributed. Using conditional independence of control variables we can write:

$$\begin{aligned} q(\boldsymbol{\theta}_{1:t} | \mathbf{y}_{1:t}) &= q(\omega_1, \xi_1, \dots, \xi_t, \psi_1, \dots, \psi_t | \mathbf{y}_{1:t}) \\ &= \mathcal{N}(\omega_1; \bar{\omega}_1, \Sigma_t^\omega) \mathcal{N}(\boldsymbol{\xi}_t; \bar{\boldsymbol{\xi}}_t, \Sigma_t^\xi) \mathcal{N}(\boldsymbol{\psi}_t; \bar{\boldsymbol{\psi}}_t, \Sigma_t^\psi). \end{aligned} \quad (5.3.7)$$

Vectors $\boldsymbol{\xi}_t = (\xi_1, \dots, \xi_t)^\top$ and $\boldsymbol{\psi}_t = (\psi_1, \dots, \psi_t)^\top$ aggregate wind speed and wind direction in time steps $1, \dots, t$. Their dimensions thus increase in time.

At each time step, moments of Gaussian pdfs in (5.3.7), mean values $\bar{\omega}_1 \in \mathbb{R}$, $\bar{\boldsymbol{\xi}}_t \in \mathbb{R}^t$, $\bar{\boldsymbol{\psi}}_t \in \mathbb{R}^t$ and corresponding variance Σ_t^ω and diagonal covariance matrices Σ_t^ξ , Σ_t^ψ , can be estimated independently from the weights and the particles $\boldsymbol{\theta}_{1:t}^{(i)} = (\omega_1^{(i)}, \boldsymbol{\xi}_t^{(i)}, \boldsymbol{\psi}_t^{(i)})^\top$:

$$\begin{aligned} \bar{\omega}_1 &= \sum_{i=1}^N w_t^{(i)} \omega_1^{(i)}, & \Sigma_t^\omega &= \sum_{i=1}^N w_t^{(i)} \left(\omega_1^{(i)} - \bar{\omega}_1 \right)^2, \\ \bar{\boldsymbol{\xi}}_t &= \sum_{i=1}^N w_t^{(i)} \boldsymbol{\xi}_t^{(i)}, & \Sigma_t^\xi[j, j] &= \sum_{i=1}^N w_t^{(i)} \left(\boldsymbol{\xi}_t^{(i)}[j] - \bar{\boldsymbol{\xi}}_t[j] \right)^2, & j &= 1, \dots, t, \\ \bar{\boldsymbol{\psi}}_t &= \sum_{i=1}^N w_t^{(i)} \boldsymbol{\psi}_t^{(i)}, & \Sigma_t^\psi[j, j] &= \sum_{i=1}^N w_t^{(i)} \left(\boldsymbol{\psi}_t^{(i)}[j] - \bar{\boldsymbol{\psi}}_t[j] \right)^2, & j &= 1, \dots, t. \end{aligned}$$

5.4 Numerical Experiment

In numerical experiment we assume an instantaneous release of radionuclide ^{41}Ar with half-life of decay 109.34 minutes. Radionuclide ^{41}Ar was chosen for two reasons: Firstly, since ^{41}Ar is a noble gas, there is no deposition and consequently no groundshine. We need to calculate only the gamma dose rate from cloudshine. Secondly, according to Tables of Radioactive Isotopes (Browne et al., 1986), the radionuclide ^{41}Ar emits gamma radiation on energy level 1293.57 keV with branching ration 99.1%. Generally, for calculation of the gamma dose rate we need to assume all the energy levels and their branching ratios specific to the given radionuclide. In the case of ^{41}Ar we can neglect the other energy levels within the remaining branching ratio 0.9% without any significant loss of accuracy. Both these facts substantially simplifies gamma dose rate calculations and makes the experiment more transparent. Since we simulate a release of a noble gas, the deposition is not calculated here.

Data assimilation is performed in time steps $t = 1, \dots, 18$. Duration of time step Δ_τ is set to 10 minutes. This step length was chosen because we assume that the radiation monitoring network provides measurements of the time integrated gamma dose rate in 10-minute intervals (Dombrowski et al., 2009).

5.4.1 Computational and Observational Grids

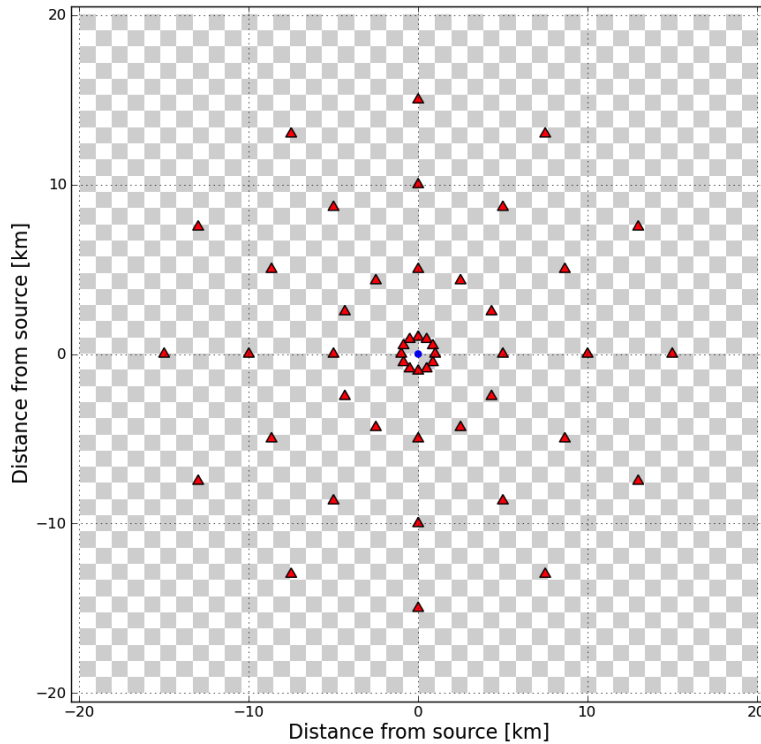


Figure 5.4.1: Illustration of computational grid and monitoring network.

The computational domain is delimited with a square centered at the location of the Czech nuclear power plant Temelin and with the side length 20km. The area is regularly covered with a rectangular grid with the grid step 1km. The total number of grids points is $41 \times 41 = 1681$. This area includes the emergency planning zone delimited with a circle of radius 13km centered at the power plant. The zone delimits potential accident site, where public is expected to be put in risk if exposed to the radioactive plume.

The measurements are assumed to come from a stationary radiation monitoring network. Let the network comprises of 48 receptors placed in the four circular bands of radii 1km, 5km, 10km, and 15km. In reality, the gamma dose rate receptors comprising the monitoring network would be placed in settled areas, e.g., in towns and villages within the zone. However, since we investigate the properties of the algorithm, the configuration of receptor points is fully justifiable for our purposes. The receptors closest to the center denote the receptors placed in the area of the power plant, the

COORDINATES OF RECEPTORS								
Rec. no.	x [m]	y [m]	Rec. no.	x [m]	y [m]	Rec. no.	x [m]	y [m]
1	0	1000	17	4330	-2500	33	-8660	-5000
2	500	866	18	2500	-4330	34	-10000	0
3	866	500	19	0	-5000	35	-8660	5000
4	1000	0	20	-2500	-4330	36	-5000	8660
5	866	-500	21	-4330	-2500	37	0	15000
6	500	-866	22	-5000	0	38	7500	12990
7	0	-1000	23	-4330	2500	39	12990	7500
8	-500	-866	24	-2500	4330	40	15000	0
9	-866	-500	25	0	10000	41	12990	-7500
10	-1000	0	26	5000	8660	42	7500	-12990
11	-866	500	27	8660	5000	43	0	-15000
12	-500	866	28	10000	0	44	-7500	-12990
13	0	5000	29	8660	-5000	45	-12990	-7500
14	2500	4330	30	5000	-8660	46	-15000	0
15	4330	2500	31	0	-10000	47	-12990	7500
16	5000	0	32	-5000	-8660	48	-7500	12990

Table 5.1: Coordinates of the receptors comprising radiation monitoring network in the numerical example.

tele-dosimetric system (TDS) on fence of the power plant. Schematic illustration of the monitoring network and the computational grid is in Figure 5.4.1. The computational points are represented with edges of the “chess board” and the receptors are denoted with the red triangles. Coordinates of the receptors are in Table 5.1.

5.4.2 Simulation of Observations

Numerical experiment is performed as a twin experiment, where the measurements are generated using a twin model and perturbed with a random noise. The twin model is a dispersion model initialized with a set of inputs defining unknown conditions of the “real” release. Convergence of the dispersion model initialized with a set of nominal inputs to the twin model is then assessed.

The nominal values of the wind speed and the wind direction are hourly meteorological forecast from a numerical weather prediction model. The true values of the wind direction are assumed to change every 10 minutes. The true wind speed is constant and systematically higher than the nominal values. Summary of setting of the nominal and the twin model is in Table 5.2:

1. Nominal values $Q^{i,*}, u_t^*, \phi_t^*$ given by an expert and the meteorological forecast (locations parameters).

PARAMETERS OF NOMINAL MODEL AND TWIN MODEL										
		Immutable variables			Mutable variables					
		Magnitude of release			Wind speed			Wind direction		
Hour	t	$Q^{i,*}$	ω_1^r	$Q^{i,r}$	u_t^*	ξ_t^r	u_t^r	ϕ_t^*	ψ_t^r	ϕ_t^r
1	1	5.0E+14	5.0	2.5E+15	2.0	0.71	2.5	270.0	0.0	270.0
1	2				2.0	0.71	2.5	270.0	10.0	280.0
1	3				2.0	0.71	2.5	270.0	20.0	290.0
1	4				2.0	0.71	2.5	270.0	30.0	300.0
1	5				2.0	0.71	2.5	270.0	40.0	310.0
1	6				2.0	0.71	2.5	270.0	50.0	320.0
2	7				2.0	0.71	2.5	280.0	50.0	330.0
2	8				2.0	0.71	2.5	280.0	60.0	340.0
2	9				2.0	0.71	2.5	280.0	70.0	350.0
2	10				2.0	0.71	2.5	280.0	60.0	340.0
2	11				2.0	0.71	2.5	280.0	50.0	330.0
2	12				2.0	0.71	2.5	280.0	40.0	320.0
3	13				2.0	0.71	2.5	290.0	20.0	310.0
3	14				2.0	0.71	2.5	290.0	10.0	300.0
3	15				2.0	0.71	2.5	290.0	0.0	290.0
3	16				2.0	0.71	2.5	290.0	-10.0	280.0
3	17				2.0	0.71	2.5	290.0	-20.0	270.0
3	18				2.0	0.71	2.5	290.0	-30.0	260.0

Table 5.2: Parameters of nominal and twin model. Nominal values $Q^{i,*}$, u_t^* , ϕ_t^* of physical quantities treated as uncertain. “Real” values $Q^{i,r}$, u_t^r , ϕ_t^r of the quantities used for simulation of measurements. Sought values of variables $\theta_t^r = (\omega_1^r, \xi_t^r, \psi_t^r)$ transforming the nominal values into the real values using parameterizations (5.3.1)–(5.3.3).

2. “Real” values of physical quantities $Q^{i,r}$, u_t^r , ϕ_t^r used for simulation of measurements.
3. Sought values of control variables $\theta_t^r = (\omega_1^r, \xi_t^r, \psi_t^r)$ transforming the nominal values into the real values using parameterizations (5.3.1)–(5.3.3).

In the experiment we expect convergence of the estimated control variables $\bar{\theta}_t$ (5.2.6) to θ_t^r . In Figure 5.4.2 we see the time integrated dose evaluated for the first three hours of the release with the nominal model (left) and the twin model (right). Radiation monitoring network \mathcal{S}^R is denoted with the red triangles. Measurements \mathbf{y}_t are sampled during the twin model propagation in 10-minute intervals according to $\mathbf{y}_t \sim \mathcal{N}(\mathcal{H}(\theta_{1:t}), \mathbf{R}_t)$, where the observation operation \mathcal{H} is given by (2.2.8)–(2.2.9). Covariance matrix \mathbf{R}_t is a diagonal matrix, where the standard deviations of elements of \mathbf{y}_t are linearly proportional to measurements:

$$\mathbf{R}_t[j, j] = (0.1\mathbf{y}_t[j] + 1.0E - 20)^2. \quad (5.4.1)$$

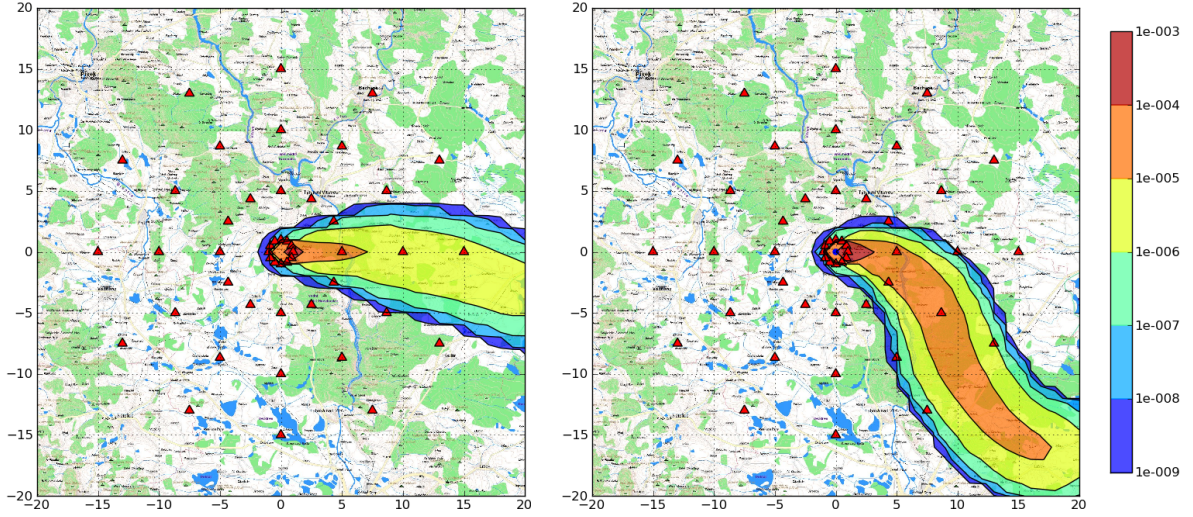


Figure 5.4.2: Time integrated gamma dose evaluated for the first three hours of the release with the nominal model (left) and the twin model (right).

Here, $\mathbf{R}_t[j, j]$ and $\mathbf{y}_t[j]$ denote the j th diagonal element of \mathbf{R}_t and the j th element of \mathbf{y}_t , respectively. Particles are initialized with values of control variables sampled from prior pdf (5.3.5), where

$$\begin{aligned} p(\omega_1) &= \log\mathcal{N}(0.5, 0.25), \\ p(\xi_1) &= \mathcal{U}(-2, 2), \\ p(\psi_1) &= \mathcal{U}(-22.5, 22.5). \end{aligned}$$

Control variables are evolved using transitional pdf (5.3.4), where

$$\begin{aligned} p(\xi_t|\xi_{t-1}) &= \mathcal{N}(\xi_{t-1}, \sigma_\xi^2), \quad \sigma_\xi = 0.4, \\ p(\psi_t|\psi_{t-1}) &= \mathcal{N}(\psi_{t-1}, \sigma_\psi^2), \quad \sigma_\psi = 2.5. \end{aligned}$$

5.4.3 Results

We run the assimilation algorithm with $N = 3000$ particles for 18 steps covering the first three hours of the release.

In Figure 5.4.3, the nominal model, the twin model, and the assimilated model are compared. The results are visualized in terms of \mathcal{D}^c integrated from time step 0 up to time steps 6, 12, and 18, respectively. We see that the nominal model without the data assimilation would predict doses smaller in magnitude and also the affected areas would be misspecified. We can observe that the expected values of \mathcal{D}^c up to time step $t = 12$ well approximate \mathcal{D}^c evaluated by the twin model. During the last six assimilation steps we observe a misfit of the wind direction. This is due to the lack of measurements in the area where the puffs (particles) were during the third hour of their propagation, see Figure 5.4.3 (bottom-right).

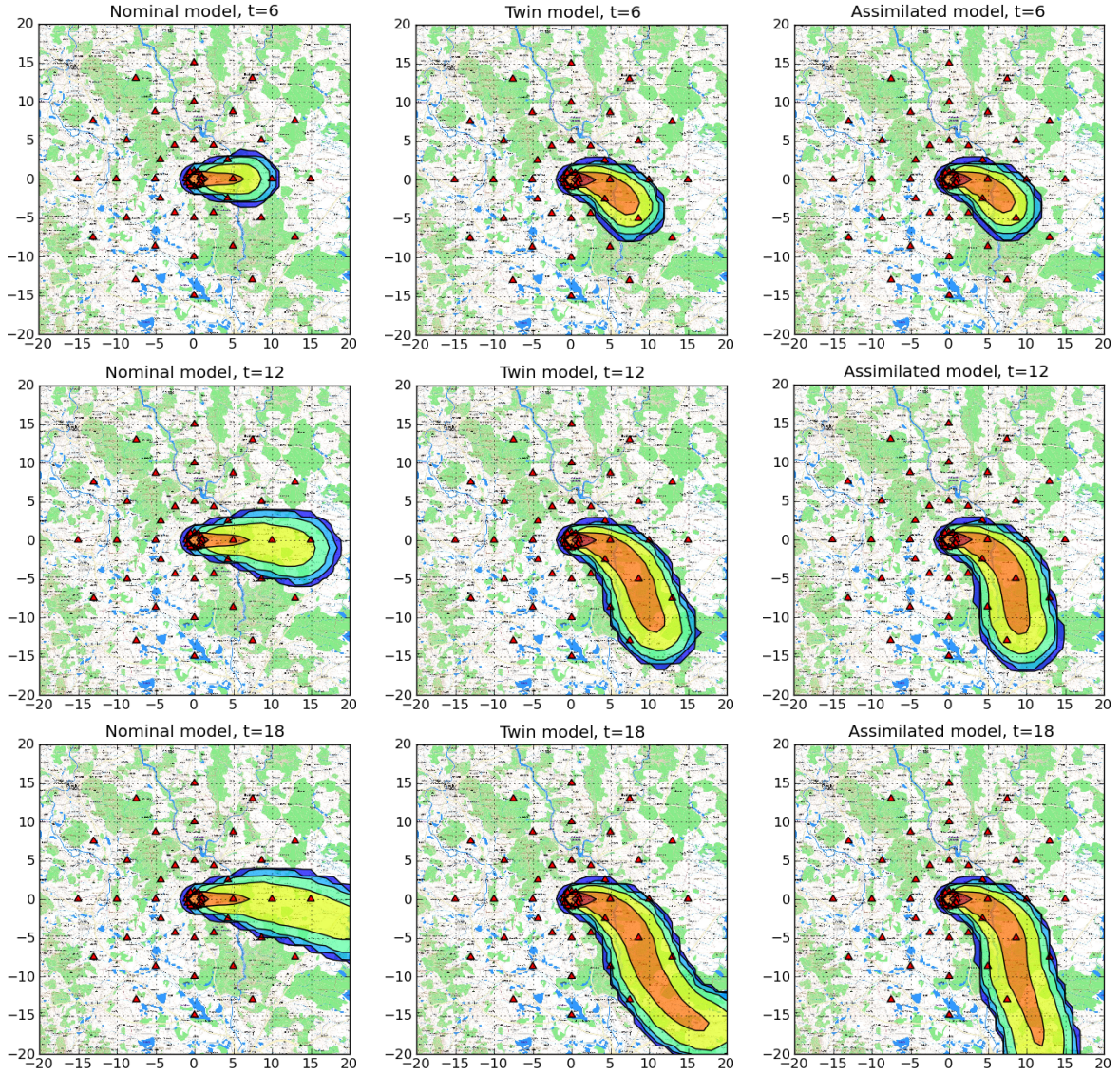


Figure 5.4.3: Comparison of the nominal model, the twin model and the assimilated model in time steps $t = 6, 12, 18$. The misfit of the wind direction in the last hour is due to the lack of measurements in the area.

In Figure 5.4.4, estimates \bar{Q}^i , \bar{u}_t , $\bar{\phi}_t$ (5.2.6) evaluated using nominal values $Q^{i,*}$, u_t^* , ϕ_t^* , weights $w_t^{(i)}$ and the states $\theta_t^{(i)}$ of the re-computed state trajectories $\theta_{1:t}^{(i)}$ in each time step are visualized. We see how the estimated values of magnitude of release, wind speed and wind direction (red lines) approach the values used for simulation of measurements (green lines). Values of the physical quantities used for propagation of the puffs are denoted with the blue dots. Only those particles with nonzero weights are visualized. During the first five steps, the magnitude of release is correctly recognized and stays tuned for the remaining time steps. Convergence to the correct wind speed and wind directions is more rapid. The lack of measured information during the last

six time steps cause, that the weights are approximately equal and the variances of the estimates increase. With the non-informative weights, the algorithm does not have enough information to correctly estimate the wind direction.

In Figure 5.4.5 we see how the expected values $\bar{\theta}_t$ of control variables (red lines) approach the true values of control variables θ_t^r (green lines) used for simulation of measurements. The gray bands denote the maximal and minimal values of particles in each time step.

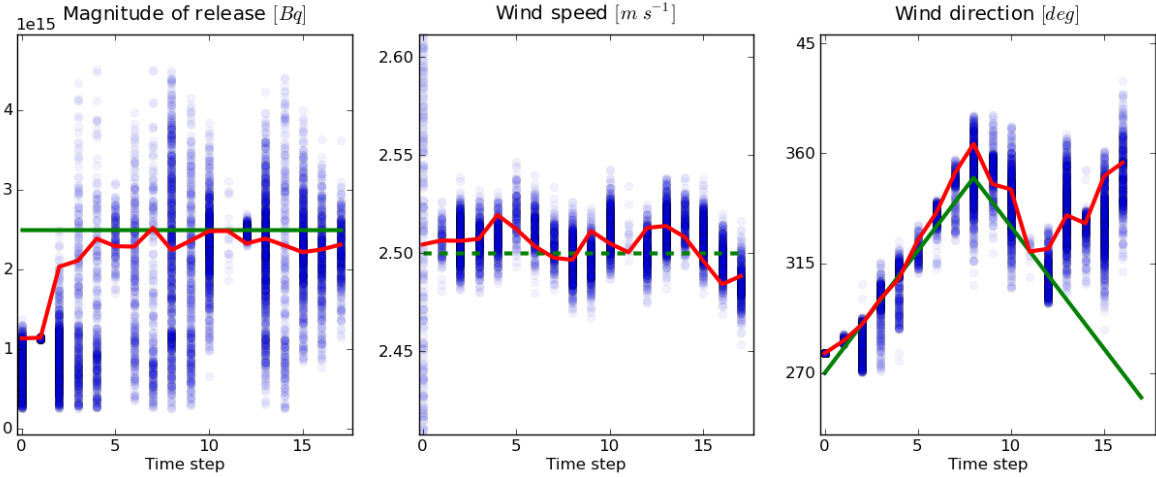


Figure 5.4.4: Estimated values of magnitude of release, wind speed and wind direction. Green lines: values used for simulation of measurements; red lines: estimated values of physical quantities; blue dots: values of particles with nonzero weights.

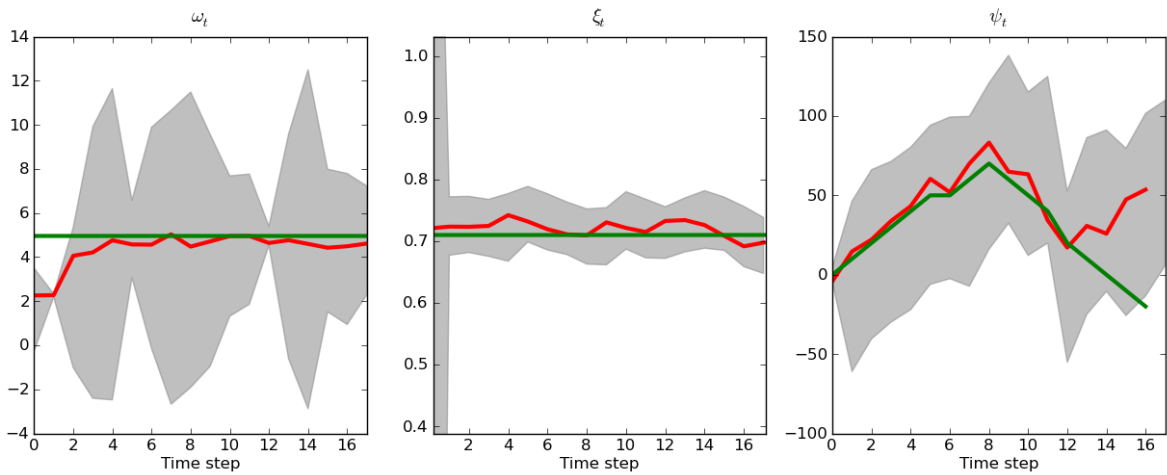


Figure 5.4.5: Estimated values of magnitude of release, wind speed and wind direction. Green lines: values used for simulation of measurements; red lines: estimated values; gray areas: regions between minimum and maximum values of the particles.

Time evolution of time integrated doses \mathcal{D}^c at selected receptor locations is visualized in Figure 5.4.6. There is a good agreement between the doses generated by the twin model and the assimilated model. In the case of receptors 40 and 41 we observe a disagreement due to misspecification of the wind direction caused by the lack of monitoring data.

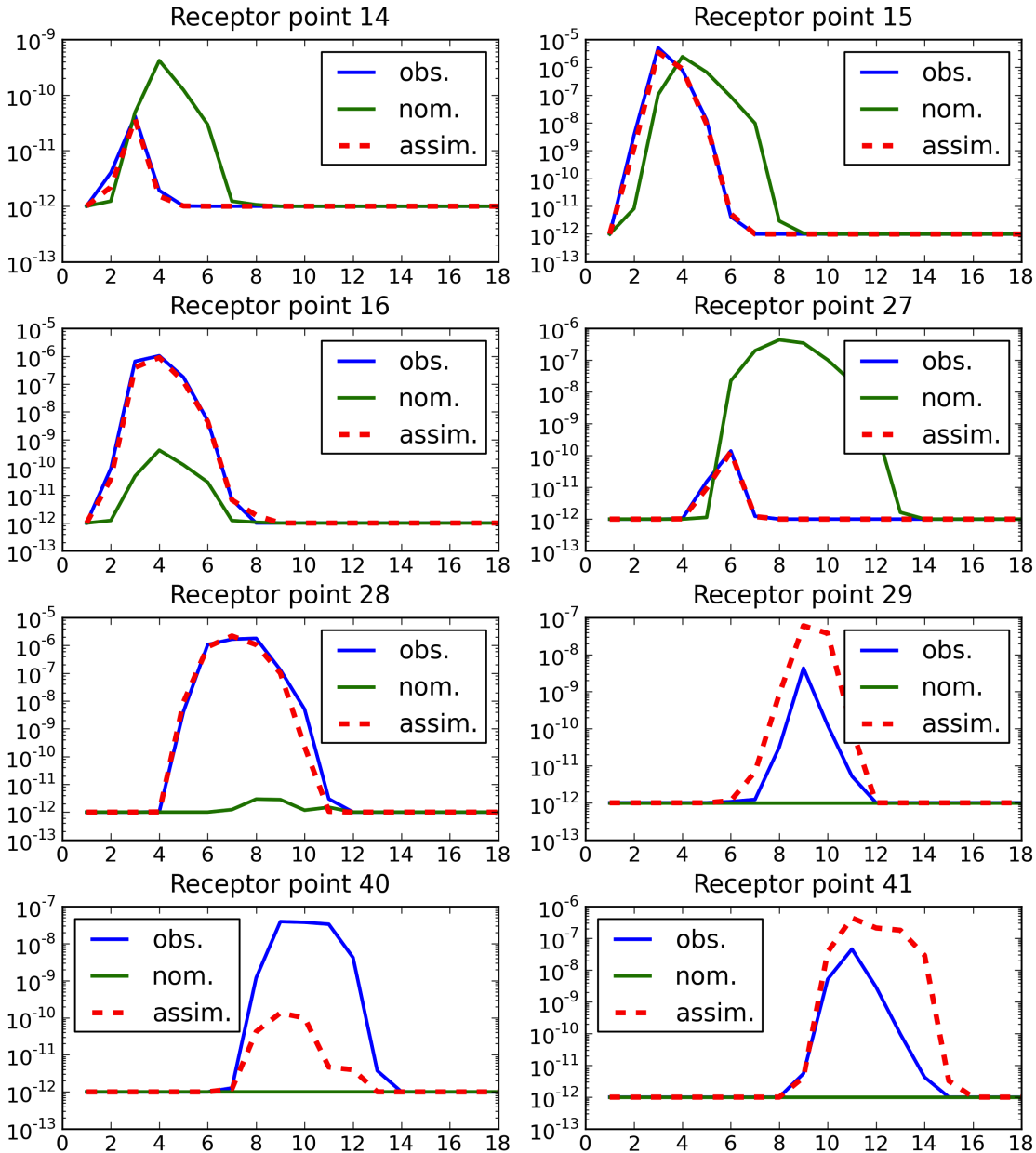


Figure 5.4.6: Time evolution of time integrated doses \mathcal{D}^c given by the twin model (blue solid lines), the nominal model (green solid lines), and the assimilated model (red dashed lines) at receptor locations 14, 15, 16, 27, 28, 29, 40 and 41 (see Table 5.1).

5.5 Summary

This chapter has developed and demonstrated a new methodology for data assimilation of gamma dose rate measurements with modeled activity concentration air. We propose to use sequential Monte Carlo methods for estimation the most important parameters of a dispersion model and thus improve the correspondence of the model output with the measurements. The methodology is based on simultaneous propagation of multiple dispersion models initialized with different inputs. The resulting algorithm seeks for the most plausible values of these parameters (here referred as control variables) using particle filtering with adaptive selection of the proposal density. Adaptive proposal selection makes the algorithm more efficient, because the trajectories of particles are sampled from a promising subspace of the full state-space. The presented form of the proposal density is a rather simple choice and more elaborated approaches can be constructed, e.g., a parametrized proposal in the form of a Gaussian mixture.

Introduced Bayesian methodology has very interesting properties suitable for the solved scenario. The probabilistic aspect of the solution optimally combines a likely answer with uncertainties of the available data. Since the uncertainty is accounted for, the physical parameters of the model are the best parameters possible, not in the sense of exact match, but because they lead to the best representation of the true system, given the assumptions that were used to build the model. The corrected parameters may in turn be used as input to long- and short-range atmospheric dispersion models, resulting in greatly improved dose rate assessment.

The algorithm was demonstrated on estimation of magnitude of release, wind speed, and wind direction of a Gaussian puff model. Since the measuring of concentration itself is not technically feasible, nonlinear observation operator for transformation of the activity concentration in air into the time integrated gamma dose rate was implemented. Selected control variables were successfully estimated and the assimilated dose rates were close to the dose rate from the twin model using a sparse observational grid. The algorithm performed well in a meandering wind field, which is particularly important under low-wind conditions. The extension of the algorithm to account for different physical effects is straightforward, however, we have to consider computational demands regarding intensive sampling during the particle filtering assimilation procedure.

Chapter 6

Data Assimilation in the Late Phase

6.1 Problem Statement

Under the term *late phase* we understand the time period after the release of radioactive material when the atmospheric transport (and subsequently the deposition) of radionuclides has finished. During the late phase, there is no more irradiation from the cloud but the deposited radioactive material causes external irradiation from groundshine and internal irradiation from inhalation of the re-suspended material. What is more, radionuclides migrate through the root system and foliage of plants into their edible parts and thus can cause internal irradiation of people and livestock when eaten. This phase extends over a period of several weeks or many years, depending on the magnitude and type of initially deposited radionuclides.

From the point of view of radiation protection, the attention is focused on the long-term monitoring of the radiation levels and modeling of its further transport towards human body through the food chain. We are concerned with the deposition modeling. Determination of the spatial and temporal distribution of radionuclides on terrain and the rate of radionuclides removal is crucial for planning of the late phase countermeasures. These regard agriculture, foodstuffs production and water-resources management (Pröhl et al., 1993).

In this chapter we propose a new data assimilation method based on the MPF framework developed in Chapter 4 for joint estimation of a spatially distributed radiological quantity and a set of parameters concerning the process of radioactivity removal.

6.2 Data Assimilation Scenario

During the late phase, the main aim of monitoring is to obtain a comprehensive picture of contamination of the environment Gering et al. (2004). The most significant monitored radiological quantities are:

- The external dose rate from deposition (*groundshine*),

- The spectrum of deposited radionuclides and the relative deposition on different surfaces,
- The contamination of reference foodstuffs.

We focus on the groundshine dose modeling, specifically, on determination of the spatial distribution of radionuclides and the groundshine dose time evolution. We approach the problem using the data assimilation, where the groundshine dose measurements are related to the predictions of deposition via groundshine dose evolution model. Here, the highest uncertainty consists (i) in the initial displacement of the deposition and (ii) in the rate of groundshine dose mitigation due to radionuclides removal and migration processes. The initial deposition displacement is fully determined by the plume depletion during the early phase. This means that the uncertainty regarding aerial pollution propagation must be considered. What regards the issue of groundshine mitigation, two dominant processes—radioactive decay and environmental removal—must be modeled. The latter is given by parametrized formula (2.2.12). Generally, the parameterization of environmental removal depends on many factors, including the place of model application. A reasonable approach is to treat the parameters as random variables and attempt for their estimation using available radiological measurements.

In this work, the following objectives of the groundshine dose modeling in the late phase are addressed:

1. The estimation of initial deposition displacement using available measurements referring to the beginning of the late phase.
2. The estimation of radiation levels in the contaminated areas and the prediction of its time evolution.
3. The estimation of the speed of radionuclides removal.

The refined estimates of the spatio-temporal distribution of radioactivity and its time evolution can in turn be used for long-term predictions.

Data assimilation in the late phase has its own specifics. The key differences compared to the data assimilation in the early phase are as follows:

High state dimension: The state vector contains the values of deposition in an ordered set of spatial points. To achieve a good spatial resolution, we want to estimate the deposition values on a dense computational grid. This means that we have to employ an estimation methodology suitable for large-scale problems, e.g., ensemble filtering.

Time constraints: With respect to the dynamics of the radionuclides transport in the late phase and its duration, the time constraints are not so strict as in the early phase. Particularly in the case of a retrospective analysis, the time constraints are of a minor interest.

Higher amount of available data: We can assume that the number of available measurements is higher than in the early phase. Monitoring strategies in the late phase combine various monitoring systems in an operational way to meet the requirements of off-site emergency management. We can assume that the observations come from the airborne gamma spectrometry. It is a powerful tool capable of rapid mapping of contamination levels in a broader scale, which was demonstrated during the Chernobyl accident (Gering et al., 2004).

With respect to the above specific properties, the data assimilation strategy must be appropriately chosen. We propose to use the marginalized particle filtering framework developed in Chapter 4. Here, the uncertain parameters of the environmental removal are estimated using the particle filter and the spatio-temporal distribution of the deposition given the parameters is estimated using the ensemble square root filter. What results is a hybrid filter, where N weighted ensemble filters are simultaneously run. Overall rate of environmental removal in the considered area is estimated using the particle filter and the ensemble filter account for local characteristics.

For numerical reasons, the calculations are performed in terms of deposition. Transformation of the deposition into the groundshine dose (2.2.10) can be simply done using the dose rate conversion factor.

6.3 Proposed Data Assimilation Methodology

Let $\mathbf{d}_t \in \mathbb{R}^{N_d}$ be a vector of deposition values in a set of computational points $\mathcal{S} = \{\mathbf{s}_1, \dots, \mathbf{s}_{N_d}\}$. Let $\boldsymbol{\theta}_t \in \mathbb{R}^{N_\theta}$ aggregate radionuclides removal rate parameters and parameters influencing magnitude and structure of model error in the ensemble filter. We use marginalized filtering framework introduced in Chapter 4, where we substitute $\mathbf{x}_t^c \equiv \mathbf{d}_t$, $\mathbf{x}_t^p \equiv \boldsymbol{\theta}_t$ in factorization (3.6.1), yielding the state vector

$$\mathbf{x}_t = \begin{bmatrix} \mathbf{d}_t \\ \boldsymbol{\theta}_t \end{bmatrix}. \quad (6.3.1)$$

Parameters $\boldsymbol{\theta}_t$ are estimated using the particle filter and the deposition field \mathbf{d}_t is estimated using the conditional ensemble square root filter. The resulting posterior is of the form given by (3.6.3).

6.3.1 State Evolution Model

Model $\mathcal{M}(\mathbf{d}, \boldsymbol{\theta}, \boldsymbol{\epsilon})$ describing the evolution of deposition \mathbf{d} is a non-linear function of parameters $\boldsymbol{\theta}$ and zero-mean mutually independent random noise $\boldsymbol{\epsilon}$,

$$\mathbf{d}_t = \mathcal{M}(\mathbf{d}_{t-1}, \boldsymbol{\theta}_t, \boldsymbol{\epsilon}_t).$$

From (2.2.11) follows that given particular values of $\boldsymbol{\theta}_t$, the model becomes linear in \mathbf{d}_t and we can construct a linear state evolution model for fixed $\boldsymbol{\theta}_{t-1}$ and $\boldsymbol{\theta}_t$ represented with a matrix \mathbf{M} ,

$$\begin{aligned}
\mathbf{d}_t &= \mathbf{M}(\boldsymbol{\theta}_t)\mathbf{d}_{t-1} + \boldsymbol{\epsilon}_t, \\
\mathbf{M}_t &= \frac{f_{\mathbf{R}}(t)f_{\mathbf{E}}(t, \boldsymbol{\theta}_t)}{f_{\mathbf{R}}(t-1)f_{\mathbf{E}}(t-1, \boldsymbol{\theta}_{t-1})}\mathbf{I}.
\end{aligned} \tag{6.3.2}$$

Determination of spatio-temporal distribution of deposition and the speed of its removal can be interpreted as estimation of the augmented state \mathbf{x}_t comprised of the vector \mathbf{d}_t of the deposition values on a grid and the vector $\boldsymbol{\theta}_t$ of variables parameterizing the removal speed. Since we attempt for estimation of the model error, its parameterization is also included into $\boldsymbol{\theta}$. The state is evolved using transitional pdf

$$\begin{aligned}
p(\mathbf{x}_t|\mathbf{x}_{t-1}) &= p(\mathbf{d}_t, \boldsymbol{\theta}_t|\mathbf{d}_{t-1}, \boldsymbol{\theta}_{t-1}) \\
&= p(\mathbf{d}_t|\mathbf{d}_{t-1}, \boldsymbol{\theta}_t, \boldsymbol{\theta}_{t-1})p(\boldsymbol{\theta}_t|\mathbf{d}_{t-1}, \boldsymbol{\theta}_{t-1}),
\end{aligned}$$

where the time evolution of $\boldsymbol{\theta}_t$ is assumed to be dependent just on its previous value,

$$p(\boldsymbol{\theta}_t|\mathbf{d}_{t-1}, \boldsymbol{\theta}_{t-1}) = p(\boldsymbol{\theta}_t|\boldsymbol{\theta}_{t-1}).$$

The time evolution of \mathbf{d}_t is given by a Gaussian pdf

$$p(\mathbf{d}_t|\mathbf{d}_{t-1}, \boldsymbol{\theta}_t, \boldsymbol{\theta}_{t-1}) = \mathcal{N}(\bar{\mathbf{d}}_{t|t-1}, \mathbf{P}_{t|t-1}), \tag{6.3.3}$$

$$\bar{\mathbf{d}}_{t|t-1} = \mathbf{M}_t\bar{\mathbf{d}}_{t-1|t-1}, \tag{6.3.4}$$

where $\bar{\mathbf{d}}_{t|t-1}$ and $\mathbf{P}_{t|t-1}$ are predictive statistics evaluated by the time update step of the ensemble filter. Since the parameterization of model error is included in $\boldsymbol{\theta}_t$, the predictive error covariance matrix $\mathbf{P}_{t|t-1}$ is a function of $\boldsymbol{\theta}_t$.

6.3.2 Observation Operator

Groundshine dose measurements given on an observational grid $\mathcal{S}_t^{\mathbf{R}} = \{\mathbf{s}_{1,t}^{\mathbf{R}}, \dots, \mathbf{s}_{N_y,t}^{\mathbf{R}}\}$ are aggregated in a vector $\mathbf{y}_t \in \mathbb{R}^{N_y}$. The measurements assumed to be normally distributed with covariance matrix \mathbf{R}_t and mutually independent given the state \mathbf{x}_t ,

$$p(\mathbf{y}_t|\mathbf{x}_t) = \mathcal{N}(\mathbf{H}\mathbf{d}_{t|t-1}, \mathbf{R}_t). \tag{6.3.5}$$

Covariance \mathbf{R}_t describes the instrumental error of the measuring device and the linear observation operator \mathbf{H} relates the deposition with the groundshine dose. In the case that the observational and the computational grids are not aligned, the operator also performs a spatial interpolation using the bilinear interpolation.

6.3.3 Evaluation of Weights

The normality of the observation model (6.3.5) implies the likelihood function used for evaluation of weights in the particle filter has the form

$$p(\mathbf{y}_t | \mathbf{y}_{1:t-1}, \mathbf{x}_t^{(i)}) \propto \det \left(\mathbf{Z}_t(\boldsymbol{\theta}_t^{(i)}) \right)^{-\frac{1}{2}} \exp \left[-\frac{1}{2} \left(\mathbf{v}_t^{(i)} \right)^T \mathbf{Z}_t^{-1}(\boldsymbol{\theta}_t^{(i)}) \mathbf{v}_t^{(i)} \right], \quad (6.3.6)$$

where $\mathbf{v}_t^{(i)} = \mathbf{y}_t - \mathbf{H} \bar{\mathbf{d}}_{t|t-1}^{(i)}$, $\mathbf{Z}_t^{(i)} = \mathbf{H} \mathbf{P}_{t|t-1}^{(i)} \mathbf{H}^T + \mathbf{R}_t$. Note, that the covariance matrices $\mathbf{Z}_t^{(i)}$ are explicitly conditioned on vectors $\boldsymbol{\theta}_t^{(i)}$ corresponding to particles.

Since the covariance square roots are stored in EnSRFs, it would be beneficial to avoid evaluation of the full covariance matrices. This can be achieved using the results of Appendix B. Let $\mathbf{F}_t^{(i)}$ and $\mathbf{S}_{t|t-1}^{(i)}$ be square roots of covariance matrices $\mathbf{Z}_t^{(i)}$ and $\mathbf{P}_{t|t-1}^{(i)}$, respectively:

$$\mathbf{Z}_t^{(i)} = \mathbf{F}_t^{(i)} \left(\mathbf{F}_t^{(i)} \right)^T, \quad \mathbf{P}_{t|t-1}^{(i)} = \mathbf{S}_{t|t-1}^{(i)} \left(\mathbf{S}_{t|t-1}^{(i)} \right)^T.$$

Using the result of Appendix B and substituting $\mathbf{B} = \mathbf{S}_{t|t-1}^{(i)}$, $\mathbf{C} = \mathbf{H}_t$, and $\mathbf{D} = \mathbf{R}_t$, it follows that

$$\begin{bmatrix} \left(\mathbf{F}_t^{(i)} \right)^T \\ \mathbf{0} \end{bmatrix} = \mathbf{T} \begin{bmatrix} \left(\mathbf{S}_{t|t-1}^{(i)} \right)^T \mathbf{H}_t^T \\ \mathbf{R}_t^{\frac{\mathbf{T}}{2}} \end{bmatrix},$$

where $\mathbf{T} \in \mathbb{R}^{N_y \times N_y}$. Having upper triangular Cholesky factor $\mathbf{F}_t^{(i)}$ of $\mathbf{Z}_t^{(i)}$, we can use (3.5.20) for computing the particle weights in logarithmic scale.

6.4 Numerical Experiment

We focus on modeling of the groundshine in the zone of emergency planning during the first two years after a severe reactor accident. In our numerical experiment we assume a deposition of radionuclide ^{134}Cs with half-life of decay $T_{1/2} = 2.0648$ years.

We want to perform a retrospective analysis using historical measurements sampled in one-month intervals for the time period of two years. The augmented state vector is of the form (6.3.1), where \mathbf{d}_t accounts for spatio-temporal distribution of the deposition and $\boldsymbol{\theta}_t$ describes the rate of radionuclides removal and the magnitude of model error. For given $\boldsymbol{\theta}_t$, deposition \mathbf{d}_t is estimated with the ensemble square root Kalman filter with multiplicative inflation of covariance (3.4.19) and evolved using the model (6.3.3).

Since the assumed time period is much shorter than the expected half-life of slow component of the environmental removal, we do not treat T^s in (2.2.12) as random and set it with a fixed value. We estimate just the half-life of the fast component T^f and its fraction d^f . Fraction of the slow component d^s is fully determined by the binding condition $d^f + d^s = 1$. Parameters $\boldsymbol{\theta}_t = (d_t^f, T_t^f, \Delta_t)^T$ are evolved using transitional pdf

$$p(\boldsymbol{\theta}_t | \boldsymbol{\theta}_{t-1}) = p(d_t^f | d_{t-1}^f) p(T_t^f | T_{t-1}^f) p(\Delta_t | \Delta_{t-1}), \quad (6.4.1)$$

where the evolution of its elements is modeled by random walk processes

$$p(d_t^f | d_{t-1}^f) = \mathcal{N}(d_{t-1}^f, \sigma_d^2), \quad \sigma_d = 0.05d_{t-1}^f + 0.01, \quad (6.4.2)$$

$$p(T_t^f | T_{t-1}^f) = \mathcal{N}(T_{t-1}^f, \sigma_T^2), \quad \sigma_T = 0.05T_{t-1}^f + 0.01, \\ p(\Delta_t | \Delta_{t-1}) = t\mathcal{N}(\Delta_{t-1}, \sigma_\Delta^2, [1, \infty]), \quad \sigma_\Delta = 0.05\Delta_{t-1} + 0.01. \quad (6.4.3)$$

Proposal density of the particle filter is chosen as (6.4.1) yielding the formula for recursive evaluation of weights

$$w_t^{(i)} \propto p(\mathbf{y}_t | \boldsymbol{\theta}_t^{(i)}) w_{t-1}^{(i)}, \quad i = 1, \dots, N.$$

6.4.1 Computational and Observational Grids

The deposition is estimated on a polar grid covering the eastern half of the zone of emergency planning using total number $N_y = 136$ observations. Rectangular observational grid with $N_d = 520$ grid points has the grid step 1.5km. Illustration of the observational and computational grid is in Figure (6.4.1). The fact that the polar computational grid and the rectangular observational grid are not aligned means that the observation operator must interpolate modeled values into the locations of receptor points. We implemented a linear observation operator \mathbf{H} using the bilinear interpolation.

6.4.2 Estimation of Prior Distribution of Deposition

Let us recall, that the initial conditions in the late phase are fully determined by the plume trajectory and plume depletion during the early phase. For simulation of the release we use atmospheric dispersion model from the environmental code HARP (HAzardous Radioactivity Propagation) (Pecha et al., 2007). It is a segmented Gaussian plume model capable for simulation of many physical processes.

We performed an extensive Monte Carlo simulation to consistently account for uncertainty connected with the plume propagation. The simulation covered a broad range of possible release scenarios, where 14 parameters $\mathbf{v} = (v_1, \dots, v_{14})^T$ of the dispersion model were treated as random. The list of parameters selected upon uncertainty study performed with the model is in Table (6.1). The total number of 5000 model realization were computed using inputs $\{\mathbf{v}^{(1)}, \dots, \mathbf{v}^{(5000)}\}$ sampled from a joint prior pdf $p(\mathbf{v})$.

Let $\{\mathbf{d}_0^{(1)}, \dots, \mathbf{d}_0^{(5000)}\}$ be deposition vectors generated using the dispersion model initialized with different sets of input parameters $\{\mathbf{v}^{(1)}, \dots, \mathbf{v}^{(5000)}\}$. Prior pdf $p(\mathbf{d}_0) = \mathcal{N}(\bar{\mathbf{d}}_0, \Sigma_0^d)$ represents an empirical distribution of the initial deposition:

$$\bar{\mathbf{d}}_0 = \frac{1}{5000} \sum_{i=1}^{5000} \mathbf{d}_0^{(i)}, \quad \Sigma_0 = \frac{1}{4999} \sum_{i=1}^{5000} (\mathbf{d}_0^{(i)} - \bar{\mathbf{d}}_0) (\mathbf{d}_0^{(i)} - \bar{\mathbf{d}}_0)^T.$$

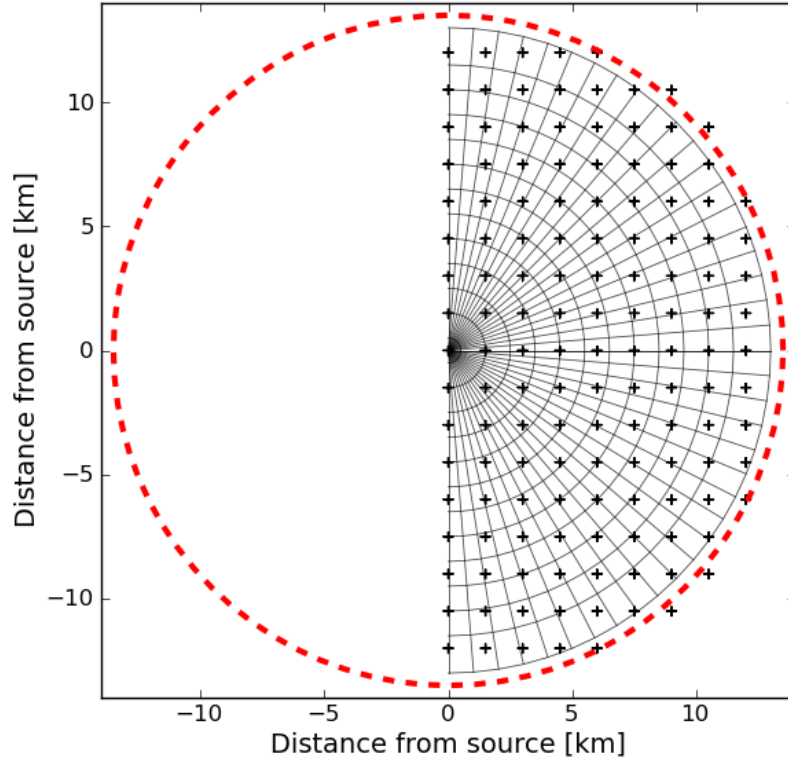


Figure 6.4.1: Illustration of computational and observational grids. We focus on the eastern half of the zone of emergency planning.

Param.	Physical effect	Param.	Physical effect
v_1	intensity of release	v_8	advection speed of plume
v_2	horizontal dispersion	v_9	wind profile
v_3	horizontal fluctuation of wind dir.	v_{10}	vertical dispersion
v_4	dry deposition of elements	v_{11}	mixing layer height
v_5	dry deposition of aerosols	v_{12}	heat capacity of the effluent
v_6	elution of elemental. iodine	v_{13}	precipitation intensity
v_7	elution of aerosols	v_{14}	time shift of precipitation

Table 6.1: Parameters treated as uncertain during Monte Carlo sampling of candidates on ensemble members.

6.4.3 Simulation of Observations

Measurements are simulated from the deposition vectors $\mathbf{d}_t^{\text{twin}}$, $t = 1, \dots, 24$, evaluated using (2.2.11) and an initial vector $\mathbf{d}_0^{\text{twin}}$ computed with the HARP model with initialized with a set of inputs \mathbf{v}^{twin} . The speed of environmental removal in the twin model is determined by the fast component with fraction $d^f = 0.54$ and half-life $T^f = 1.20$ years.

Measurement vectors \mathbf{y}_t are sampled from $\mathbf{d}_t^{\text{twin}}$ in receptor locations and perturbed with zero-mean Gaussian noise according to

$$\mathbf{y}_t \sim \mathcal{N}(\mathbf{H}\mathbf{d}_t^{\text{twin}}, \mathbf{R}_t). \quad (6.4.4)$$

The standard deviation of the observation error is a linear function of the measured values $\mathbf{y}_t^{\text{twin}} = \mathbf{H}\mathbf{d}_t^{\text{twin}}$,

$$\mathbf{R}_t[j, j] = (0.1\mathbf{y}_t^{\text{twin}}[j] + 500)^2, \quad j = 1, \dots, N_y.$$

Deposition generated using the twin model is in Figure 6.4.2 (top).

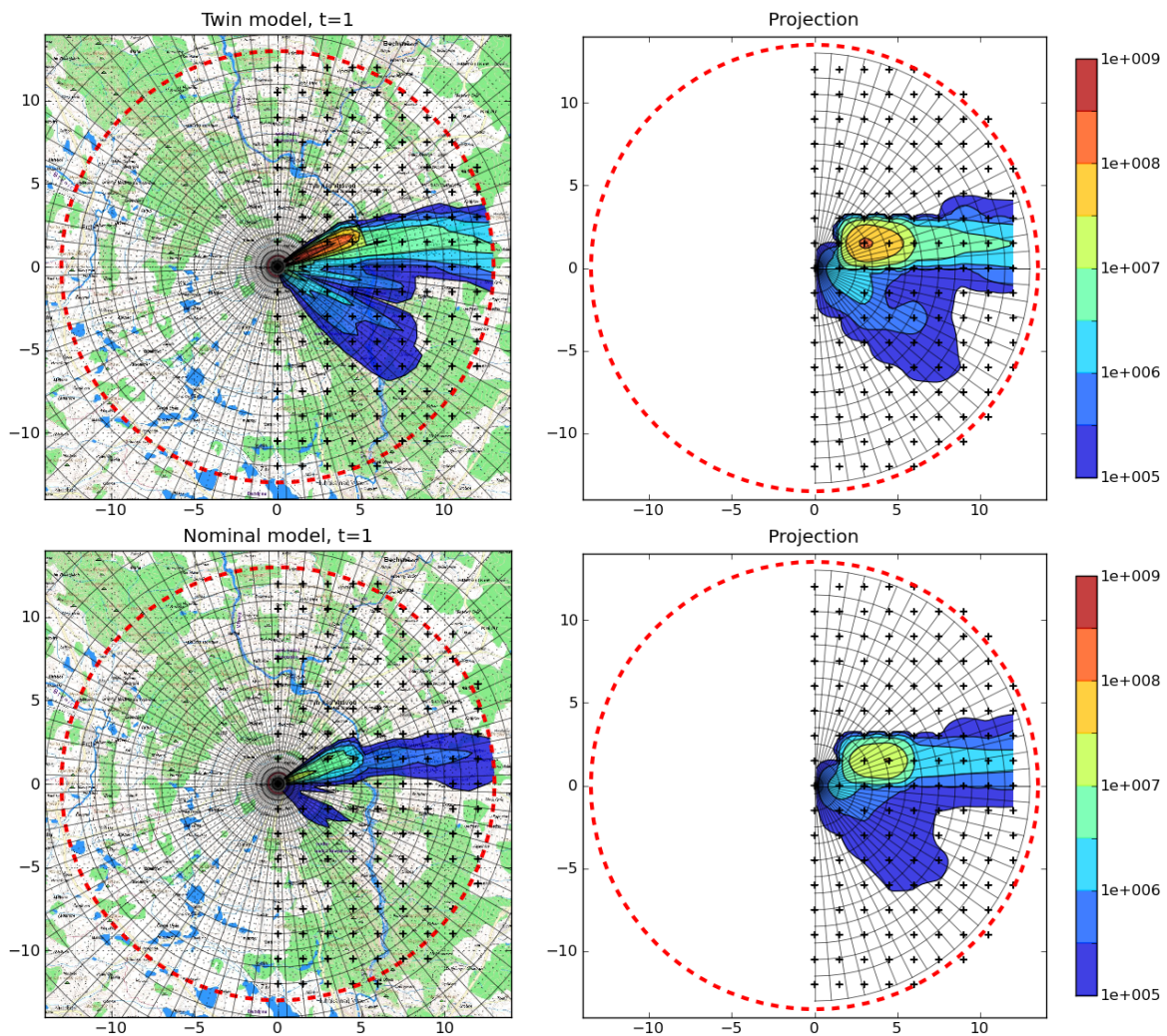


Figure 6.4.2: Left column: Visualization of initial deposition of the twin model $\mathbf{d}_0^{\text{twin}}$ (top) and of the initial ensemble mean (bottom). Right column: Interpolation of $\mathbf{d}_0^{\text{twin}}$ projected into the space of observations using (6.4.4) (top) and interpolation of the initial ensemble mean projected into the space of observations using (6.4.4) (bottom).

6.4.4 Selection of Prior Ensemble

EnSRFs within the MPF framework are initialized with a prior ensemble. This ensemble represents our initial belief on distribution of the deposition at the beginning of the late phase. In Section 6.4.2 we estimated the prior distribution of the deposition using 5000 realizations generated with the HARP system. However, to achieve a better agreement of the initial ensemble with the spatial localization of the deposition, we can use measurements \mathbf{y}_0 referring to the beginning of the late phase and select those realizations from the set $\{\mathbf{d}_0^{(1)}, \dots, \mathbf{d}_0^{(5000)}\}$, which are in the best agreement with the measurements. This procedure increases the representativeness of the prior ensemble. Realizations are weighted with the likelihood function

$$p(\mathbf{y}_0 | \mathbf{d}_0^{(i)}) \propto \det(\mathbf{Z}_0)^{-\frac{1}{2}} \exp \left[-\frac{1}{2} (\mathbf{y}_0 - \mathbf{H}\bar{\mathbf{d}}_0^{(i)})^T \mathbf{Z}_0^{-1} (\mathbf{y}_0 - \mathbf{H}\bar{\mathbf{d}}_0^{(i)}) \right],$$

$$\mathbf{Z}_0 = \mathbf{H}\Sigma_0^d \mathbf{H}^T + \mathbf{R}_0.$$

Resulting weights are in Figure 6.4.3. We used the multinomial re-sampling and selected 20 realizations which were included into the prior ensemble. 2-dimensional visualization of the prior ensemble mean is in Figure 6.4.2 (bottom).

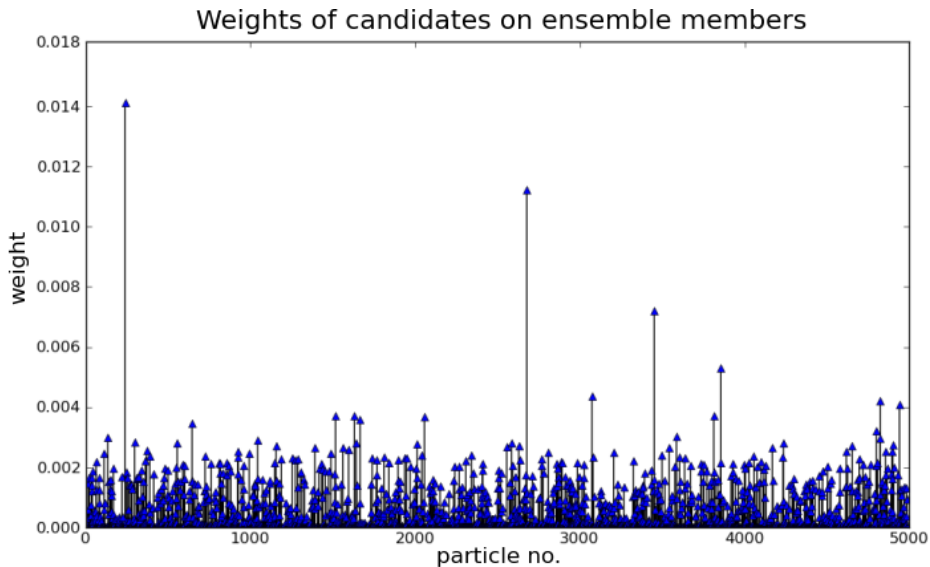


Figure 6.4.3: Weights of candidates $\mathbf{d}_0^{(i)}$ on members of initial ensemble.

6.4.5 Results

We run the data assimilation algorithm with 100 particles for 24 steps, i.e., 100 ensemble square root filters were run using different parameters $\boldsymbol{\theta}_t^{(i)}$ in respective time steps. In Figure 6.4.4 we see the deposition values for a randomly selected receptor location. We

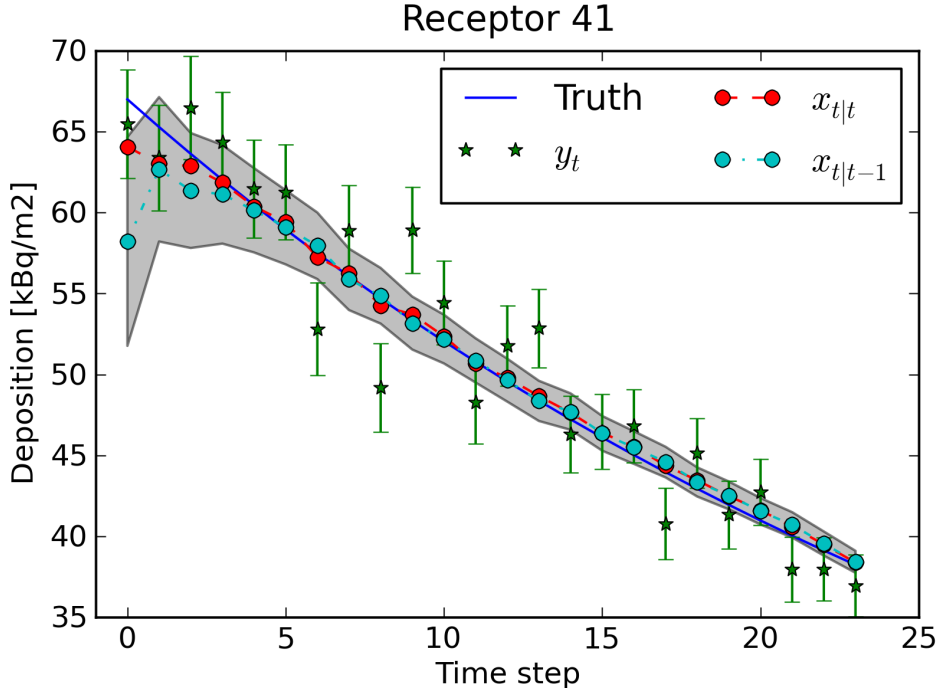


Figure 6.4.4: Results for a selected observation location. Blue line: true deposition (twin model); green dots: measurements and their standard deviations; cyan dots: prior estimates (forecasts); gray area: standard deviation of the forecast error; red dots: posterior estimates.

see that the posterior values (red dots) becomes identical with the true deposition (blue line) given by the twin model. Also that the variance of estimates (gray area) decreases with time.

In Figure 6.4.5 we see spatial visualization of the data assimilation results for time step 0, 8, 16, and 24. The nominal model, the twin model and the assimilated model are compared in respective time steps. We see that the ensemble localization procedure perform well and the initial estimate of affected area is similar to that given by the twin model. Already after the first assimilation cycle we obtain a good agreement between the assimilated model and the twin model. In the remaining time steps we observe, how the assimilated model approaches the twin model. To achieve a good agreement in all the computational points, more data assimilation cycles would be needed.

Besides the time evolution of the deposition we also estimate the speed of radionuclides removal given by the fast component of the environmental removal. Estimated parameters d^f and T^f are assumed to be time invariant. Comparison of the “true” parameters used for the simulation of measurement and the average values of the estimates is in Table 6.2. We observe a good correspondence of the estimates and the true values. The estimates can be in turn used as an input into the subsequent predictive models regarding further transport of radionuclides through the environment.

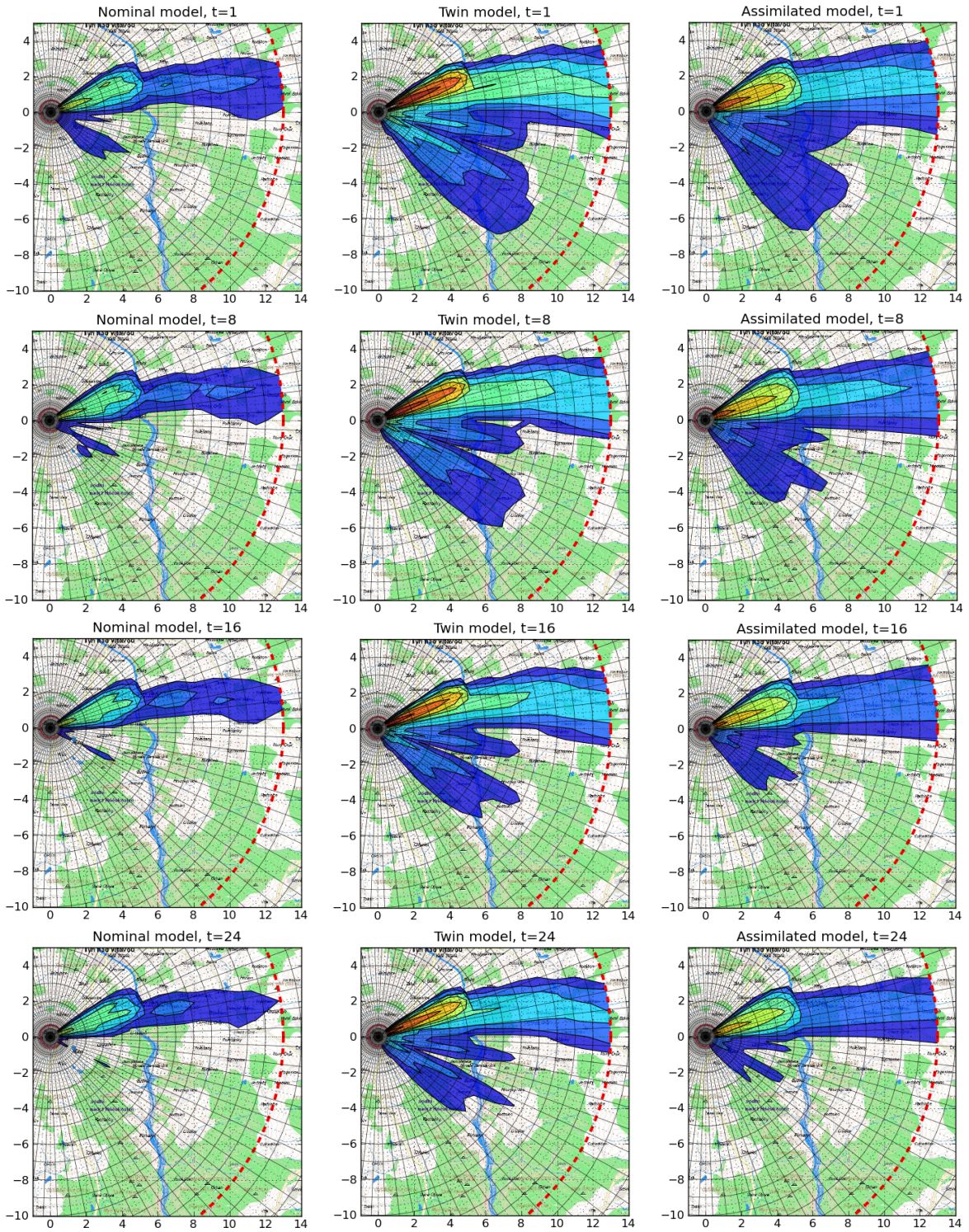


Figure 6.4.5: Visualization of assimilation results in time steps 0, 8, 16, and 24. Nominal model (prior mean), twin model (measurements) and assimilated model (posterior mean) are in first, second and third column, respectively. Color scale is the same as in Figure 6.4.2.

Parameter	“True” values	Mean estimated values
d^f	0.54	0.57
T^f	1.20	1.26

Table 6.2: Comparison of “true” parameters used for simulation of measurements with those estimated using the data assimilation procedure.

The mean value of the estimated multiplicative inflation factor used for correction of model error was 2.27 which indicate the fact that the spread of the initial ensemble was heavily underestimated.

6.5 Summary

This chapter has addressed the problem of data assimilation in the late phase of a radiation accident. We were concerned with the task of data assimilation of the forecasted spatio-temporal distribution of deposition with the groundshine dose measurements.

In (Palma, 2005), ensemble Kalman filtering has been identified as the most promising approach for this task. We developed this idea further and applied the MPF framework introduced in Chapter 4 for estimation of spatio-temporal distribution of the groundshine in tandem with the speed of environmental removal. In the proposed data assimilation method, particle filter approximates the posterior pdf of the global speed of radionuclides removal, whereas the conditional ensemble square root filter accounts for local variations in the deposition field reflected in groundshine dose measurements.

The performance of the method was demonstrated on a twin experiment, where the groundshine dose evolution model was assimilated with groundshine dose measurements. A release of ^{134}Cs was simulated with the atmospheric dispersion model embedded in the decision support system HARP. We performed an extensive Monte Carlo simulation of the possible release scenarios in order to account for uncertainty regarding the plume propagation during the early phase. Deposition fields resulting from 20 most plausible release scenarios were used for initialization of the ensemble filters attached to particles. The estimated deposition field approached that evaluated using the twin model. The rate of environmental removal also was correctly identified. The results are promising, however, the operational applicability remains to be demonstrated on real deposition data.

Chapter 7

Developed Software

In this chapter we describe different software tools developed for purposes of testing of data assimilation methods and handling of the meteorological and other data. The tools were developed in Python and C++ and they became parts of the decision support system HARP (Pecha et al., 2007).

7.1 Visualization System

The visualization system is capable of producing publishing-ready visualizations of radiological and meteorological quantities on a scalable map background. It is suitable particularly for visualization of spatial data given on a polar or a rectangular grid. Besides the visualization of the static data, the system also allows for animation of the plume movement, which can be used for examination of the radionuclides distribution in time. All the visualizations of spatial data in this dissertation were created using the system. The system also contains a set of tools for basic operations with the map, e.g., measuring of distances in the map, transformation of geographical latitude-longitude coordinates into the UTM (Universal Transverse Mercator) coordinate system and vice versa.

In Figure 7.2.1, time integrated activity concentration in air due to a simulated release from the Czech NPP Temelin is visualized.

7.2 Preprocessor of Meteorological Data

Meteorological preprocessor is a tool for viewing and transformation of the meteorological data entering the HARP system. The preprocessor transforms the input 3-dimensional HIRLAM (HIGH Resolution Limited Area Model) forecasts into the format supported by the HARP system. In Figure 7.2.2, a sample wind field describing the flow in vicinity of the Czech NPP Dukovany is visualized. Wind speed and direction on the red grid is the HIRLAM data and the preprocessor performs its interpolation on the green polar grid used by the HARP system.

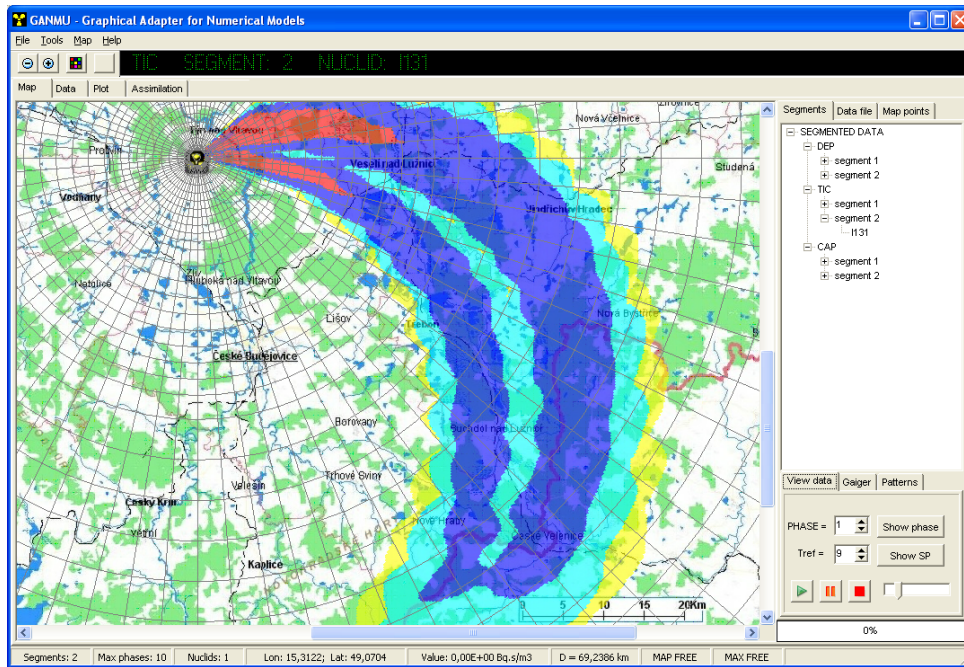


Figure 7.2.1: Spatial data visualization system. Visualization of a simulated release from the Czech NPP Temelin.

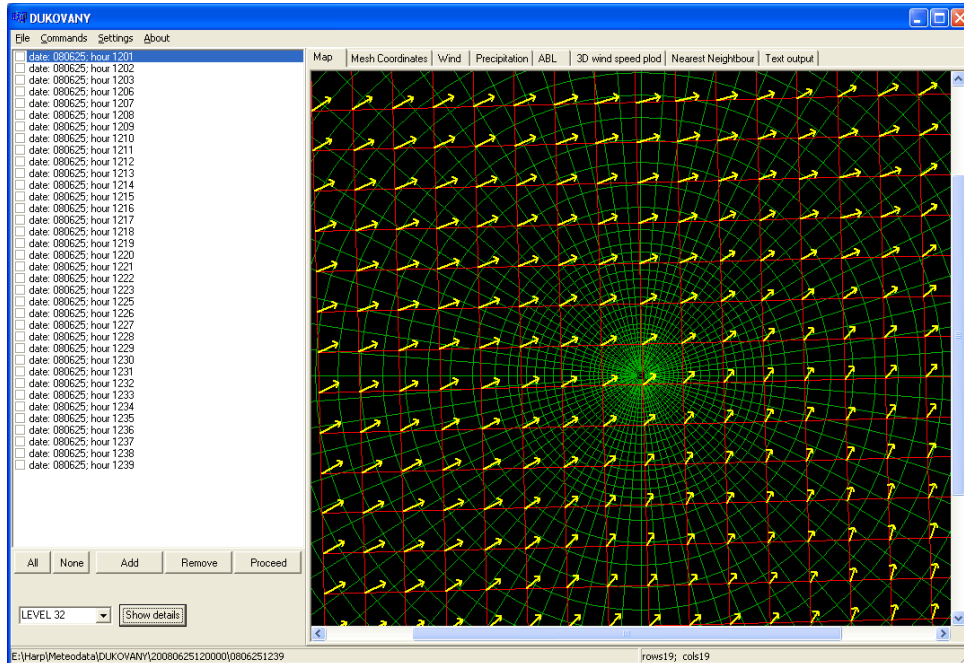


Figure 7.2.2: Meteorological data preprocessor. Visualization of a sample wind field describing the flow in vicinity of the Czech NPP Dukovany. HIRMAL data on the red rectangular grid is interpolated into the points of the green polar grid used by the HARP system.

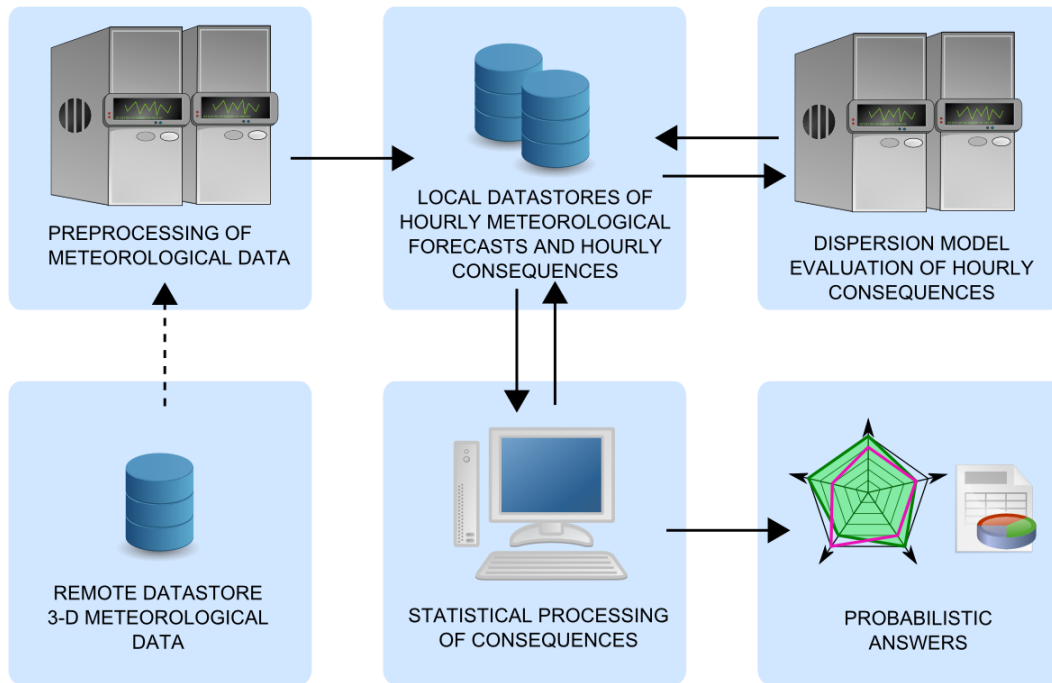


Figure 7.2.3: A diagram of the Monte Carlo framework for repetitive evaluation of dispersion models.

7.3 Framework for Monte Carlo Sampling

For purposes of extensive Monte Carlo simulations with the dispersion models we implemented a versatile framework (Hofman and Pecha, 2011). The framework is suitable for automated repetitive evaluation of a dispersion model using different inputs (meteorological conditions and/or source term). The three main fields of its application are as follows:

- Application in the field of probability safety assessment,
- Simulation of consequences of long term discharges of radionuclides into the atmosphere,
- Data assimilation in the early phase and the late phase of a radiation accident.

The diagram of the framework is in Figure 7.2.3. Firstly, meteorological forecasts are fetched from a remote data-store and transformed into hourly meteorological forecasts using meteorological preprocessor. Hourly forecast are stored on a local data-store. Secondly, an ADM is repeatedly evaluated using different meteorology and/or different source term. Generally, an arbitrary ADM can be inserted there. Hourly-evaluated consequences are stored in the local data-store. User can then access the data-store and perform statistical manipulations with the data. The system is equipped with a user friendly graphical user interface for visualization of probabilistic answers.

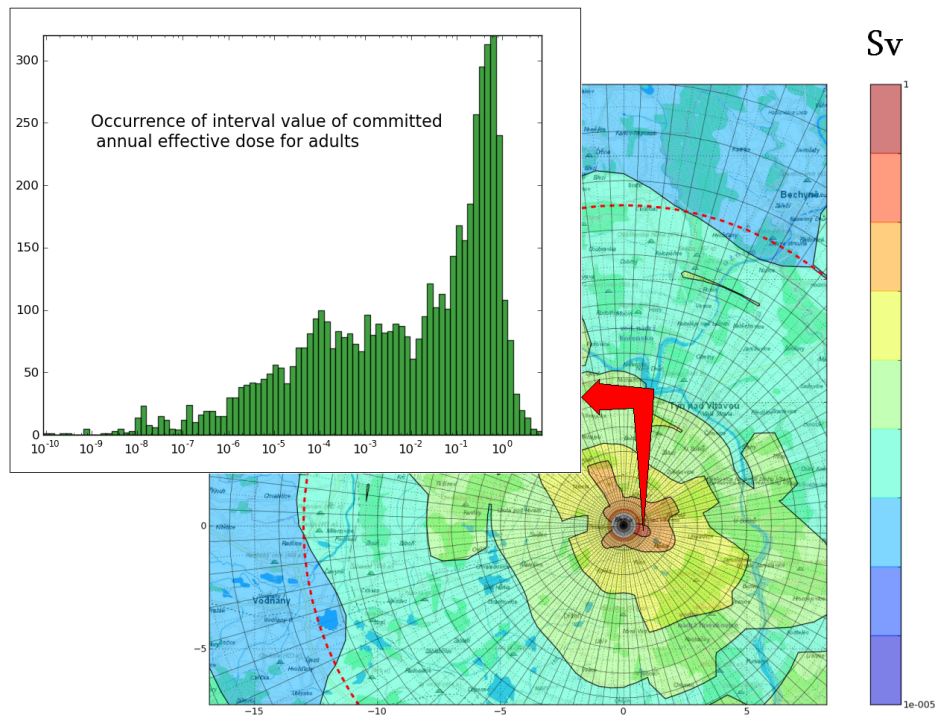


Figure 7.3.1: Example of a graphical output from the system. Background: visualization of expected spatial distribution of total committed dose for adults based on a sample two-year meteorological sequence (17520 hourly releases). Foreground: histogram representing distribution of committed doses in the highlighted point close to the source.

In Figure 7.3.1 we see an example of the system output. In background, there is a visualization of the expected spatial distribution of total committed dose for adults based on a sample two-year meteorological sequence (17520 hourly releases). In foreground, there is a histogram representing distribution of committed doses in the highlighted point close to the source.

Chapter 8

Conclusion

This dissertation has addressed the application of advanced data assimilation methods in the field of radiation protection. We focused on exploitation of particle filtering and marginalized particle filtering for assessment of radiation situation in the early and the late phase of a radiation accident. Respective data assimilation methodologies were formalized using consistent Bayesian framework and notation.

The research has demonstrated that the particle filtering approach, when applied in these areas, provides useful insights into the problems of interest, and results in improved versatility over more traditional approaches, e.g. Kalman filtering. Data assimilation systems based on particle filtering have a potential to be used for real-world emergency response in the near future.

Since no data from real reactor accident were available, all experiments were performed as twin experiments. In the twin experiments, measurements are simulated using a model of the system under investigation and perturbed with a random noise. The convergence of the estimated values to the known “background truth” can be then easily assessed.

The contributions of this dissertation and recommendations for the future research are presented in this chapter.

8.1 Summary of Contributions

The contributions of this thesis are now summarized chapter by chapter.

Chapter 2: This chapter concerned the physical models used in this dissertation.

Firstly, theoretical aspects of atmospheric dispersion modeling and radiological modeling were provided. Secondly, developed numerical schemes used for practical implementation of the models were described. For demonstration of the data assimilation algorithms developed in subsequent chapters we implemented the Gaussian puff model evaluating activity concentration in air. For evaluation of measurements we implemented an observation operator for transformation of the activity concentration in air into the time integrated gamma dose rate.

Chapter 3: Data assimilation was put into context of the Bayesian filtering. An overview of the sequential data assimilation methods was provided with the focus on state space models. Kalman filtering, ensemble filtering, particle filtering, and marginalized particle filtering is presented together with description of a numerically efficient implementation of the filters. The chapter primarily serves as a literature review of relevant Bayesian methods that are applied in subsequent chapters.

Chapter 4: In this chapter, the issues of adaptive tuning of inflation factor and other parameters within an assimilation scheme based on ensemble filtering was addressed. The developed framework based on the original MPF was presented as a new method for merging particle filters with analytically intractable approximate filters. The performance of the method for tuning of ensemble filters was presented on two scenarios with 40-variable Lorenz-96 model and compared with the “best tuned” ensemble filters.

Chapter 5: This chapter considered on-line estimation of the source term and the mean wind field during the plume propagations in the early phase of a radiation accident. This task has been traditionally addressed using the Kalman filters, where the non-linear state and the measurement models were approximated using the first-order Taylor expansion. To avoid this, we proposed a new particle filtering data assimilation methodology with adaptive selection of the proposal density. Our method can be used with an arbitrary parameterized atmospheric dispersion model. The resulting algorithm performed well in the simulated instantaneous release scenario with the meandering wind field. The correction factors of the release magnitude, wind speed and wind direction were well estimated from a limited set of gamma dose rate measurements. The adaptive selection of the proposal density ensured effective exploration of the state space.

Chapter 6: Application of the hybrid filtering methodology developed in Chapter 4 was extended to the problem of data assimilation in the late phase. The assimilation scenario for identification of the affected areas and the determination of the groundshine time evolution was formulated. In the proposed data assimilation algorithm, the particle filter estimated the magnitude of model error and the global speed of radionuclides removal, whereas the conditional EnSRF accounted for local variations in the deposition field. The assimilation performance was demonstrated using a simulated release, where an extensive Monte Carlo simulation was performed to account for uncertainty regarding the initial displacement of radionuclides. The speed of radionuclides removal was identified with high accuracy. The disadvantage of this methods is its high computational cost, where a number of ensemble filters must be run in parallel. However, in the case of retrospective analysis, the computational cost is an issue of a minor importance.

Chapter 7: Review of different software tool supporting the development and testing of the data assimilation methods was provided.

8.2 Future Research Directions

Based on the entire research in this work, we suggest to keep focus on sequential Monte Carlo methods in future investigations towards the operational application of data assimilation in the examined field. Among the possible future research topics belong:

- The extension of the data assimilation methodology for the early phase to continuous releases approximated by a sequence of puffs. Since this will increase the number of estimated parameters and bring a significant increase of computational cost, a parallel implementation of the algorithm will be needed.
- The application of the data assimilation algorithm for the late phase with a more elaborated deposition models based on multiple interacting compartments. This step will provide a background for further application of data assimilation in the propagation of radionuclides through the food chain.
- The twin experiments only provide a way for the initial validation of a considered data assimilation method. It is desirable to validate the data assimilation methods against existing real-case measurements.
- The implementation of the developed data assimilation algorithms into the HARP system.

Appendix A

Mean Value and Covariance of a Mixture of Gaussians

Assume a weighted mixture of n Gaussian distributions $\mathcal{N}(\mathbf{x}; \boldsymbol{\mu}^{(i)}, \mathbf{P}^{(i)})$ of a random variable \mathbf{x} with mean values $\boldsymbol{\mu}^{(i)}$ and covariance matrices $\mathbf{P}^{(i)}$, $i = 1, \dots, n$:

$$p(\mathbf{x}) = \sum_{i=1}^n w^{(i)} \mathcal{N}(\mathbf{x}; \boldsymbol{\mu}^{(i)}, \mathbf{P}^{(i)})$$

The mean $\mathbb{E}[\mathbf{x}]$ and covariance $\mathbb{E}[(\mathbf{x} - \mathbb{E}[\mathbf{x}])^2]$ of \mathbf{x} can be calculated as follows:

$$\begin{aligned} \mathbb{E}[\mathbf{x}] &= \int \mathbf{x} p(\mathbf{x}) d\mathbf{x} \\ &= \sum_{i=1}^n w^{(i)} \int \mathbf{x} \mathcal{N}(\mathbf{x}; \boldsymbol{\mu}^{(i)}, \mathbf{P}^{(i)}) d\mathbf{x} \\ &= \sum_{i=1}^n w^{(i)} \boldsymbol{\mu}^{(i)}, \\ \mathbb{E}[(\mathbf{x} - \mathbb{E}[\mathbf{x}])^2] &= \int (\mathbf{x} - \mathbb{E}[\mathbf{x}])^2 p(\mathbf{x}) d\mathbf{x} \\ &= \sum_{i=1}^n w^{(i)} \int (\mathbf{x} - \mathbb{E}[\mathbf{x}])^2 \mathcal{N}(\mathbf{x}; \boldsymbol{\mu}^{(i)}, \mathbf{P}^{(i)}) d\mathbf{x} \\ &= \sum_{i=1}^n w^{(i)} \int [(\mathbf{x} - \boldsymbol{\mu}^{(i)}) + (\boldsymbol{\mu}^{(i)} - \mathbb{E}[\mathbf{x}])]^2 \mathcal{N}(\mathbf{x}; \boldsymbol{\mu}^{(i)}, \mathbf{P}^{(i)}) d\mathbf{x} \\ &= \sum_{i=1}^n w^{(i)} \left[\mathbf{P}^{(i)} + (\boldsymbol{\mu}^{(i)} - \mathbb{E}[\mathbf{x}])^2 \right] \\ &= \sum_{i=1}^n w^{(i)} \mathbf{P}^{(i)} + \sum_{i=1}^n w^{(i)} (\boldsymbol{\mu}^{(i)} - \mathbb{E}[\mathbf{x}])^2. \end{aligned}$$

Appendix B

Computation of Time Update Using Square Roots

Let $\mathbf{A} \in \mathbb{R}^{n \times n}$, $\mathbf{B} \in \mathbb{R}^{n \times n}$, $\mathbf{C} \in \mathbb{R}^{m \times n}$, $\mathbf{D} \in \mathbb{R}^{n \times n}$ be real matrices. Following Simon (2006), let us suppose that we can find an orthogonal matrix $\mathbf{T} \in \mathbb{R}^{2n \times 2n}$ such that

$$\begin{bmatrix} \mathbf{A}^T \\ \mathbf{0} \end{bmatrix} = \mathbf{T} \begin{bmatrix} \mathbf{B}^T \mathbf{C}^T \\ \mathbf{D}^{\frac{T}{2}} \end{bmatrix} \quad (8.2.1)$$

$$= \begin{bmatrix} \mathbf{T}_1 & \mathbf{T}_2 \end{bmatrix} \begin{bmatrix} \mathbf{B}^T \mathbf{C}^T \\ \mathbf{D}^{\frac{T}{2}} \end{bmatrix} = \begin{bmatrix} \mathbf{T}_1 \mathbf{B}^T \mathbf{C}^T + \mathbf{T}_2 \mathbf{D}^{\frac{T}{2}} \end{bmatrix}, \quad (8.2.2)$$

where $\mathbf{T}_1, \mathbf{T}_2 \in \mathbb{R}^{n \times n}$. From orthogonality of \mathbf{T} follows that

$$\mathbf{T}^T \mathbf{T} = \begin{bmatrix} \mathbf{T}_1^T \\ \mathbf{T}_2^T \end{bmatrix} \begin{bmatrix} \mathbf{T}_1 & \mathbf{T}_2 \end{bmatrix} = \begin{bmatrix} \mathbf{T}_1^T \mathbf{T}_1 & \mathbf{T}_1^T \mathbf{T}_2 \\ \mathbf{T}_2^T \mathbf{T}_1 & \mathbf{T}_2^T \mathbf{T}_2 \end{bmatrix} = \begin{bmatrix} \mathbf{I} & \mathbf{0} \\ \mathbf{0} & \mathbf{I} \end{bmatrix},$$

and consequently

$$\mathbf{T}_1^T \mathbf{T}_2 = \mathbf{T}_2^T \mathbf{T}_1 = \mathbf{0}, \quad (8.2.3)$$

$$\mathbf{T}_1^T \mathbf{T}_1 = \mathbf{T}_2^T \mathbf{T}_2 = \mathbf{I}, \quad (8.2.4)$$

where $\mathbf{0}$ and \mathbf{I} are zero and identity matrices, respectively. Using (8.2.2) we can write

$$\begin{aligned} \begin{bmatrix} \mathbf{A} & \mathbf{0} \end{bmatrix} \begin{bmatrix} \mathbf{A}^T \\ \mathbf{0} \end{bmatrix} &= \begin{bmatrix} \mathbf{H}_t \mathbf{B} & \mathbf{D}^{\frac{1}{2}} \end{bmatrix} \begin{bmatrix} \mathbf{T}_1^T \\ \mathbf{T}_2^T \end{bmatrix} \begin{bmatrix} \mathbf{T}_1 \mathbf{B}^T \mathbf{C}^T + \mathbf{T}_2 \mathbf{D}^{\frac{T}{2}} \end{bmatrix} \\ &= \begin{bmatrix} \mathbf{H}_t \mathbf{B} & \mathbf{D}^{\frac{1}{2}} \end{bmatrix} \begin{bmatrix} \mathbf{T}_1^T \mathbf{T}_1 \mathbf{B}^T \mathbf{C}^T + \mathbf{T}_1^T \mathbf{T}_2 \mathbf{D}^{\frac{T}{2}} \\ \mathbf{T}_2^T \mathbf{T}_1 \mathbf{B}^T \mathbf{C}^T + \mathbf{T}_2^T \mathbf{T}_2 \mathbf{D}^{\frac{T}{2}} \end{bmatrix}. \end{aligned}$$

From identities (8.2.3)–(8.2.4) follows

$$\begin{aligned} \mathbf{A} \mathbf{A}^T &= \mathbf{C} \mathbf{B} \mathbf{T}_1^T \mathbf{T}_1 \mathbf{B}^T \mathbf{C}^T + \mathbf{D}^{\frac{1}{2}} \mathbf{T}_2^T \mathbf{T}_2 \mathbf{D}^{\frac{T}{2}} \\ &= \mathbf{C} \mathbf{B} \mathbf{B}^T \mathbf{C}^T + \mathbf{D}^{\frac{1}{2}} \mathbf{D}^{\frac{T}{2}}. \end{aligned}$$

So if we can find an orthogonal matrix $\mathbf{T} \in \mathbb{R}^{2n \times 2n}$ such that (8.2.1) is fulfilled, then matrix \mathbf{A} is equal to transpose of square root of $\mathbf{Z} = \mathbf{A}\mathbf{A}^T$. We can use various methods to find the orthogonal matrix and resulting square root of \mathbf{Z} , e.g., Householder transform, Gram-Schmidt orthogonalization, or Givens rotations (Golub and Van Loan, 1996). Different methods give us different square roots of \mathbf{Z} . From QR decomposition we obtain an upper triangular factor of the Cholesky decomposition of \mathbf{Z} .

Bibliography

- Anderson, J., 2007a: An adaptive covariance inflation error correction algorithm for ensemble filters. *Tellus A*, **59** (2), 210–224.
- Anderson, J., 2007b: Exploring the need for localization in ensemble data assimilation using a hierarchical ensemble filter. *Physica D: Nonlinear Phenomena*, **230** (1-2), 99–111.
- Anderson, J. and S. Anderson, 1999: A Monte Carlo implementation of the nonlinear filtering problem to produce ensemble assimilations and forecasts. *Monthly Weather Review*, **127**, 2741–2758.
- Andrieu, C., N. De Freitas, A. Doucet, and M. Jordan, 2003: An introduction to MCMC for machine learning. *Machine learning*, **50** (1), 5–43.
- Andrieu, C., A. Doucet, and R. Holenstein, 2010: Particle Markov chain Monte Carlo methods. *Journal of the Royal Statistical Society: Series B (Statistical Methodology)*, **72** (3), 269–342.
- Astrup, P., C. Turcanu, R. Puch, C. Palma, and T. Mikkelsen, 2004: Data assimilation in the early phase: Kalman filtering RIMPUFF. *Risø NL*.
- Barratt, R., 2001: *Atmospheric dispersion modelling: an introduction to practical applications*. Earthscan.
- Bengtsson, T., C. Snyder, and D. Nychka, 2003: Toward a nonlinear ensemble filter for high-dimensional systems. *Journal of Geophysical Research*, **108** (D24), 8775.
- Browne, E., R. Firestone, and V. Shirley, 1986: Table of radioactive isotopes.
- Burgers, G., P. van Leeuwen, and G. Evensen, 1998: Analysis scheme in the ensemble Kalman filter. *Monthly Weather Review*, **126**, 1719–1724.
- Carruthers, D., H. Edmunds, K. Ellis, C. McHugh, B. Davies, and D. Thomson, 1995: Atmospheric Dispersion Modelling System (ADMS): Comparisons with data from the Kincaid experiment. *International Journal of Environment and Pollution*, **5** (4), 382–400.

- Cheremisnoff, N., 2002: *Handbook of air pollution prevention and control*. Butterworth-Heinemann.
- Choppin, G., J. Liljenzin, and J. Rydberg, 2002: *Radiochemistry and nuclear chemistry*. Butterworth-Heinemann.
- Cimorelli, A., et al., 2004: *AERMOD: description of model formulation (EPA-454/R-03-004)*. US Environmental Protection Agency.
- Daley, R., 1993: *Atmospheric data analysis*. Cambridge Univ Pr.
- Dee, D., 1995: On-line estimation of error covariance parameters for atmospheric data assimilation. *Monthly weather review*, **123** (4), 1128–1145.
- Dempster, A., N. Laird, D. Rubin, et al., 1977: Maximum likelihood from incomplete data via the EM algorithm. *Journal of the Royal Statistical Society. Series B (Methodological)*, **39** (1), 1–38.
- Dombrowski, H., S. Neumaier, I. Thompson, and F. Wissmann, 2009: EURADOS inter-comparison 2006 to harmonise European early warning dosimetry systems. *Radiation Protection Dosimetry*, **135** (1), 1.
- Douc, R. and O. Cappé, 2005: Comparison of resampling schemes for particle filtering. *Proceedings of the 4th International Symposium on Image and Signal Processing and Analysis, 2005. ISPA 2005.*, IEEE, 64–69.
- Doucet, A., N. De Freitas, and N. Gordon, 2001: *Sequential Monte Carlo methods in practice*. Springer Verlag.
- Drews, M., B. Lauritzen, and H. Madsen, 2005: Analysis of a Kalman filter based method for on-line estimation of atmospheric dispersion parameters using radiation monitoring data. *Radiation protection dosimetry*, **113** (1), 75.
- Eleveld, H., Y. Kok, and C. Twenhöfel, 2007: Data assimilation, sensitivity and uncertainty analyses in the Dutch nuclear emergency management system: a pilot study. *International Journal of Emergency Management*, **4** (3), 551–563.
- Eleveld, H. and C. Twenhöfel, 2004: Improving the reliability of the prognosis of atmospheric dispersion using data assimilation. *Ninth International Conference on Harmonisation within Atmospheric Dispersion Modelling for Regulatory Purposes*, 1–4.
- Evensen, G., 1994: Sequential data assimilation with a nonlinear quasi-geostrophic model using Monte Carlo methods to forecast error statistics. *Journal of Geophysical Research*, **99**, 10–10.
- Gaspari, G. and S. Cohn, 1999: Construction of correlation functions in two and three dimensions. *Quarterly Journal of the Royal Meteorological Society*, **125** (554), 723–758.

- Gelman, A., 2004: *Bayesian data analysis*. CRC press.
- Gering, F., W. Weiss, E. Wirth, R. Stapel, P. Jacob, H. Müller, and G. Pröhl, 2004: Assessment and evaluation of the radiological situation in the late phase of a nuclear accident. *Radiation protection dosimetry*, **109** (1-2), 25.
- Gifford, F., 1976: Turbulent diffusion-typing schemes: A review. *Nuclear Safety*, **17** (1), 68–86.
- Golikov, V., M. Balonov, V. Erkin, and P. Jacob, 1999: Model validation for external doses due to environmental contaminations by the Chernobyl accident. *Health physics*, **77** (6), 654.
- Golub, G. and C. Van Loan, 1996: *Matrix computations*. Johns Hopkins Univ Pr.
- Gordon, N., D. Salmond, and A. Smith, 2002: Novel approach to nonlinear/non-Gaussian Bayesian state estimation. *Radar and Signal Processing, IEE Proceedings F*, IET, Vol. 140, 107–113.
- Gurjar, B., 2008: *Air Pollution: Health and Environmental Impacts*. CRC.
- Hager, W., 1989: Updating the inverse of a matrix. *SIAM review*, **31** (2), 221–239.
- Hanna, S., G. Briggs, and R. Hosker Jr, 1982: Handbook on atmospheric diffusion. Tech. rep., National Oceanic and Atmospheric Administration, Oak Ridge, TN (USA). Atmospheric Turbulence and Diffusion Lab.
- Hofman, R. and P. Pecha, 2011: Application of regional environmental code HARP in the field of off-site consequence assessment. *Proc. of International topical meeting on probabilistic safety assessment and analysis, PSA2011*.
- Hofman, R., P. Pecha, and E. Pechová, 2008: A simplified approach for solution of time update problem during toxic waste plume spreading in atmosphere. *Proc. of 12th Inter. Conf. on Harmonization within Atmospheric Dispersion Modelling for Regulatory Purposes, HARMO-12, Hrvatski Meterološki Časopis*, 510–515.
- Holmes, N. and L. Morawska, 2006: A review of dispersion modelling and its application to the dispersion of particles: An overview of different dispersion models available. *Atmospheric Environment*, **40** (30), 5902–5928.
- Homma, T., 2002: OSCAAR Development and Applications. *International MACCS user group I*, 57.
- Houtekamer, P. and H. Mitchell, 2001: A sequential ensemble Kalman filter for atmospheric data assimilation. *Monthly Weather Review*, **129** (1), 123–137.

- Houtekamer, P., H. Mitchell, G. Pellerin, M. Buehner, M. Charron, L. Spacek, and B. Hansen, 2005: Atmospheric data assimilation with an ensemble Kalman filter: Results with real observations. *Monthly Weather Review*, **133** (3), 604–620.
- IAEA, 2003: Testing of environmental transfer models using Chernobyl fallout data from the Iput River catchment area, Bryansk Region, Russian Federation. Part of the IAEA Co-ordinated Research Project on Biosphere Modelling and Assessment (BIOMASS). Technical Report.
- Ide, K., P. Courtier, M. Ghil, and A. Lorenc, 1997: Unified notation for data assimilation: Operational, sequential and variational. *J. Meteor. Soc. Japan*, **75** (1B), 181–189.
- Jazwinski, A., 1970: *Stochastic processes and filtering theory*. Academic Pr.
- Jeffreys, H., 1961: *Theory of Probability*. Oxford University Press.
- Jeong, H., E. Kim, K. Suh, W. Hwang, M. Han, and H. Lee, 2005: Determination of the source rate released into the environment from a nuclear power plant. *Radiation protection dosimetry*, **113** (3), 308.
- Julier, S. and J. Uhlmann, 1997: A new extension of the Kalman filter to nonlinear systems. *Int. Symp. Aerospace/Defense Sensing, Simul. and Controls*, Vol. 3, 26.
- Jung, Y., W. Park, and O. Park, 2003: Pollution dispersion analysis using the puff model with numerical flow field data. *Mechanics research communications*, **30** (4), 277–286.
- Kalman, R., 1960: A new approach to linear filtering and prediction problems. *Journal of Basic Engineering*, **82** (1), 35–45.
- Kalnay, E., 2003: *Atmospheric modeling, data assimilation, and predictability*. Cambridge Univ Pr.
- Kovalets, I., V. Tsiouri, S. Andronopoulos, and J. Bartzis, 2009: Improvement of source and wind field input of atmospheric dispersion model by assimilation of concentration measurements: Method and applications in idealized settings. *Applied Mathematical Modelling*, **33** (8), 3511–3521.
- Li, H., E. Kalnay, and T. Miyoshi, 2009: Simultaneous estimation of covariance inflation and observation errors within an ensemble Kalman filter. *Quarterly Journal of the Royal Meteorological Society*, **135** (639), 523–533.
- Lillington, J., 2004: *The future of nuclear power*. Elsevier Science Ltd.
- Lorenz, E. and K. Emanuel, 1998: Optimal sites for supplementary weather observations: Simulation with a small model. *Journal of the Atmospheric Sciences*, **55**, 399–414.

- Ludwig, F., L. Gasiorek, and R. Ruff, 1977: Simplification of a Gaussian puff model for real-time minicomputer use. *Atmospheric Environment (1967)*, **11 (5)**, 431–436.
- Mandel, J., 2006: *Efficient implementation of the ensemble Kalman filter*. University of Colorado at Denver and Health Sciences Center.
- Mitchell, H. and P. Houtekamer, 2000: An adaptive ensemble Kalman filter. *Monthly Weather Review*, **128 (2)**, 416–433.
- Oh, M. and J. Berger, 1992: Adaptive importance sampling in Monte Carlo integration. *Journal of Statistical Computation and Simulation*, **41 (3)**, 143–168.
- Onishi, Y., O. Voitsekhovich, and M. Zheleznyak, 2007: *Chernobyl—what have we learned?: the successes and failures to mitigate water contamination over 20 years*. Springer.
- Overcamp, T. and R. Fjeld, 1987: A Simple Approximation for Estimating Centerline Gamma Absorbed Dose Rates Due to a Continuous Gaussian Plume. *Health physics*, **53 (2)**, 143.
- Palma, C., 2005: Data assimilation for off-site nuclear emergency management, report RODOS(RA5)-RE(04)-01.
- Palma, C., et al., 2003: Data assimilation in the decision support system RODOS. *Radiation protection dosimetry*, **104 (1)**, 31.
- Park, S. and L. Xu, 2009: *Data assimilation for atmospheric, oceanic and hydrologic applications*. Springer Verlag.
- Päsler-Sauer, J., 2000: Description of the atmospheric dispersion model ATSTEP. *Report of project RODOS (WG2)-TN (99)-11*.
- Pasquill, F., 1961: The estimation of the dispersion of windborne material. *Meteorol. Mag*, **90 (1063)**, 33–49.
- Pecha, P. and R. Hofman, 2008: Fitting of segmented gaussian plume model predictions on measured data. *Proc. of 22th European Simulation and Modelling Conference ESM'2008, Le Havre, France*.
- Pecha, P., R. Hofman, and E. Pechová, 2007: Training simulator for analysis of environmental consequences of accidental radioactivity releases. *Proc. of 6th EUROSIM Congress on Modelling and Simulation, Ljubljana, Slovenia*.
- Peterka, V., 1981: Bayesian system identification. *Automatica*, **17 (1)**, 41–53.
- Pröhl, G., W. Friedland, and H. Müller, 1993: Potential reduction of the ingestion dose after nuclear accidents due to the application of selected countermeasures. *Radiation Protection Dosimetry*, **50 (2)**, 359.

- Quelo, D., B. Sportisse, and O. Isnard, 2005: Data assimilation for short range atmospheric dispersion of radionuclides: a case study of second-order sensitivity. *Journal of environmental radioactivity*, **84** (3), 393–408.
- Rao, K., 2005: Uncertainty analysis in atmospheric dispersion modeling. *Pure and Applied Geophysics*, **162** (10), 1893–1917.
- Raza, S., R. Avila, and J. Cervantes, 2001: A 3-D Lagrangian (Monte Carlo) method for direct plume gamma dose rate calculations. *Journal of Nuclear Science and Technology*, **38** (4), 254–260.
- Ristic, B., S. Arulampalam, and N. Gordon, 2004: *Beyond the Kalman filter: Particle filters for tracking applications*. Artech House Publishers.
- Rubinstein, R. and D. Kroese, 2008: *Simulation and the Monte Carlo method*. Wiley-Interscience.
- Saha, S., E. Özkan, V. Šmídl, and F. Gustafsson, 2010: Marginalized particle filters for Bayesian estimation of noise parameters. *Proc. of the 13th International Conference on Information Fusion*, Edinburgh, UK.
- Saji, G., 2003: A new approach to reactor safety goals in the framework of INES. *Reliability Engineering and System Safety*, **80** (2), 143–161.
- Schön, T., F. Gustafsson, and P. Nordlund, 2005: Marginalized particle filters for mixed linear/nonlinear state-space models. *IEEE Transactions on Signal Processing*, **53** (7), 2279–2289.
- Simon, D., 2006: *Optimal state estimation: Kalman, H_∞ and nonlinear approaches*. John Wiley and Sons.
- Tennekes, H. and J. Lumley, 1972: *A first course in turbulence*. MIT press.
- Thiessen, K., et al., 2005: Model testing using data on Cs-137 from Chernobyl fallout in the Iput River catchment area of Russia. *Journal of environmental radioactivity*, **84** (2), 225–244.
- Thrun, S., W. Burgard, and D. Fox, 2005: *Probabilistic Robotics (Intelligent Robotics and Autonomous Agents)*. MIT press.
- Thyker-Nielsen, S., S. Deme, and E. Lång, 1995: *Calculation Method for Gamma Dose Rates From Gaussian Puffs*. Risø National Laboratory.
- Thyker-Nielsen, S., S. Deme, and T. Mikkelsen, 1999: *Description of the atmospheric dispersion module RIMPUFF*. Risø National Laboratory.
- Tippett, M., J. Anderson, C. Bishop, T. Hamill, and J. Whitaker, 2003: Ensemble square-root filters. *Mon. Weather Rev*, **131**, 1485–1490.

- Twenhöfel, C., M. van Troost, and S. Bader, 2007: Uncertainty analysis and parameter optimization in early phase nuclear emergency management. RIVM, tech. rep.
- Wang, B., X. Zou, and J. Zhu, 2000: Data assimilation and its applications. *Proceedings of the National Academy of Sciences of the United States of America*, **97** (21), 11 143.
- Welch, G. and G. Bishop, 1995: An introduction to the Kalman filter. *University of North Carolina at Chapel Hill*.
- Whitaker, J. and T. Hamill, 2002: Ensemble data assimilation without perturbed observations. *Monthly Weather Review*, **130**, 1913–1924.
- Yuschenko, S., I. Kovalets, V. Maderich, D. Treebushny, and M. Zheleznyak, 2005: Modelling the radionuclide contamination of the black sea in the result of chernobyl accident using circulation model and data assimilation. *Radioprotection*, **40**, 685–691.
- Zannetti, P., 1986: A new mixed segment-puff approach for dispersion modeling. *Atmospheric Environment (1967)*, **20** (6), 1121–1130.
- Zannetti, P., 1990: *Air pollution modeling*. Van Nostrand Reinhold.
- Zheng, D., J. Leung, B. Lee, and H. Lam, 2007: Data assimilation in the atmospheric dispersion model for nuclear accident assessments. *Atmospheric environment*, **41** (11), 2438–2446.

Index

- absorbed dose, 20
- activity, 19
- activity concentration in air, 15, 16, 20, 24
- advection-diffusion equation, 11, 12
- analysis, 29, 33
- atmospheric dispersion modeling, 9

- background field, 29
- Bayes formula, 31, 32
- Becquerel, 20

- cloudshine, 2, 20
- conjugate prior, 32
- control variables, 4, 65
- covariance localization, 41

- data assimilation, 29
- data update, 29
- decay constant, 19
- decay law, 20
- decay rate, 19
- diffusivity coefficients, 10
- dispersion coefficients, 15, 17
- dose rate conversion factor, 20, 22

- early phase, 2, 65
- effective height, 17
- elevated source, 17
- ensemble inflation, 41
- ensemble Kalman filter, 34
- ensemble square root filter, 37
- environmental removal, 22
- Eulerian model, 12
- extended Kalman filter, 34

- forecast, 29, 33

- Gaussian plume model, 13, 14
- Gaussian puff model, 13, 16
- groundshine, 2, 22, 81, 85

- half-life, 20

- importance sampling, 44
- inflation factor, 41

- Kalman filter, 32

- Lagrangian model, 12
- late phase, 2, 81
- length-scale parameter, 41
- likelihood function, 50
- Lorenz-96 model, 56

- marginal likelihood, 36
- Markov process, 31
- mixing layer, 17

- observation operator, 31

- parametrized model, 4
- particle filtering, 42
- plume reflection, 17
- posterior, 30
- prior, 30
- proposal density, 43, 47

- radioactive decay, 19, 22
- radioactivity, 19

- sampling-importance-resampling, 47
- sampling-importance-sampling, 45
- Schur product, 41
- semi-infinite approximation, 20
- Sherman–Morrison–Woodbury formula, 37

shielding factor, 22
spurious covariances, 41
state transition operator, 31
state transition pdf, 32
stationary parameters, 67
statistical inference, 30, 31
stochastic process, 31
systematic re-sampling, 47

time update, 29
turbulent diffusion, 10
twin experiments, 6, 73, 87

virtual source, 16, 17

zone of emergency planning, 85